Model Predictive Control of Fuel-Cell-Car-Based Smart Energy Systems in the Presence of Uncertainty

Ph.D. Thesis

Farid Alavi

Delft University of Technology, 2019

ISBN 978-94-6366-149-2

Cover design by Farid Alavi.
Printed by Gildeprint.

Model Predictive Control of Fuel-Cell-Car-Based Smart Energy Systems in the Presence of Uncertainty

PROEFSCHRIFT

ter verkrijging van de graad van doctor
aan de Technische Universiteit Delft,
op gezag van de Rector Magnificus Prof. Dr. Ir. T.H.J.J. van der Hagen;
voorzitter van het College voor Promoties,
in het openbaar te verdedigen op
Woensdag 3 april 2019 om 12:30 uur

door

Farid ALAVI
Master of Science in Electrical Engineering - Control
Isfahan University of Technology, Iran
geboren te Bandar Emam Khomeini, Iran

This dissertation has been approved by the
promotor: Prof. dr. ir. B. De Schutter, and
promotor: Prof. dr. ir. N. van de Wouw

Composition of the doctoral committee:

Rector Magnificus,	chairperson
Prof. dr. ir. B. De Schutter,	promotor
Prof. dr. ir. N. van de Wouw,	promotor

Independent members:

Prof. dr. ir. H. La Poutre,	Delft University of Technology
Prof. dr. ir. Z. Lukszo,	Delft University of Technology
Prof. dr. C. Ocampo-Martinez,	Technical University of Catalonia
Prof. dr. A. Parisio	The University of Manchester
Dr. M. Lazar,	Eindhoven University of Technology

This research is supported by the NWO-URSES project Car as Power Plant, which is financed by the Netherlands Organization for Scientific Research (NWO).

This dissertation has been completed in fulfillment of the requirements of the Dutch Institute of Systems and Control (DISC) for graduate study.

Published and distributed by: Farid Alavi

ISBN 978-94-6366-149-2

Keywords: model predictive control, energy management systems, fuel cell cars, microgrid, min-max control

Printed in the Netherlands

"Simple causal reasoning about a feedback system is difficult because the first system influences the second and second system influences the first, leading to a circular argument. This makes reasoning based upon cause and effect tricky, and it is necessary to analyze the system as a whole."

K. J. Åström and R. M. Murray, Feedback Systems: An Introduction for Scientists and Engineers.

Acknowledgements

My PhD research program allowed me to learn and grow. This process of learning and growing would not be possible without the help of my first promotor, Professor Bart De Schutter. I was privileged to have him as my promotor and I would like to express my sincere gratitude to him. He has been an excellent mentor for me during the last years.

I would also like to thank my second promotor, Professor Nathan van de Wouw, for all his help and guidance. He helped me a lot in improving the quality of this thesis and I am very grateful for that.

The CaPP research group had a nice atmosphere and I enjoyed working with the group. I am very grateful to Professor Zofia Lukszo for the fruitful discussions about the CaPP project. I would like to thank other researchers in the group, specially Esther, Vincent, Reinier, Samira, and Giannis for their kindness and help.

I am forever thankful to my old friends, specially Reza, Bardia, Soheil, Mostafa, and Amir Reza.

I sincerely thank my volleyball-player friends, including Arash, Masoud, Sahar, Hamid, Hengameh, Amin, Maryam, Javad, Farzaneh, Matin, Siamak, and Aydin for creating lots of happy memories for me.

Since my arrival in the Netherlands, a lot of my friends helped me to get familiar with the new environment, to enjoy my time in the Netherlands, and to understand different cultures of the world. Among these friends are Behnam, Francesco, Graziana, Frederik, Shuai, Sjoerd, Arman, Mohammad Reza, Mahya, Amir, Yashar, Cecilia, Laura, Cristiano, Matiya, Tina, Arash, Ali, Shima, Hossein, and Amin.

I had very kind and friendly colleagues and their presence made the atmosphere of my work better. I would like to thank them all, specially Tomas, Hai, Jia, Anahita,

Abhimanyu, Max, Vittorio, Jesus, Jeroen, Tim, Maolong, Carlos, Bart, Filippo, Baptiste, Yu, Sophie, Zhou, and Reinier.

My special thanks go to Cees for helping me in translating the abstract of my thesis into Dutch.

I would like to express my deep gratitudes to my parents, my siblings, and my brother in law. Their support has been a valuable gift in my life.

At last, I would like to thank the one who showed me the dawn of a new life, my charming wife, Behtab.

Farid Alavi
The Netherlands, March 2019

Summary

In this thesis, we design control algorithms for power scheduling of a fleet of fuel cell cars in a microgrid. Fuel cell cars are a relatively new type of vehicles. The driving force of these cars comes from an electrical motor and in order to generate the required electricity for the operation of the motor, the vehicle is equipped with a fuel cell system. The purpose of the fuel cell system is to convert the chemical energy of hydrogen into electricity. By considering the fact that fuel cell cars have the ability to generate electricity from hydrogen, these type of vehicles can be considered as a new type of flexible power plant. The idea of generating electricity inside a parking lot by using fuel cell cars is what we refer to as the Car as Power Plant (CaPP) concept. In this PhD thesis, we consider the power scheduling problem of a fleet of fuel cell cars in the CaPP concept. Several robust model predictive control methods are developed to determine the power generation schedule of the fuel cell cars inside the microgrid.

In the first part of this thesis, we present an overview of the CaPP concept from the technical, socio-economical, and control point of view. The focus of this part is on the development of a min-max model predictive control method for a CaPP microgrid system, where the worst-case performance of the system is optimized. To this end, we first model the CaPP microgrid by using the mixed logical dynamical framework. In addition, the operational cost function of the system is determined while taking into account the uncertainty in the prediction of the residual load of the microgrid. A min-max optimization problem is constructed and solved to minimize the highest possible operational cost for all possible realizations of uncertainty, while the power balance of the microgrid is maintained.

In the second part of the thesis, we develop an alternative approach, called disturbance feedback min-max model predictive control. In this alternative approach, we

consider a feedback law that uses the disturbance of the previous time step. Therefore, the branches of possible state trajectories in the future are closer together compared to the conventional min-max approach. As a result, the disturbance feedback min-max approach is less conservative compared to the min-max approach. Even though a disturbance feedback min-max approach results in a satisfactory performance of the system, this method is not applicable for a large-scale system, due to the computational complexity of the resulting optimization problem. To solve the scalability issue of the proposed approaches, three distributed control methods based on the dual decomposition, alternating direction method of multipliers (ADMM), and proximal ADMM are developed. As a result of using the developed distributed control methods, the driving patterns of the fuel cell cars can be kept private. In other words, no privacy sensitive data on the usage of the cars is collected by a central control agent. The improvement in the privacy of the car owners, and also reduction in the computation time of the controller are the two main advantages of the proposed distributed control algorithms.

In the last part of the thesis, a different approach is used to schedule the power generation profiles of the fuel cell cars. In the previous parts, the power scheduling profile of each individual fuel cell car was determined by the control system. In other words, the individual fuel cell cars were considered as power generation units. In this part, we consider an entire parking lot for fuel cell cars as a single power generation unit and the control system determines the power generation profile of several parking lots inside a microgrid. One advantage of this approach is the ability to control a large fleet of fuel cell cars without requiring a complex communication network. By considering this approach, three model predictive control methods are designed with three different approaches, namely, the nominal, the min-max, and the min-max-regret approach. Moreover, we present two methods that can be used to reduce the complexity of the optimization problems for the min-max and min-max-regret approach. These two methods allow us to identify a relatively small region inside the search space where the optimal point is located and, hence, the optimization problems of the proposed approaches become tractable.

Samenvatting

In dit proefschrift ontwerpen we regeltechnische algoritmes voor het plannen van het vermogen van een vloot van brandstofcelauto's in een micronetwerk. Brandstofcelauto's zijn een relatief nieuw type voertuigen die aangedreven worden door een elektrische motor. Het voertuig is uitgerust met een brandstofcelsysteem om de benodigde hoeveelheid elektriciteit voor de motor te genereren. Het doel van het brandstofcelsysteem is het converteren van chemische energie van waterstof naar elektriciteit. Aangezien brandstofcelauto's in staat zijn elektriciteit te genereren uit waterstof, kan men dit type voertuigen beschouwen als een nieuw type flexibele energiecentrale. Het concept om elektriciteit te genereren in een parkeerplaats door gebruik te maken van brandstofcelauto's, wordt ook wel het *Car as Power Plant* (CaPP) (auto als energiecentrale) concept genoemd. In dit proefschrift wordt het vermogensplanningsprobleem beschouwd voor een vloot van brandstofcelauto's in het CaPP raamwerk. Om stroomopwekkingschema's te bepalen van de brandstofcelauto's in een micronetwerk, worden robuuste *Model Predictive Control* (MPC) (modelgebaseerde voorspellende regeling) methodes ontworpen.

In het eerste deel van dit proefschrift wordt een overzicht van het CaPP concept gepresenteerd vanuit een technisch, socio-economisch en regeltechnisch perspectief. De focus van dit onderdeel is op de ontwikkeling van een min-max MPC methode voor een CaPP micronetwerk-systeem, waarbij de systeemprestatie in het slechtste geval wordt geoptimaliseerd. Hiertoe wordt allereerst het CaPP micronetwerk gemodelleerd met behulp van het *Mixed Logical Dynamical* (gemengde logische dynamische) raamwerk. Daarnaast wordt de operationele kostenfunctie van het systeem bepaald, waarbij er rekening gehouden wordt met de onzekerheid in de voorspelling van de resterende belasting van het micronetwerk. Een min-max optimalisatieprobleem wordt opgesteld en opgelost om de hoogst mogelijke operationele kosten te

minimaliseren voor alle mogelijke realisaties van de onzekerheid, terwijl de vermogensbalans van het micronetwerk in stand gehouden wordt.

In het tweede deel van dit proefschrift wordt er een alternatieve aanpak ontwikkeld, genaamd *disturbance feedback* (terugkoppeling van de verstoring) min-max MPC. In deze alternatieve aanpak wordt er een terugkoppelingsregeling beschouwd die de verstoring van de vorige tijdstap gebruikt. Hierdoor liggen de mogelijke toestandstrajecten in de toekomst dichter bij elkaar in vergelijking met de conventionele min-max aanpak. Daardoor is de *disturbance feedback* min-max aanpak minder conservatief dan de min-max aanpak. Alhoewel een *disturbance feedback* min-max aanpak resulteert in een bevredigende prestatie van het systeem, is deze methode niet toepasbaar voor grootschalige systemen door de reken-complexiteit van het resulterende optimalisatieprobleem. Om de schaalbaarheidsproblematiek van voorgestelde methodes op te lossen, worden er drie gedistribueerde regelmethoden ontwikkeld, gebaseerd op duale decompositie, *alternating direction method of multipliers* (ADMM) (alternerende-richting methode van vermenigvuldigers) en proximale ADMM. Als gevolg van het gebruik van de ontwikkelde gedistribueerde regelmethodes, kunnen de rijpatronen van de brandstofcelauto's privaat gehouden worden. Met andere woorden, er wordt geen privacygevoelige informatie over het gebruik van de auto's verzameld door een centrale regelagent. De verbetering in privacy van de auto-eigenaren en ook de vermindering in rekentijd van de regelaar zijn de twee belangrijkste voordelen van de voorgestelde gedistribueerde regelalgoritmes.

In het laatste deel van het proefschrift wordt er een andere aanpak voor het plannen van de stroomopwekkingsprofielen van de brandstofcelauto's gebruikt. In de voorgaande delen werd het stroomopwekkingsprofiel van iedere individuele brandstofcelauto bepaald door het regelsysteem. Met andere woorden, de individuele brandstofcelauto's werden geschouwd als stroomopwekkingseenheden. In dit deel wordt de gehele parkeerplaats van brandstofcelauto's als een enkele stroomopwekkingseenheid beschouwd en het regelsysteem bepaalt het stroomopwekkingsprofiel van verscheidene parkeerplaatsen in een micronetwerk. Een voordeel van deze methode is de mogelijkheid om een grote vloot van brandstofcelauto's te regelen, zonder dat er een complex communicatienetwerk nodig is. Voor deze aanpak worden er drie MPC methodes ontworpen met drie verschillende aanpakken, namelijk het nominale, min-max en min-max-*regret* (spijt) aanpak. Daarnaast worden er twee methodes voorgesteld die kunnen worden gebruikt om de complexiteit van de optimalisatieproblemen van de min-max en min-max-*regret* aanpak te verlagen. Deze twee methodes maken het mogelijk om een relatief klein gebied binnen de zoekruimte te identificeren waarin het optimale punt zich bevindt en daarom de optimalisatieproblemen van de voorgestelde aanpakken haalbaar maken.

Contents

List of Figures

List of Tables

1 Introduction

This chapter presents the motivation for the research and also the research goals and main contributions. In Section 1.1, we explain the detailed motivation for the research of this thesis. In Section 1.2, the goals of the research are introduced and the main contributions of this thesis are highlighted. Section 1.3 presents the outline of the rest of this thesis.

1.1 Motivation for the research

In recent years, we have seen an increase in the share of renewable energy sources (RES) in the total power generation for electrical networks. Two commonly known examples of RES are wind turbines and solar photovoltaic (PV) panels. This increase is one step forward towards reducing the emission of carbon dioxide (CO_2) and, at the same time, reducing the use of fossil fuels for electrical power generation. However, most of the available RES have intermittent power generation capacity by nature. The capacity of power generation for a RES is highly dependent on the weather condition. For example, for a wind turbine, the speed of the wind and, for a PV system, the intensity of sunlight, are important factors in power generation. Therefore, the power generation of RES are not as predictable and as controllable as the power generation by a conventional power plant.

To stabilize and to operate a power network in a desired operational condition, the amount of generated power should be equal to the load at each time instant. If the share of RES power generation is extremely low compared to the power generation of conventional power plants, the intermittent power generation of RES does not threaten the stability of the power network. Similar to the current approach in dealing with uncertainty in the realization of the load, i.e., using primary, secondary

control levels, the uncertainty in the power generation of the RES can be compensated by adapting the power generation of conventional generators using such primary and secondary control levels as well. However, if the share of RES in the total power generation of the power grid reaches a considerable level, the aforementioned approach is not feasible, because the primary and secondary controllers can only adjust the power generation of a unit up to a certain limit.

Microgrids are a relatively new type of power systems that can incorporate a high share of RES, while the microgrid still maintains the power balance. We define a microgrid as a small-scale power network in which the generators are equipped with smart control and communication systems and there is a considerable reserve capacity for generation and storage of electricity. We assume that an energy management system is responsible for the correct operation of the microgrid by collecting information from all the devices that consume electricity and sending control commands to different generators. The problem of maintaining the power balance with intermittent power generation of RES can be solved by adjusting the power generation or storage of reserve units.

In this thesis, we consider a fleet of fuel cell cars as the reserve units of a microgrid. A fuel cell car has the ability to convert chemical energy of hydrogen into electricity and, if the car is not used for transportation, it is potentially a power generation unit. The concept of using fuel cell cars for the power generation inside a microgrid is called Car as Power Plant (CaPP). Figure 1.1 indicates a microgrid structure that is considered in this thesis. In this figure, the red lines indicate the data exchange within the control system, while the dashed blue lines represent the electrical connections of the microgrid. The energy management system of the microgrid maintains the power balance of the microgrid by updating the power generation profiles of the fuel cell cars on a regular basis. To this end, a model predictive control (MPC) system is a promising solution for the considered energy management system, because MPC has intrinsic robust features and is able to deal with the constraints in the system. The main motivation of this thesis is to explore potential MPC solutions for the energy management of a CaPP system, while we consider the uncertainty in the system. Here, uncertainty in the system is originated from inaccurate predictions in the microgrid's load or the number of available cars in the geographical area of the microgrid. Designing a control algorithm without considering these uncertainties may result in a weak performance or even a power unbalance situation.

1.2 Research goals and main contributions

The goal of this thesis is developing new MPC strategies for a CaPP system, i.e., for a microgrid where fuel cell cars act as power generation units. Based on the review of the current control methods for the energy management systems in Chapter 2, the following challenges have been identified in that chapter. First of all, a model

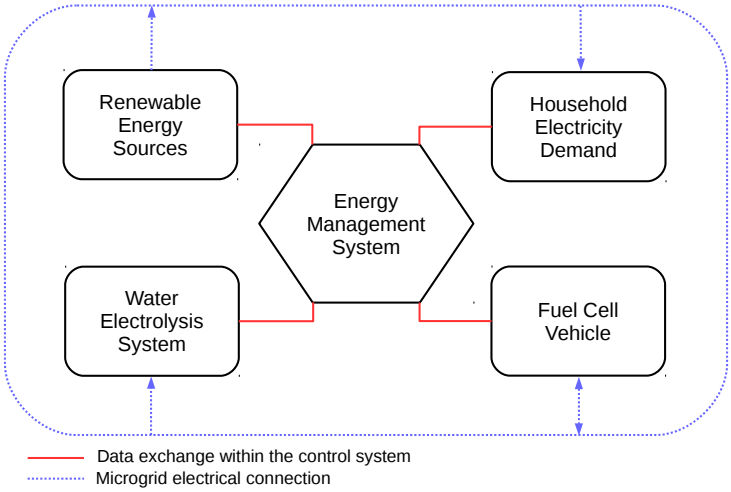

Figure 1.1: The schematic representation of the microgrid considered in this thesis.

for the CaPP system is needed to serve as a basis for MPC-based controllers. The following challenges arise when considering the design of such controllers. New MPC strategies should also be able to optimize the operational cost of the system while considering the uncertainty in the system, to preserve the privacy of the fuel cell car owners, and to deal with a large number of fuel cell cars in the system.

The main contributions of this thesis, aligned with these challenges, consist of:

- **Developing a mixed logical dynamical model for the microgrid.**

  The fuel cell cars are modeled by considering several operational modes, such as transportation, refilling, and power generation modes. A water electrolysis system is also modeled and, finally, the whole microgrid of Figure 1.1 is modeled by a mixed logical dynamical model. Development of such a model paves the way to use MPC for the energy management system of the microgrid.

- **Developing a min-max MPC approach for the microgrid.**

  A min-max MPC approach is developed for the microgrid that is able to minimize the operational cost of the system for the worst-case uncertainty, while the power balance of the microgrid is maintained for any realization of the uncertainty. The developed control approach emphasizes the use of the fuel cell cars in both the power generation mode and the transportation mode.

- **Developing control strategies with enhanced privacy for the fuel cell car owners.**

  While the fuel cell cars are considered as the power generation units in the microgrid, these also act as private transportation means for their owners. As

such, sharing information about the driving patterns of the cars with the energy management system may be considered as violating the privacy rights of the car owners. We develop three MPC control strategies that eliminate the use of any information about the driving patterns of the cars with the energy management system. Even though all of these MPC control strategies preserve the privacy of the car owners, these strategies posssess different characteristics regarding the scalability and performance of the system.

- **Developing scalable control strategies for a large microgrid.**

  An MPC control system needs to solve an optimization problem at each sampling time instant. Considering that these optimization problems should be solved relatively fast for a large system with hundreds of fuel cell cars, we develop several distributed control strategies that support a computationally more efficient implementation compared to a central control strategy. In other words, we make the control of energy management system scalable. Even though all of these strategies are scalable, these strategies possess different characteristics regarding the performance of the system.

- **Developing an MPC approach based on minimizing the regret of the decision maker.**

  The general approach in defining the cost function of an MPC controller is to consider the operational cost of the system. We develop an alternative approach that considers the regret of the decision maker as the cost function of the MPC controller. We show that the developed approach would optimize the same objective as the one that a human operator would try to optimize. The developed approach may also reach a better solution compared to the min-max MPC approach, in terms of a posteriori closed-loop operational cost, in presence of uncertainty in the system.

- **Developing methods to simplify the optimization problem of the MPC controller.**

  In each chapter, we formulate a specific optimization problem to be solved in the MPC controller. In most of the cases, we derive technical results in order to reduce the search space of the optimization problem. These technical results are not only useful in making the optimization problems of this thesis tractable, but these may inspire other researchers in similar fields to reduce the computational complexity of their optimization problems.

1.3 Thesis outline

The organization of this thesis and the relation between different chapters are presented in Figure 1.2. The arrows in this figure indicate the preferred reading order.

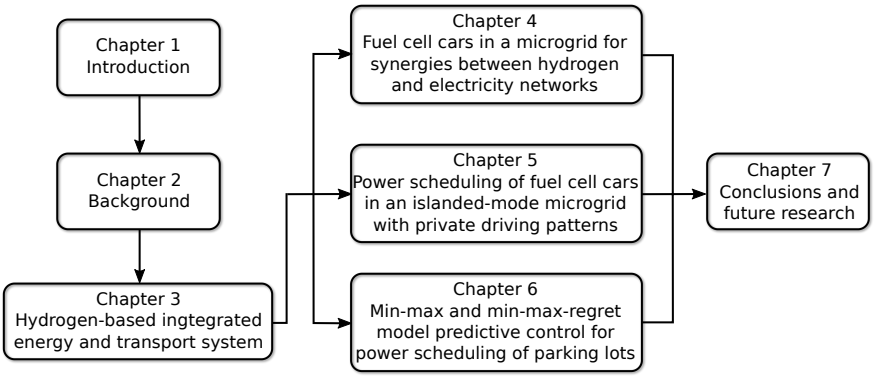

Figure 1.2: Structure of this thesis. The arrows indicate preferred reading order.

After the introduction to this thesis in this chapter, we present background information and a survey on the current state of the art methods in Chapter 2. A detailed explanation of fuel cell systems and the CaPP concept, as well as a review of the current control methods for energy management systems of microgrids are presented in Chapter 2.

In Chapter 3, the CaPP concept is analyzed from three different perspectives, including a techno-economical perspective, a control system perspective, and a socio-technical perspective. The aim of this chapter is to show that a CaPP system is feasible and economically viable and, at the same time, to show different aspects of the system to the reader.

In Chapter 4, a min-max MPC controller is designed for the energy management system of the microgrid of Figure 1.1. In this chapter, we show how we can model a microgrid with fuel cell cars that are both used for transportation and power generation. Note that inaccuracies in the prediction of the load or in the number of cars inside the geographical area of the microgrid results in uncertainties in the control system. Therefore, a min-max MPC is developed for the system to minimize the operational cost of the system for the worst-case scenario of the uncertainty, while the power balance of the microgrid is guaranteed to be maintained.

To reduce the conservatism of the min-max MPC approach of Chapter 4, we develop a disturbance feedback min-max MPC approach in Chapter 5. We also develop three distributed control methods that make the optimization problem of the MPC controller scalable. Another advantage of the developed distributed control methods is the enhancement of the privacy of the fuel cell car owners; by using the developed distributed control methods of Chapter 5, no privacy-sensitive data regarding the driving behavior of the car owners is shared with any agent in the system.

In Chapter 6, an MPC controller is designed for the energy management system of the microgrid that optimizes the same objective as the one that a human operator

would try to optimize. We develop an MPC controller based on minimizing the regret of the decision maker, rather than the regular cost function of the system. Our simulations show that by considering the presence of uncertainty in the system, there are cases where the developed MPC controller outperforms the conventional min-max control strategy.

Finally, Chapter 7 concludes the thesis. Some recommendations for future research directions regarding the CaPP concept are also presented in this chapter.

2 Background on Fuel Cell Cars and Smart Energy Systems with Vehicle-to-Grid Operation

In this chapter, fuel cell cars and their operation in the vehicle-to-grid mode are introduced in Section 2.1. Furthermore, the concept of car as power plant is presented in Section 2.2, where a fleet of fuel cell cars is used for the task of power generation within a microgrid. Considering the fact that this thesis is focused on the energy management system within the car as power plant concept, after introducing three different control levels in power systems, we focus of the power scheduling problem of distributed energy sources and some existing methods in the literature are reviewed in Section 2.3.

2.1 Fuel cell cars

In fuel cell electric vehicles (FCEVs), the driving power of the car is provided by the electricity that comes from a fuel cell stack. Figure 2.1 depicts a schematic representation of such vehicles from an energy flow perspective. Depending on the design of the vehicle, the engine of an FCEV can be an alternating current (AC) or direct current (DC) electrical motor. To create a suitable voltage and current for the operation of the electrical motor based on the driving conditions, and also to manage the charging mode and discharging mode of the battery, a power electronic management system is used. Providing electricity for running the engine is realized by using a fuel cell stack and a battery. Note that even though the presence of a battery makes the structure of an FCEV similar to an electrical vehicle (EV), the difference between these two types of vehicles is in the size of their batteries and the existence of a fuel cell system.

An FCEV requires a much smaller battery compared to an EV and the reason is

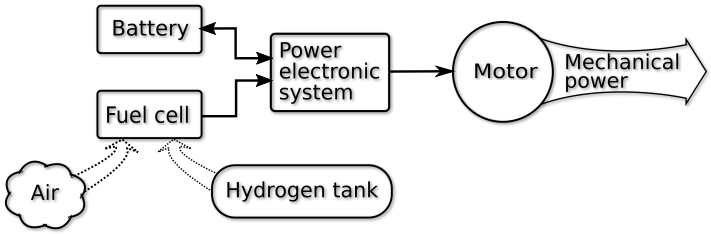

Figure 2.1: Schematic representation of the internal structure of a fuel cell car.

that an FCEV is equipped with a fuel cell system that provides almost all the energy that the vehicle needs. Therefore, in contrast to an EV, the battery of an FCEV is not the main source for providing energy and it is mainly used for providing extra power when there is a demand for rapid acceleration. Note that there is a type of electrical vehicles, in which the fuel cell system is used as a range extender of the vehicle [92]. In this specific type of vehicles, the fuel cell stack is smaller and the battery is larger compared to a normal FCEV. In fact, these type of vehicles can be considered as an EV with an onboard charging system in the form of fuel cell stack. In this thesis, we consider a normal fuel cell vehicle, i.e., a vehicle in which the main driving power comes from a fuel cell stack.

The fuel cell stack is used to convert chemical energy of hydrogen into electricity. This conversion in the form of energy is a result of a chemical reaction inside the fuel cell as follows [35]:

$$2\mathrm{H}_2 + \mathrm{O}_2 \rightarrow 2\mathrm{H}_2\mathrm{O}. \tag{2.1}$$

The chemical reaction (2.1) is in fact the process of burning hydrogen. However, in a fuel cell system, this chemical reaction is realized in a specific manner, in which the electrons of the hydrogen molecules are separated from their respective protons at the beginning of the process. This step is done by using a membrane that only allows the protons to pass through. Figure 2.2 gives a schematic representation of this process. As the protons pass through the membrane and reach the other side of the membrane, i.e., cathode, these react with the oxygen (O_2) in the air and new molecules of water are created. The extra electrons required for this chemical reaction are provided by the existing electrons in the cathode plate. Therefore, the whole process results in a shortage of electrons at one side, i.e. the cathode side, and an excess of electrons at the other side, i.e., the anode side. Consequently, these two sides will have a difference in their electrical potential and a flow of electrons, or electrical current, will occur if there is an electrical circuit outside of the fuel cell connecting the anode and cathode.

The source of energy in FCEVs is hydrogen and this kind of gas is stored using a high-pressure tank inside the vehicle. The typical pressure of the gas in such storage tanks is around 700 bar. With this pressure, a tank with a normal volume of around 122 liter can provide almost 5 kg of hydrogen, which is sufficient to drive a car for

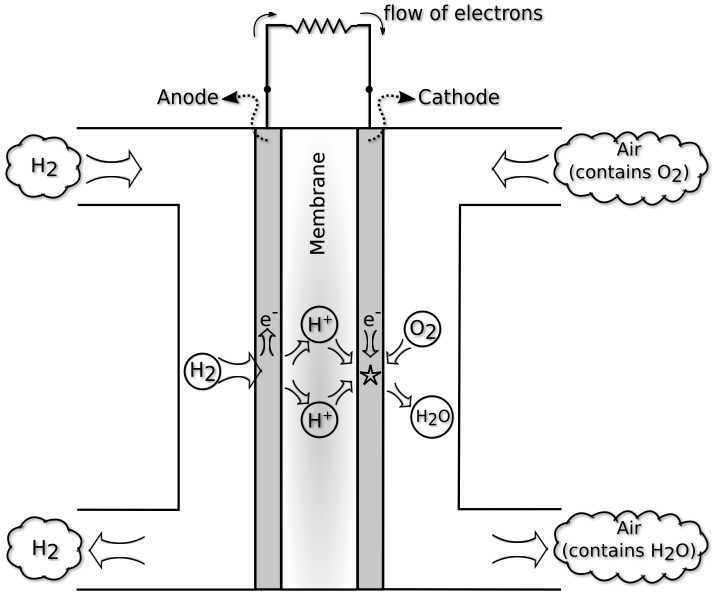

Figure 2.2: Conversion of hydrogen into water inside a fuel cell. An important result of this conversion is a flow of electrons (electrical current) in a circuit outside of the fuel cell.

about 500 km. Even though these numbers can be dependent of the specific design of a vehicle, it is important to point out that with the current level of technology, fuel cell cars can be built and used on the road efficiently. Examples of such fuel cell cars are the Hyundai ix35, the Toyota Mirai, the Honda Clarity, and the Mercedes-Benz F-Cell. Even though hydrogen is an explosive gas, the safety level of FCEVs is high, thanks to a conservative design of the hydrogen tanks. A recent study [57] shows that FCEVs are accepted as a safe type of vehicle and [81] argues that FCEVs will be more common in the future. The aforementioned commercial models of fuel cell cars have passed the required level of certification to be used on public roads in Europe. A hydrogen tank can be fully charged in less than 5 minutes, and this fast charging procedure combined with the relatively long driving range is an advantage of FCEVs compared to EVs.

2.2 Car as power plant

Power systems are accommodating an increasing amount of renewable generation. However, Renewable Energy Sources (RES) such as the sun or the wind are variable, uncertain, and not dispatchable. Therefore electricity is not always produced when it is needed by the users. Flexibility sources such as dispatchable generation, storage, demand side response, and increased interconnection are needed to integrate more renewable power generation into power systems [42, 95].

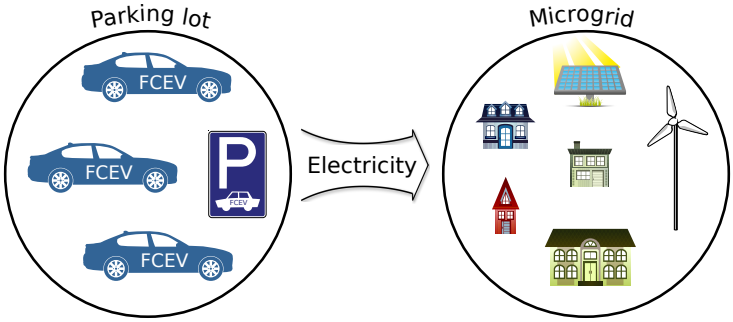

Figure 2.3: The concept of car as power plant, in which fuel cell cars are used both for transportation and power generation.

Electric vehicles can provide the flexibility needed in future electric power systems. Although plug-in EVs represent a new source of variability due to their charging needs, this variability can be managed via smart charging strategies [90], and the vehicles' batteries can also be used to store surplus renewable generation. Moreover, plug-in EVs can become dispatchable power plants by providing power or balancing services via vehicle-to-grid (V2G) technology [50].

Fuel cell electric vehicles, with hydrogen as fuel, can be used to support the operation of power systems with a large participation of RES. These are particularly suited to provide peak power or spinning reserves to the grid [56, 52]. Because these use hydrogen as a fuel, they do not draw power from the grid, and if aggregated, they can provide large amounts of power. In contrast to plug-in EVs, if FCEVs have a connection to a hydrogen source, they can be operated continuously regardless of the level of fuel stored in their tank [56]. Through the use of FCEVs for both transportation and power generation, we can explore the synergies that can be created between hydrogen and electricity networks.

In this section, we present the Car as Power Plant (CaPP) [88] concept. CaPP introduces a flexible multi-modal energy system that uses FCEVs as dispatchable power plants [32]. It is based on the fact that FCEVs, when parked, can produce electricity from hydrogen in a cleaner and more efficient way than the current power system, thereby producing waste products (water and heat) that can be re-used [88, 59]. Since cars are used for driving only around 5% of the time [88], there is a big potential to replace peak power plants with a large fleet of FCEVs or to reduce the need to build new plants in the future. Additionally, heat generated in the fuel cells can be used locally if the FCEVs are connected directly to a building's heat network [52]. Figure 2.3 depicts the concept of CaPP, where the fuel cell cars are not only an integral part of the transportation system, but also are part of the power generation units in a microgrid.

The CaPP concept can be implemented in different settings and for different types of applications. When applied in a parking lot, a large fleet of parked cars can

be used to provide power to the grid through an aggregator that sells power on behalf of the drivers. In residential microgrid settings, residents of the neighborhood can use their FCEVs to provide power to the local grid at times of low renewable power generation. In buildings with high electricity and heat demand, such as hospitals, the CaPP system can be implemented not only to use the electricity and heat from vehicles, but also to provide a large back-up capacity to the building.

This thesis focuses on the power scheduling problem of a microgrid including the CaPP system. We consider a residential microgrid with distributed generators that are used to serve local loads and to produce hydrogen, which acts as energy storage medium. This gaseous fuel is used by cars to drive, and additionally, it can be used to generate power when renewable power sources are scarce. This system is studied from the operational control perspective, as operational control is one of the main challenges in the implementation of microgrids [67].

The operational control aspects to take into account in the CaPP microgrid are the scheduling of the FCEVs and the electrolyzer in the power-to-gas (P2G) system. In the literature, the scheduling problem of grid-integrated vehicles in microgrids is usually addressed with centralized optimization approaches, where the resources from plug-in EVs are managed by minimizing power losses in the system [51] or by minimizing the operating costs [11]. In a microgrid with renewable resources, a power-to-gas (P2G) system and vehicle-to-grid (V2G) power from FCEVs, the V2G scheduling problem is addressed by minimizing the power imported from the grid [84]. The operation of electrolyzers in P2G systems is also addressed with optimization approaches in the literature [53, 48, 77]. Similar control objectives are used, e.g., for maximizing the profits from wind power export to the grid while taking into account the hydrogen demand [53]. In [91], the sizing of the solar Photo Voltaic (PV) panels and techno-economic aspects of a PV-to-hydrogen system with fuel cell buses are studied using a simple control algorithm.

2.3 Energy management systems

Different levels of control can be used in order to maintain the power balance of a microgrid. Traditionally, three control levels exist in power systems, namely primary, secondary, and tertiary control. In primary and secondary control [82, 83, 49], the objective of the control system is to keep the voltage and frequency of the power system at a specific value. In tertiary control [38], set points for the amount of power generation are determined for each generator. In this level, the objective is to minimize the operational cost of the system while considering the power balance condition and the system constraints, such as the maximum power generation of each generator. In this thesis, we consider tertiary control, or the power scheduling, problem of a microgrid.

The control system that manages the demand and production of the electricity in a smart grid, of which the distributed power generation based on fuel-cell cars

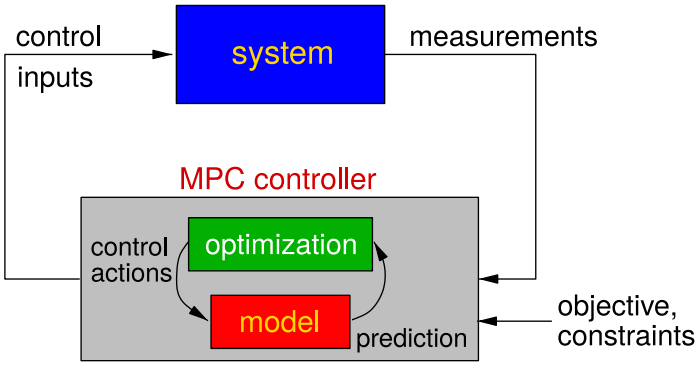

Figure 2.4: Model predictive control loop.

is an example, is called an energy management system. In recent years, several works have considered controller design for such systems. In [22], the problem of charging and discharging of EVs in a smart grid is considered in order to reach a power balance in the system and gain the maximum operational benefit. Two optimization methods based on centralized and decentralized schemes are proposed. However, the developed distributed solution requires the exchange of solutions for each agent during several iterations. Therefore, the network traffic is typically high in this approach.

2.3.1 Model predictive control method

Due to the intrinsic robust features and the ability to deal with the constraints in the system, Model Predictive Control (MPC) is a method that has gained much attention in design of an energy management system for smart grid applications. As Figure 2.4 depicts, an MPC controller consists of two main parts. The first part is a model of the system by which we can predict the future behavior of the system for a given control input. The second part is an optimization procedure that optimizes the operational cost of the system subject to possible constraints on inputs, states, or outputs of the system. By solving such an optimization problem, the MPC controller determines a sequence of control inputs that represent the control inputs from the current time step to a specific time step in the future. Here, by a time step we mean specific time instants where the interval between any two consecutive time instants are equal to a specific number that we call sampling time[1]. The first part of the control input sequence is then applied to the system. At the next time step, the controller updates the system states using the measurement devices and the whole process mentioned above repeats one more time.

[1]Note that in MPC usually a discrete-time model is used to determine the system states at specific time instants, i.e., at time steps. If we define sampling time, T_s, as a constant real number, then the time steps are determined by $t_k = kT_\mathrm{s}$, for all $k \in \mathbb{Z}^+$, where $\mathbb{Z}^+$ indicates the set of non-negative integers.

2.3.2 MPC in energy management systems

In [10], a distributed MPC method to operate a microgrid is developed. The problem of power scheduling in a microgrid is reviewed in [66] and [75]. Another example of using MPC in the operation of a microgrid system is [78], where it is assumed that the controlled microgrid has a renewable energy source, a storage battery system, and some electrical loads. The designed control algorithm is based on an optimization problem that takes into account the cost of system operation. However, the paper [78] neglects binary variables that determine different operational modes of devices and, hence, some part of the operational cost is not considered.

In [25], control of a microgrid that contains several power plants, a photovoltaic system, and a fuel cell system is considered. The problem is formulated with mixed-logical dynamical models and the optimization problem is solved with multiparametric programming techniques. Another example of using MPC in the control of microgrids that contain fuel cells and solar photovoltaic systems is [97]. In this paper, a method is developed to control the system via the market trades. However, the developed method cannot guarantee the stability of the system.

The design of an MPC controller in order to operate several devices in a smart grid is discussed in [69]. In this paper, the optimization problem is expressed as a mixed integer linear programming problem. However, [69] assumes that the future load profile is predetermined and that there is no uncertainty in the system.

In order to deal with the uncertainty in the energy management systems, robust control techniques are used in [68] and [40]. A stochastic optimization in the energy management system is developed in [68], while in [40] a minimax formulation is used. In [37], a method is developed in order to model the uncertainty in power systems as a polytope, while the appropriate control strategy in order to deal with the modeled uncertainty is not discussed.

Three different methods to deal with the uncertainty in the power systems are discussed in [14]. The first method simply considers some plants in the standby operation mode in order to provide excess electricity if it is needed. The second method uses stochastic optimization in order to set an appropriate power production profile for each plant. However, this method requires a priori knowledge about the uncertainties in the system. The last method employs robust optimization which guarantees the stability of the system in presence of all the possible disturbances. The advantage of the third method compared to the second method is that accurate information about the uncertainties is not necessary.

Min-max MPC and stochastic MPC are two widely used methods in dealing with uncertainty in power networks. An advantage of using min-max MPC compared to stochastic MPC is that we only need to determine an interval for the realization of the uncertainty; no extra information about the uncertain parameter, such as the probability distribution function, is needed. Even though the min-max MPC method has the advantage of simplicity, it suffers from a high level of conservatism. In reality, the worst-case scenario will be realized rarely and this is the reason that

a min-max approach has a lower performance compared to the other robust MPC methods.

In [87] an alternative method, called min-max disturbance feedback, is proposed where a feedback law is considered in the control system that includes the uncertainty of the model. In a similar concept, [58] shows that the feedback on the disturbance creates a set of possible state trajectories in the form of a tube.

The control methods mentioned above focus on designing a controller with a centralized architecture, in which there is a single controller that receives all the information of the system and determines the control inputs for all the agents in the system. An alternative solution involves a distributed architecture, in which several agents inside the system interact to determine the control inputs of the system. A distributed control architecture can be used to reduce the computational complexity of the optimization problem in model predictive controllers. In this method, the optimization problem is reformulated as several smaller optimization problems and each problem is solved separately. Dual decomposition [15] and the alternating direction method of multipliers (ADMM) [16] are two well-known methods in distributed control. An alternative method is called proximal ADMM [27], where a proximal term is added to the cost function of the dual problem and a result is the faster convergence toward the solution. However, these methods have been originally developed for the convex programming problems. Using these methods to solve a non-convex optimization problem may result in a suboptimal solution, because of a duality gap between primal and dual problems [15]. If the distributed generation units inside a microgrid have ON/OFF switching signals, the energy management system will face a non-convex optimization problem for power scheduling of the generation units and, hence, the conventional distributed control methods might be inefficient.

The control methods discussed so far in this chapter are based on defining the objective of the optimization problem in the MPC controller as the operational cost of the system. However, an alternative approach is to define the objective of the optimization problem as the regret of the decision maker. To the author's best knowledge, there is not any reference on defining the regret in energy management systems. In the field of operations research, the regret of a decision maker is defined in [12]. Here, by the regret, we mean the difference between the best possible performance of the system and the actual system performance. While in a conventional min-max control approach, the objective is to minimize the worst-case operational cost, in the min-max-regret approach the objective is to minimize the biggest possible regret of a decision maker. In [20], the possible advantages of considering the regret over the operational cost are considered for a travel choice problem, where the decision makers, i.e., travelers, can choose either a route with risky travel time or wait for more information to select the fastest route. The authors in [20] show that a decision maker with regret minimization approach can reach a better solution by waiting for extra information to select the fastest route, while using an approach to minimize the operational cost results in making the decision too early, choosing slower route, and, hence, an increase in the final operational cost. Note that in [20]

the travel time is an important factor in determining the operational cost. The interested reader is referred to [2] and the references therein for a review on min-max and min-max regret approaches for optimization problems with uncertainties.

2.4 Conclusions

For the CaPP system, we need a suitable energy management system that is able to schedule the power generation of fuel cell cars in the presence of physical constraints and uncertainties in the microgrid's load or the number of cars connected to the microgrid. Min-max MPC has already been used to solve similar problems. However, the current min-max MPC methods have to be modified in order to be suitable for the application of the CaPP system. In addition, a drawback of the current min-max MPC methods is the high level of conservatism. In this thesis, we aim to develop a min-max MPC strategy that is suitable for the CaPP system. In addition, we develop a disturbance feedback min-max MPC approach for the CaPP system that has a lower level of conservatism compared to the conventional min-max methods. As will be shown in the next chapters, the optimization problem of the MPC controller for the CaPP system is not convex and in order to obtain the advantages of a distributed control approach, we need to modify currently distributed control methods to make those suitable for the CaPP system. Finally, we propose an alternative approach for solving the power scheduling problem by considering the regret of a human operator. The regret of a decision maker in energy management systems is not defined yet. In this thesis, in addition to defining the regret for the CaPP system, we create an MPC controller that minimizes the regret of the operator of the CaPP system.

3 Hydrogen-Based Integrated Energy and Transport System

In this chapter, we analyze the Car as Power Plant (CaPP) system from three different perspectives. To this end, the city of Hamburg in the year 2050 is considered as a case study. In the first part of this chapter, the techno-economic analysis of the CaPP system is presented. The second part is dedicated to the design of a control system for the operation of fuel cell cars inside the CaPP system, and the last part presents the results of our analysis from a socio-technical point of view. The aim of this chapter is to illustrate different methods for analyzing the emergence and operation of a CaPP system.

The research presented in this chapter is a joint work with other researchers and has been published in [31].

3.1 Introduction

Emphasizing the necessity of developing richer interdisciplinary research on future energy systems, our aim in this chapter is to provide a single comprehensive framework from different perspectives for designing a complex socio-technical system that we call car as power plant. We show that technical, economic, operational, and social aspects are necessary ingredients to obtain a complete understanding of the system [18]. The emphasis is on the fact that the system design and the operation are deeply intertwined. We will show that a stand-alone technical, economic, or social analysis can be incomplete without considering the two other aspects. To this end, we introduce a fully renewable energy system for a smart city in 2050, inspired by the city of Hamburg in Germany, and perform a comprehensive analysis based on technical, economic, operational, and social properties. We have chosen the year

2050 to show that the European Union's ambition towards a carbon-free energy transition in 2050 is indeed realizable.

The rest of this chapter is organized as follows. Section 3.2 describes the future energy system in the city of Hamburg, including all the components we consider in the design. Section 3.3 is dedicated to the techno-economic analysis of the described system to achieve a 100% renewable and self-sufficient energy system. Section 3.4 summarizes the control strategies that are applied to minimize the fuel consumption in the FCEVs while guaranteeing the supply-demand balance. In Section 3.5, we perform the optimal scheduling from a socio-technical point of view taking into account the different contracts between the agents in the system. Section 3.6 concludes the chapter.

3.2 System description

The smart city used as an illustrative example for 2050 is designed in such a way that it fulfills the following design requirements: 1) energy and transport systems use only electricity and hydrogen as energy carriers and are all electric in end use; 2) the city uses only hydrogen as seasonal energy storage and as fuel to power all road transport vehicles; 3) the smart city architecture can be extended to a network of multiple smart city areas and renewable hydrogen and electric energy hubs or centers [8, 60]; 4) the smart city can be integrated into existing infrastructure and buildings; 5) the operation of the smart city is not dependent on an in-urban area underground hydrogen pipeline transport network; 6) the smart city uses abundant renewable energy sources in Europe: local solar and large scale wind only; 7) the smart city is independent of natural gas and district heating grids.

The size of the hydrogen-based integrated energy and transport system in the smart city area for this study is determined by using the dispersion of supermarkets and petrol stations in Europe and Germany. Accordingly, we selected 2000 households since for every 2000 households there is a medium-sized supermarket and one petrol station [28]. On average 2000 households in Germany correspond to 4210 people, with in total 2330 passenger cars and 140 other vehicles, according to German national statistical data [28, 30]. Note that these numbers may vary in 2050 based on the societal profile and social behaviors at that time. The floor area of residential and services buildings is derived from national statistical data and scaled to 2000 households. An average dwelling has a floor area of 92m^2. Residential and service sector roofs are used for solar electricity systems and for rainwater collection. Solar electricity systems are installed on roof areas: 9m^2 per person on residential buildings and 4m^2 per person on service sector buildings area [65].

Figure 3.1 illustrates the energy system in the smart city and its key components. Based on [65], hydrogen is produced within the urban areas from local surplus solar energy and from shared large-scale wind energy. Hydrogen is transported via tube trailers from the urban areas to hydrogen fueling stations, to other hydrogen hubs/-

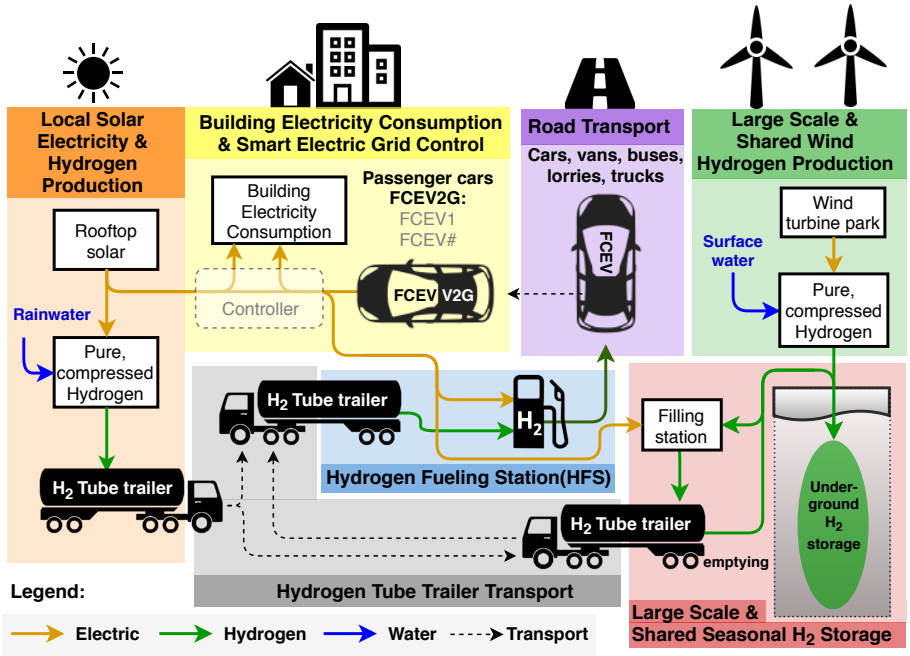

Figure 3.1: Hydrogen-based integrated energy and transport system and its key elements.

consumers, or to the large-scale and shared underground seasonal hydrogen storage [17]. Even though an underground hydrogen pipeline can also be used, we consider the tube trailers for the sake of minimizing the investment costs. The whole system has the following 7 major elements (see Figure 3.1):

1. Local solar electricity and hydrogen production: local rooftop solar electricity and rainwater collection, purification, and storage systems produce solar electricity and pure water both for the building consumption and for hydrogen production.

2. Building electricity consumption and smart electric grid control: the smart electric grid has a centralized controller, that manages all buildings, grid connected fuel cell electric vehicles (FCEVs), hydrogen fueling station, solar electricity and hydrogen production, and the tube trailer filling station at the seasonal hydrogen storage. Any shortage of electricity is met by the electricity produced from hydrogen through parked and "Vehicle-to-Grid" (V2G) connected fuel cell electric vehicles (FCEV2G).

3. Hydrogen tube trailer transport: tube trailers towed by tube trailer tractors transport hydrogen from either the local solar hydrogen production or the seasonal hydrogen storage to the hydrogen fueling station or from the local solar hydrogen production to the seasonal hydrogen storage.

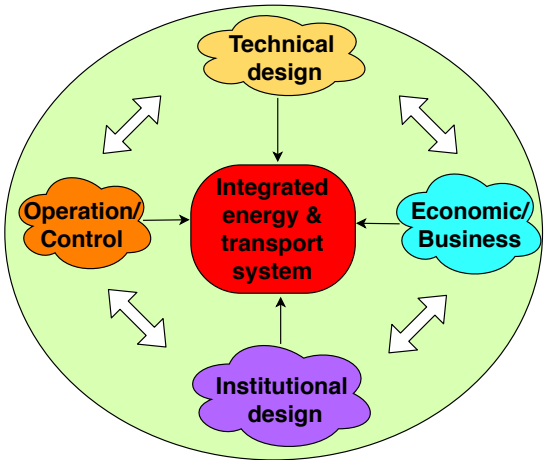

Figure 3.2: Analysis framework for the design of the future smart city area.

4. Hydrogen fueling stations: the FCEVs can be refilled at these stations.

5. Road transport: a fleet of road transport FCEVs including passenger cars, vans, buses, lorries, and trucks.

6. Large-scale and shared wind hydrogen production: an off-site large-scale wind turbine park is shared with other smart city areas and renewable hydrogen hubs or centers. All wind electricity is used with purified water for hydrogen production, which can be stored in a large-scale seasonal hydrogen storage.

7. Large-scale and shared seasonal hydrogen storage: underground salt caverns can be used for large-scale hydrogen storage.

To design a smart city based on the CaPP concept, we propose an analysis framework (cf. Figure 3.2) combining four perspectives: technical, economic, operational including control, and institutional perspective. In the following sections, we show how these perspectives can be combined to obtain a complete system design.

3.3 Techno-economic analysis

In this section, the techno-economic analysis of the considered smart city is presented. Our approach is based on: 1) technological and economical characterization for the system components; 2) hourly simulation of all energy flows and technical sizing of the system components; 3) cost of energy calculated based on the sizing and economic characterization of the system components.

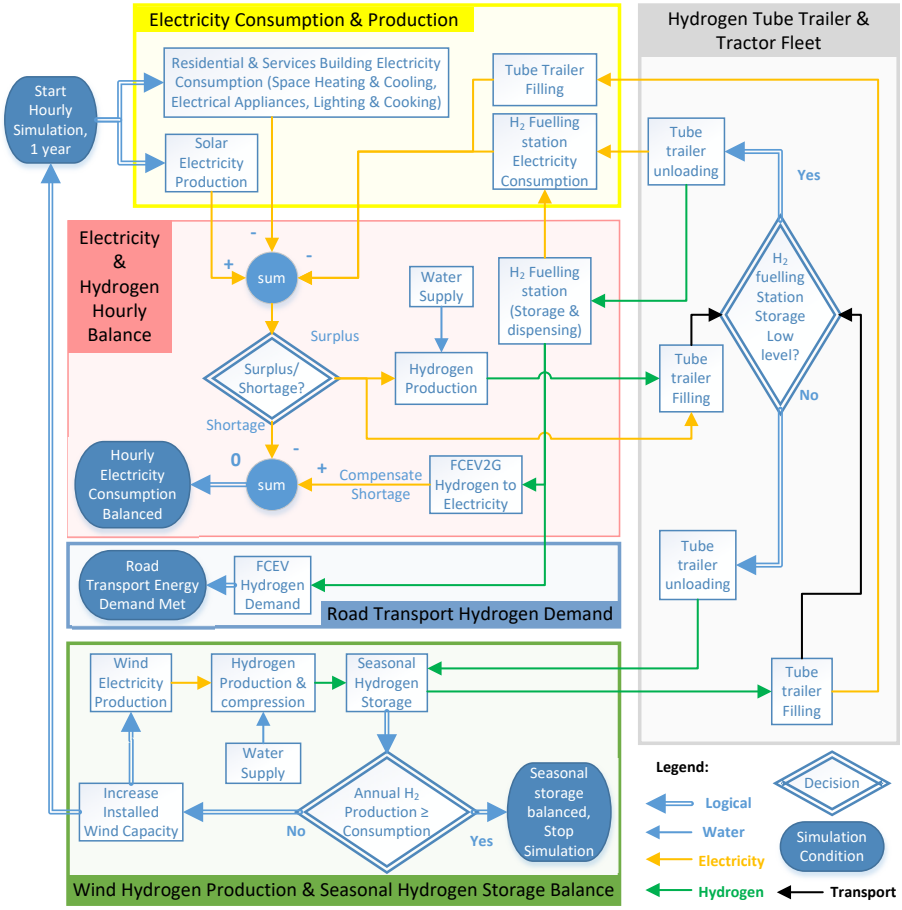

Figure 3.3: Simplified hourly simulation scheme for a hydrogen-based integrated energy and transport system.

3.3.1 A heuristic model for the CaPP system

Figure 3.3 displays the simplified simulation scheme of the system. We know that the hourly electricity and hydrogen balance has to be met, either by converting surplus electricity into hydrogen or converting stored hydrogen into electricity. The net consumed hydrogen from the seasonal hydrogen storage in underground salt caverns needs to be zero on a yearly basis. The hourly simulation is done for the entire year 2014 to size the system components in such a way that there is no curtailment of electricity.

Figure 3.3 shows the hourly simulation scheme to investigate the system state in 2050. The yellow rectangle at the top includes the services and residential buildings, hydrogen fueling station, seasonal hydrogen storage electricity consumption, and

solar electricity production. The hourly electricity consumption profile of the all-electric residential and services sector buildings includes space heating and cooling, hot water, lighting, cooking, and electrical appliances, and is based on the following inputs:

- National annual energy consumption data for hot water, lighting, cooking, and electrical appliances [28];
- Hourly normalized electricity and heating consumption profiles [64];
- Estimations on efficiency improvements in the year 2050, technology change (heat pumps), and energy reduction [65];
- Relations for determining space heating and cooling demand in buildings based on the heating and cooling data [21, 24, 1] derived from local air temperature logs [26, 74] and the European heating and cooling index [76, 94, 46, 47];

Hourly hydrogen consumption for transport (blue, in Figure 3.3) of the passenger cars, vans, buses and trucks is based on the German national annual driving data [54, 55], the estimated fuel economy in 2050 [65], and a repeating weekly fueling profile.

3.3.2 Cost of energy

We applied the cost calculation methods described in [65] in which the different economic lifetimes, operation, and maintenance costs of the various components and a weighted average cost of capital of 3% [45], are taken into account. The Total Cost (TC) of the hydrogen-based integrated energy and transport system in this smart city in k€/year is the sum of the total annual Capital Costs (CC) and the Operation and Maintenance Costs (OMC) of the individual subsystems. The Levelized Cost of Energy of electricity ($LCoE_e$) from wind and solar does not include the energy storage; therefore, the System Levelized Cost of Energy (SLCoE) is introduced [65]. The SLCoE is built up from the cost of energy for electricity consumption in buildings $SLCoE_e$ (€/kWh) and the hydrogen consumption for driving $SLCoE_H$ (€/kg H_2). SLCoE can be calculated by allocating a share of the total cost of the smart city area energy system [65].

3.3.3 Simulation of the CaPP system using a heuristic approach

Energy balance

Based on the hourly simulation, the annual energy balance is defined and presented in Figure 3.4.

When analyzing the annual system behavior, we investigated production and transport of hydrogen and the seasonal and tube-trailer hydrogen storage, see Figure 3.4(a). In the period October-March, the hydrogen consumption is higher than the

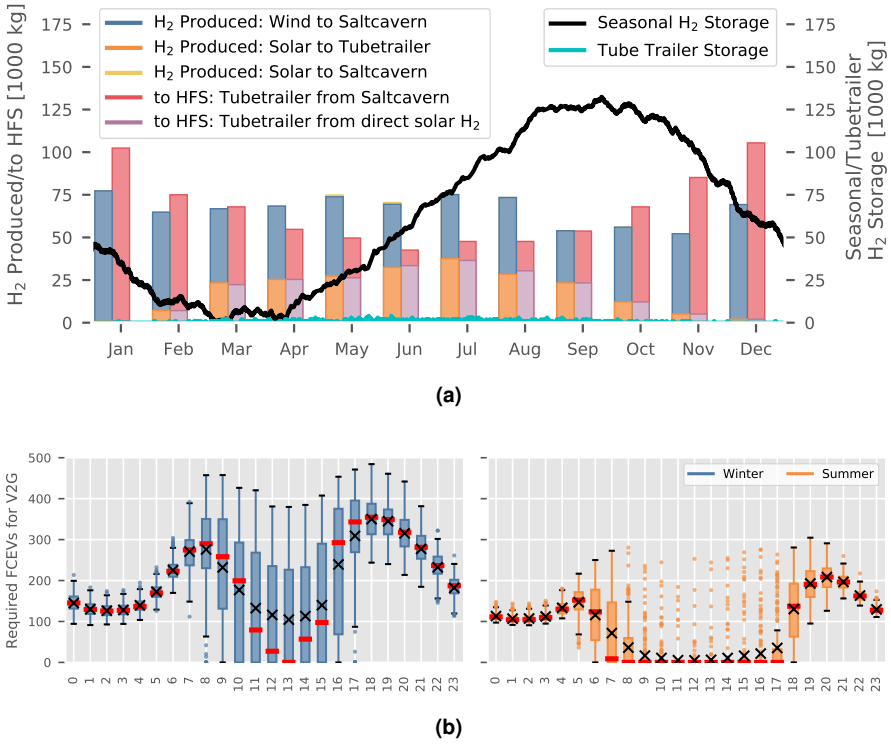

Figure 3.4: (a) Hydrogen production and transport (left axis) and seasonal and tube trailer hydrogen storage (right axis), (b) FCEV2G operation during winter (left) and summer (right) period per hour of the day.

production and the majority of the hydrogen production comes from wind. From April to September the hydrogen consumption is lower than the production due to increasing solar energy and reduced building electricity consumption, resulting in more stored hydrogen. For the entire year, all hydrogen from solar surplus electricity is going to the hydrogen fueling station, except that in May and June approximately 2000 kg is stored in the underground storage (see also Figure 3.5).

In Figure 3.4(b), the FCEV2G power demand over the winter (left) and summer (right, days 91-274 of the year) period is displayed for every hour of the day in box plots (based on a normal distribution). Dots indicate outliers. Daily averages and medians are respectively displayed as black x marks and red horizontal lines in the bars. The annual peak of 485 cars (21%) occurs during winter at 18h. During the night hours (23h-4h), on average between 100-200 cars are required (4-9%). Around 4h FCEV demand starts rising to an average of 280 (12%) at 8h in winter and 150 (6%) at 5h in summer. At these morning peak hours, solar electricity starts covering the daytime electricity demand. In winter, the average minimum for the number of cars is 105 (5%) at 13h and in summer it is less than 25 cars (1%) from 9h-16h. The

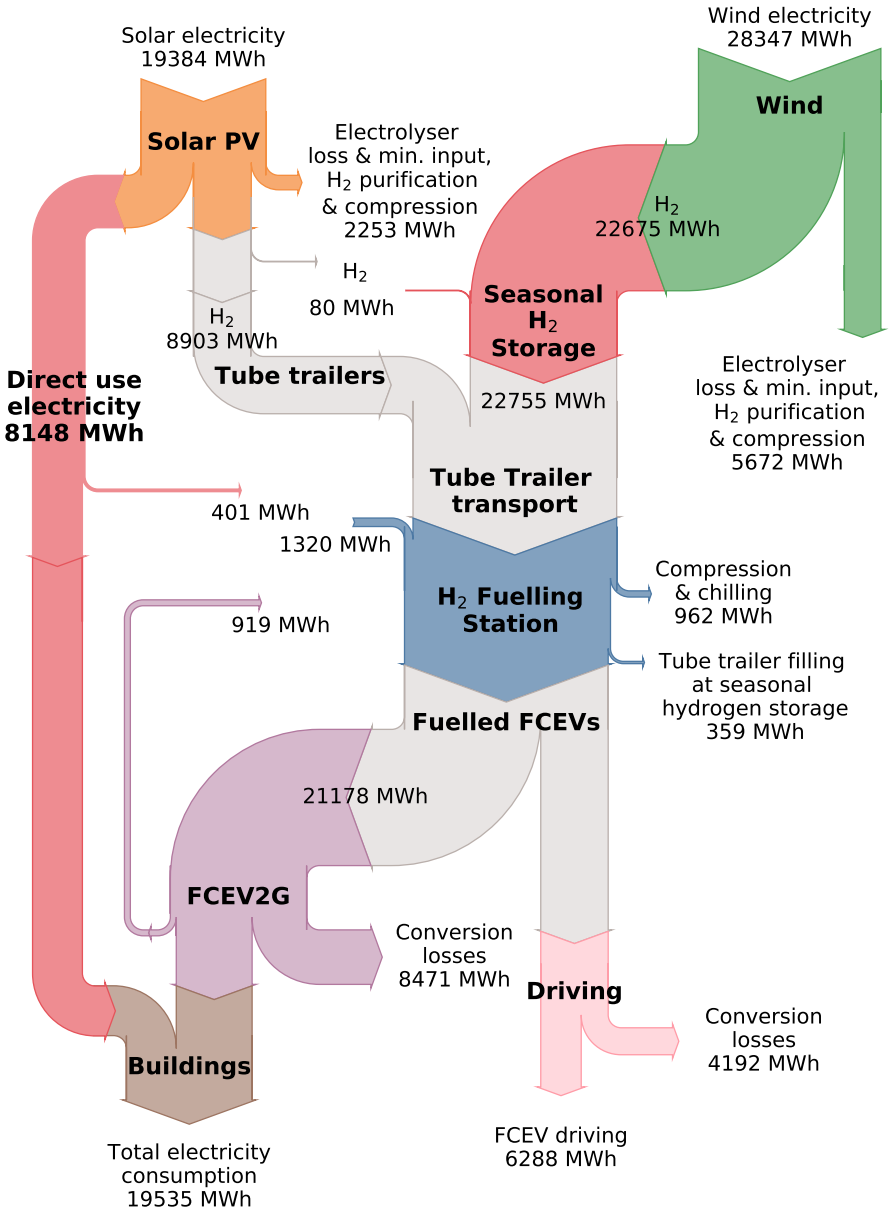

Figure 3.5: Annual energy balance for a 2050 fully renewable electricity, heating and road transport system for the city of Hamburg.

average evening peak is 350 cars (15%) at 18h in winter and 210 cars (9%) at 20h in summer. Relatively more cars are needed during morning and evening hours. Also, some cars are likely to be used for driving and not available for power production

Table 3.1: Calculated capital (CC), operation & maintenance (OMC), and total costs (TC) for the subsystems in the smart city area.

Subsystems	CC [k€/yr]	OMC [k€/yr]	TC [k€/yr]
Solar Electricity	406	199	605
Solar H_2 Production	273	70	343
Wind Electricity	360	226	586
Wind H_2 Production	142	89	231
Hydrogen Fueling Station	352	63	416
Seasonal H_2 Storage	259	11	270
H_2 Tube Trailers Transport	143	151	293
FCEV2G, Smart Grid, & Control	268	72	341
Total System Cost of Energy	2,204	881	3,085

in the CaPP system, but on average this is still less than 15% of the cars. In the calculation of the V2G power production we used 10 kW output per car, i.e., only 10% of the rated fuel cell power.

Cost analysis

Before we analyze the operation of the CaPP system, an analysis of the economic feasibility is presented. Table 3.1 shows the aggregated results of the cost of the subsystems and components as presented in Figure 3.1.

The Total Cost (TC) of the smart city area energy system is 3085 k€/year and it is the sum of the total annual Capital Costs (CC) of 2204 k€/year and the Operation and Maintenance Costs (OMC) of 881 k€/year of the individual subsystems. The $LCoE_e$ from wind and solar is respectively 0.03 €/kWh and 0.02 €/kWh. The $SLCoE_e$ is 0.11 €/kWh and the $SLCoE_H$ of 3.3 €/kg H_2. These values are comparable with other fully renewable future integrated energy systems [45].

3.4 Optimal scheduling of power generation of fuel cell cars

Promising conclusions from the techno-economic feasibility lead us to the question how the fuel cell cars can be used efficiently for power balancing of the smart city area. To this end, we further adjust the model of the hydrogen-based integrated energy and transport system to make it suitable to be controlled by a model predictive controller.

We assume that the energy management system is responsible for maintaining the power balance of the integrated energy and transport system in a smart city area. By using the historical data of the load and of the solar photo voltaic (PV) cells'

power generation, we can predict the residual load of the smart city area at any time step k, $P_{\mathrm{res}}(k)$, i.e., the actual load subtracted by the power generation of the PV cells. If the residual load has a negative sign, this indicates that the total power generation of the PV system is larger than the load; the excess of power is used in an electrolyzer and so the power balance is maintained. In the case that the load is larger than the power generation of PV systems, the total power generation of fuel cell cars should be equal to the residual load of the smart city area to maintain the power balance constraint. The task of the control system is to determine the power generation profile of each fuel cell car such that the power balance of the smart city area is always maintained, while the operational cost of the system is minimized. The aim of the control system is to minimize the FCEV2G, Smart Grid, & Control cost from Table 3.1.

3.4.1 Discrete-time model of the CaPP system

In this section, we present a discrete-time model for the system, where the sampling time is indicated by T_{s}. The fuel levels of the fuel cell cars, $x_{\mathrm{f},i}$, for $i \in \mathcal{I}$, are considered as the system states, where $\mathcal{I} = \{1, \ldots, N_{\mathrm{veh}}\}$ indicates the index set of all cars. Here, N_{veh} is the number of fuel cell cars. In the following cases, the fuel level of car i changes:

- Power generation mode: if the generated power at time step k is $u_{\mathrm{f},i}(k)$, the fuel level is decreased by $\alpha_i u_{\mathrm{f},i}(k) + \beta_i$, where α_i and β_i are two constant parameters that can be determined from the specifications of the fuel cell stack of car i.
- Refueling mode: fuel cell car i is refilled at step k if the binary refueling signal, $s_{\mathrm{r},i}(k)$, is equal to 1. In this case, the fuel level of that car will be at its maximum level, $\bar{x}_{\mathrm{f},i}$, at the next time step. Note that this criterion requires a large enough (larger than 15 min) time step.
- Transportation mode: if car i is used for transportation at time step k, then the fuel level of that car is reduced by a predetermined value $\gamma_i(k)$. The value of $\gamma_i(k)$ can be predicted by using the historical data of the driving patterns of car i. If the car is not in transportation mode at time step k, then $\gamma_i(k) = 0$.

Given the above operational modes for a fuel cell car, the evolution of the system states can be written as

$$\begin{aligned} x_{\mathrm{f},i}(k+1) =& x_{\mathrm{f},i}(k) - s_{\mathrm{f},i}(k)\left(\alpha_i u_{\mathrm{f},i}(k) + \beta_i\right) T_{\mathrm{s}} \\ &+ s_{\mathrm{r},i}(k)\left(\bar{x}_{\mathrm{f},i} - x_{\mathrm{f},i}(k)\right) - \gamma_i(k). \end{aligned} \tag{3.1}$$

In (3.1), $s_{\mathrm{f},i}(k)$ is a binary variable that indicates the on/off operational mode of fuel cell i at time step k. The maximum capacity of fuel in car i is denoted by $\bar{x}_{\mathrm{f},i}$. The vector of control inputs related to fuel cell car i, is represented by u_i and it is defined as $u_i(k) = \left[u_{\mathrm{f},i}(k)\ s_{\mathrm{f},i}(k)\ s_{\mathrm{r},i}(k)\right]^T$.

Another state of the system is $x_{\mathrm{s}}(k)$, the total amount of hydrogen that is present inside the smart city at time step k. The process of producing hydrogen is related to the power generation of renewable energy sources. Therefore, it is possible to determine the amount of hydrogen, $h_{\mathrm{s}}(k)$, that is added to the smart city area at time step k inside the prediction window. Therefore, we can write the following equation for the amount of stored hydrogen at each time step k:

$$x_{\mathrm{s}}(k+1) = x_{\mathrm{s}}(k) + h_{\mathrm{s}}(k) - \sum_{i \in \mathcal{I}} s_{\mathrm{r},i}(k) \left(\bar{x}_{\mathrm{f},i} - x_{\mathrm{f},i}(k) \right). \tag{3.2}$$

The last part of (3.2) indicates the amount of hydrogen used to refuel the fuel cell cars.

The operation of system is subjected to several constraints as follows:

- If a fuel cell is off then its total power generation is zero, i.e.,

$$\text{if } s_{\mathrm{f},i}(k) = 0 \text{ then } u_{\mathrm{f},i}(k) = 0. \tag{3.3}$$

- A fuel cell cannot be in both the refueling and the power generation modes at the same time, i.e.,

$$\text{if } s_{\mathrm{f},i}(k) = 1 \text{ then } s_{\mathrm{r},i}(k) = 0, \tag{3.4}$$
$$\text{if } s_{\mathrm{r},i}(k) = 1 \text{ then } s_{\mathrm{f},i}(k) = 0. \tag{3.5}$$

- If a car is used for the transportation, it cannot be connected to the smart city area's power network or be refueled. Therefore,

$$\text{if } \lambda_i(k) = 0 \text{ then } s_{\mathrm{f},i}(k) = s_{\mathrm{r},i}(k) = 0, \tag{3.6}$$

  where $\lambda_i(k)$ is a binary variable that represents the transportation mode of fuel cell car i at time step k. If $\lambda_i(k) = 1$, the car is available inside the smart city area for power generation. Conversely, if $\lambda_i(k) = 0$ the car is used in the transportation mode. We assume that the drivers announce the use of their cars for transportation and, hence, the value of $\lambda_i(k)$ can be predetermined for all i and k.

- The driver of each fuel cell car can set a minimum level, $\underline{x}_{\mathrm{f},i}$, on the remaining fuel of the car. In addition, there is a maximum fuel level, $\bar{x}_{\mathrm{f},i}$, for each car. Therefore,

$$\underline{x}_{\mathrm{f},i} \leq x_{\mathrm{f},i}(k) \leq \bar{x}_{\mathrm{f},i}. \tag{3.7}$$

- If the residual load of the smart city area is lower than zero, the power balance of the smart city area is maintained by the operation of the electrolyzer. In the case that the residual load is more than zero, the total power generation of fuel cell cars should be equal to the residual load of the smart city area, at

each time step k. In other words, if we define $P_{\mathrm{d}}(k) = \max\{0,\ P_{\mathrm{res}}(k)\}$, we require the following constraint:

$$\sum_{i \in \mathcal{I}} u_{\mathrm{f},i}(k) = P_{\mathrm{d}}(k). \tag{3.8}$$

By adopting a similar procedure as in [3], Equations (3.1)-(3.2) together with the constraints in (3.3)-(3.8) can be rewritten as a so-called mixed logical dynamical model of the form

$$\begin{aligned} &x(k+1) = x(k) + B_1 u(k) + B_2 z(k) + B_3(k) \\ &E_1 u(k) + E_4 x(k) + E_5 \geq E_3 z(k). \end{aligned} \tag{3.9}$$

In (3.9), $x(k)$ and $u(k)$ are the system states and the control inputs and are defined as $x(k) = \left[x_1^T(k)\ \ldots\ x_{N_{\mathrm{veh}}}^T(k)\ x_{\mathrm{s}}(k)\right]^T$ and $u(k) = \left[u_1^T(k)\ \ldots\ u_{N_{\mathrm{veh}}}^T(k)\right]^T$, respectively, and $z(k)$ is a vector of auxiliary variables. The interested reader is referred to Chapters 4 and 5 for more details on how to derive such a mixed logical dynamical model.

The operational cost of a fuel cell car consists mainly of two factors. The first factor is the degradation of the fuel cell stack; here, switching the operation mode and the power generation of a fuel cell are considered to be the two important causes of degradation. The second factor is the fuel consumed inside the car, which is an affine function of the generated power. Therefore, the total cost function of the system is

$$J(k) = \sum_{i \in \mathcal{I}} \sum_{j \in \mathcal{J}} W_{\mathrm{s},i} |\Delta s_{\mathrm{f},i}(k+j)| + W_{1,i} u_{\mathrm{f},i}(k+j) + W_{0,i} s_{\mathrm{f},i}(k+j), \tag{3.10}$$

where $\mathcal{J} = \{0,\ \ldots\ N_{\mathrm{p}} - 1\}$, N_{p} is the prediction horizon, and $W_{\mathrm{s},i}$, $W_{1,i}$, and $W_{0,i}$ are three constant coefficients related to fuel cell car i that represent the cost of switching the operation mode, the cost of power generation, and the cost of standby mode operation, respectively. In (3.10), the value of $\Delta s_{\mathrm{f},i}(k+j)$ indicates the difference in the value of $s_{\mathrm{f},i}$ in two consecutive time steps as

$$\Delta s_{\mathrm{f},i}(k+j) = s_{\mathrm{f},i}(k+j) - s_{\mathrm{f},i}(k+j-1),$$

which represents the switching on and off of the fuel cell.

3.4.2 Optimization problem of model predictive controller

The vector of optimization variables, $\tilde{V}(k)$, has to be determined at time step k and this vector is defined as follows:

$$\tilde{V}(k) = \left[\tilde{u}^T(k)\ \tilde{x}^T(k)\ \tilde{z}^T(k)\right]^T, \tag{3.11}$$

where a tilde notation over a variable means the stacked version of that variable over the prediction window. For example, $\tilde{u}(k)$ is defined as

$$\tilde{u}(k) = \left[u^T(k)\ u^T(k+1)\ \dots\ u^T(k+N_\mathrm{p}-1)\right]^T.$$

By adding some extra auxiliary variables to $\tilde{z}(k)$ in (3.11) and by defining a vector c in an appropriate way, we can rewrite the cost function (3.10) as $J(k) = c^T\tilde{V}(k)$. In addition, we can define the matrix A and the vector b such that the constraints in (3.9) for all the time steps in the prediction window can be expressed as $A\tilde{V}(k) \leq b$. Hence, the optimization problem of the model predictive controller at time step k can be written as

$$\begin{aligned} &\min_{\tilde{V}(k)}\ c^T\tilde{V}(k) \\ &\text{subject to } A\tilde{V}(k) \leq b \end{aligned} \tag{3.12}$$

The vector of optimization variables $\tilde{V}(k)$ in (3.12) includes both continuous variables, such as the amount of power generation for each fuel cell car, and binary variables, such as the refilling commands for the fuel cell cars. Therefore, the optimization problem (3.12) is a mixed integer linear programming problem and can be solved by the standard solvers such as CPLEX [23] or Gurobi [39].

3.4.3 Simulation of the CaPP system using model predictive control

Assumptions in the model predictive control approach

We have considered 2300 fuel cell cars inside the system, where the parameters α_i and β_i in (3.1) are randomly chosen from a uniform distribution in an interval $[0.03, 0.05]$ kg/kWh for α_i and an interval $[0.001, 0.009]$ kg/h for β_i for all $i \in \mathcal{I}$. The maximum power generation of each fuel cell car, $\bar{u}_{\mathrm{f},i}$ for all $i \in \mathcal{I}$, is assumed to be 10 kW.

The maximum capacity of hydrogen tank in each car, $\bar{x}_{\mathrm{f},i}$ for all $i \in \mathcal{I}$, is set to be 6.5 kg. In addition, we assume that the minimum level of fuel for the power generation mode, $\underline{x}_{\mathrm{f},i}$ for all $i \in \mathcal{I}$, is 1.5 kg. The sampling time of the system, T_s, is assumed to be 1 hour. As the required time for the refueling process of the cars is less than a single time step and by following the standard tuning rule in MPC [33], we have selected the prediction horizon, N_p, equal to 4 in order to cover the most important dynamics of the system. The values of $W_{\mathrm{s},i}$, $W_{1,i}$, and $W_{0,i}$ are randomly chosen from a uniform distribution in the interval of $[0.5, 1.5]$.

Results

The operation of a smart city area with the specifications described in Section 3.2 is simulated for a time span of a year. The computation time required to solve the optimization problem (3.12) in general grows exponentially when the size of the problem increases. In our case, it is impractical to solve problem (3.12) for 2300 cars

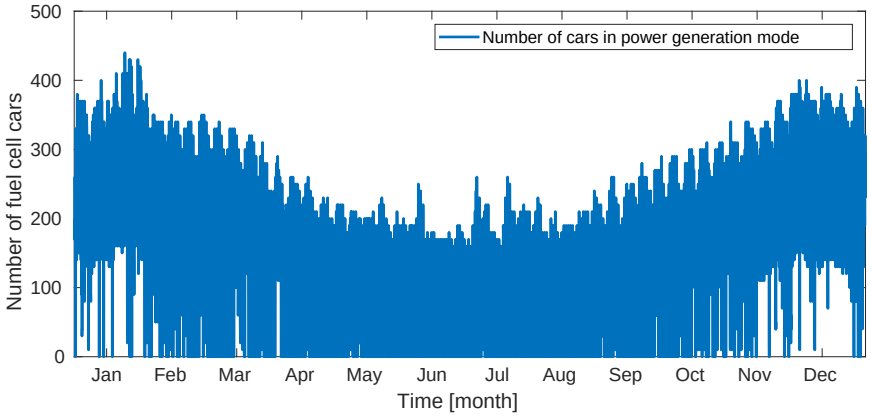

Figure 3.6: Number of cars in the power generation mode during one year.

with a normal personal computer. There are generally two approaches to decrease the computation time and to make the problem tractable. The first approach is to use a distributed control architecture, see, e.g., [96]. The second approach is to adopt a decentralized control architecture where the overall system is decomposed into several subsystems and each subsystem has its own control system that is not dependent to other subsystems.

In our study, we use the latter approach, as it has the advantage of simplicity. We consider 10 subsystems, where each subsystem consists of 230 fuel cell cars. In order to maintain the power balance condition of the smart city area, each subsystem is assigned to generate one tenth of the total residual load of the smart city area. As a result, the computation time is decreased significantly. In a Linux machine with Intel Xeon CPU with 3.7 GHz clock speed and 16 GB of RAM memory, it takes on average about 0.46 second to solve the optimization problem of each time step. Considering the time step of 1 hour, the optimization problems are thus solved fast enough for a real-time application.

The obtained results show that, in general, the amount of stored hydrogen is increasing during the spring and summer, while in the fall and winter the amount of stored hydrogen decreases, which confirms the results of Figure 3.4(a). Also the simulation results illustrated in Figure 3.6 show that the total number of cars that are used in the power generation mode is lower in the spring and summer compared to the other times of the year, which confirms the results of Section 3.3.

3.5 Institutional analysis

In order to have a complete design and operational system, we need to consider social aspects and interactions that influence such system. From a socio-technical system perspective, we view the smart city area as the combination of physical and

social subsystems [71]. In this view, the actors in the social subsystem make decisions or take actions that influence the operation of the physical system. The use of an FCEV as a power plant, thus, depends on both the driver (to make the car available) and the aggregator (to start-up the car), which then, calls for new institutions. To operate FCEVs while taking into account drivers' needs, we focus on the contractual relationship between drivers and the aggregator. We, then, use another modeling technique, i.e Agent-Based Modeling and Simulation (ABMS), and formalize the vehicle-to-grid contracts to show the role of contract parameters in the participation of drivers when supplying power to the smart city.

3.5.1 Vehicle-to-grid contracts

In [72] and [73], three contract types are conceptualized: price-based, volume-based, and control-based contracts. As the name indicates, in price-based contracts, a price signal is used to activate the V2G power from a vehicle. In volume-based contracts, the volume committed is used as a boundary condition. Finally, with control-based contracts, any connected vehicle may be used to support the system as long as there is enough fuel available for driving. Each contract type consists of parameters that define the availability and the conditions under which the aggregator may use the vehicle.

Based on the analyses of Sections 3.3 and 3.4, the number of vehicles needed at a certain hour is between 400 and 500 (cf. Figures 3.4(b) and 3.6). Therefore, the number of discharging points for V2G is set to 500. Considering the fact that the total number of FCEVs in the system is more than 2000 and only 500 connection points present in the system, we consider the use of control-based contracts with voluntary plug-in. We expect that there is need for a commitment of plug-in time and volume, since the limited discharging points would lead to unfulfilled contracts.

3.5.2 Agent-based model

As introduced above, we use agent-based modeling and simulation to explore the agents' actions and their effects on the aggregated vehicle availability and system performance. As shown in Figure 3.7, we create agents that represent actors in the social subsystem that own and operate components in the physical subsystem. Buildings produce electricity with PV panels for their own consumption and feed the excess to the grid. Together with the wind energy produced outside and transported to the smart city grid, the excess PV generation is used for hydrogen production. Drivers refill their FCEVs at the hydrogen fueling station. Whenever the PV generated in the buildings is not sufficient, FCEVs are used to supply V2G power. To manage the availability of FCEVs in the system for V2G, the drivers sign a control-based V2G contract with the aggregator. This defines when the vehicles will be plugged in, and to what extent the aggregator is allowed to use them.

In the rest of this section, the agent-based model is described in more detail.

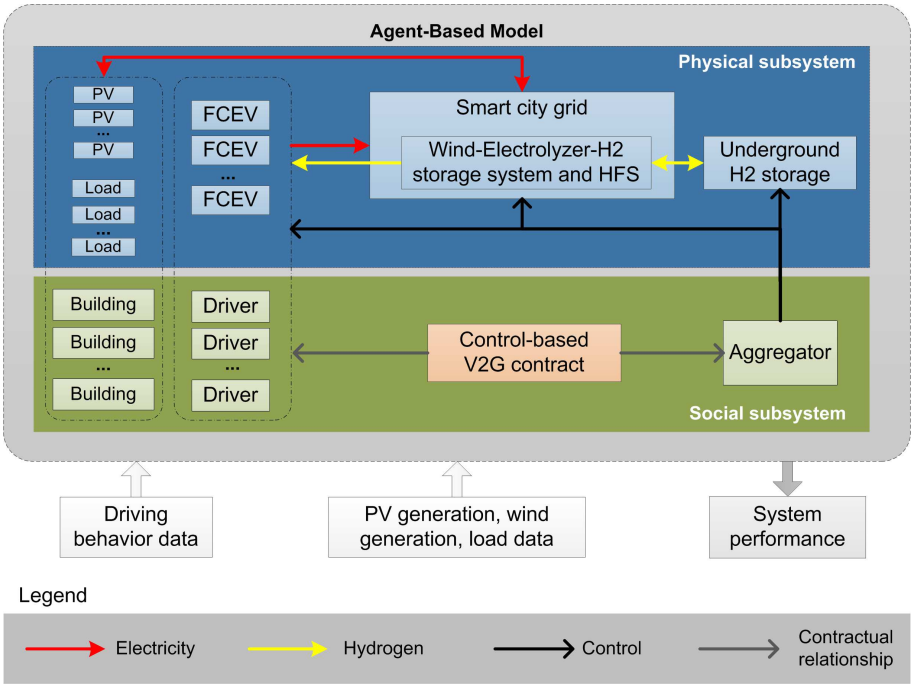

Figure 3.7: Agent-based model concepts.

Agents

Driver agent This agent type represents the characteristics of the driver as well as those of his/her car. The main states of the agent include the driving schedule (weekdays and weekends), the plug-in profile (either 'home' or 'work' hours), the fuel level, and the state of the vehicle (driving, refueling, plugged in, V2G). The driver agent also owns a control-based V2G contract that consists of the guaranteed fuel.

Building agent Commercial and retail buildings are represented as agents that consume and produce electricity with rooftop photovoltaic (PV) systems.

Aggregator agent The aggregator manages the supply and demand in the smart city. It owns an electrolyzer-hydrogen storage system (Hydrogen Fueling Station), used to produce hydrogen using electricity and to provide hydrogen to drivers. An underground hydrogen storage is also operated by the aggregator to exchange hydrogen in the case of surplus or shortage.

Process overview

The order in which actions take place in the simulation is depicted in Figure 3.8.

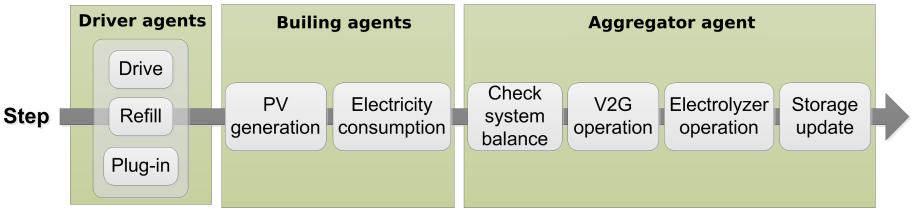

Figure 3.8: The order of taking actions in the agent-based simulation.

Driver agent Drivers follow their driving schedule to drive from home to work and vice versa. After arrival, drivers check the fuel level in their vehicle and decide to refill if it is low. Each driver has either a "home" or "work" plug-in profile that indicates whether he plugs in his vehicle when parked at home or at work.

Building agent Building objects have PV panels that produce electricity, either used for own consumption or to produce hydrogen when generated in excess.

Aggregator agent Every hour the aggregator checks the system balance and determines the residual demand. If needed, available FCEVs are used for V2G. Similarly as in [70, 71], we use a fair scheduling mechanism for the aggregator to operate available vehicles based on their total number of start-ups. Thus, available vehicles that have been used less frequently will be started up first. When there is a surplus solar generation from the buildings and whenever wind power is being generated, the electrolyzers are used to produce hydrogen. Finally, if the level of hydrogen stored in the fueling station is too low or too high, some amount of hydrogen is exchanged with the seasonal underground hydrogen storage.

Agent-based model assumptions

- Drivers live and work within the smart city.
- Drivers have constant driving schedules throughout the simulation.
- The use of dischargers for plugging in is based on a first-come first-serve rule.
- Once plugged in, cars are not disconnected until they leave for their next trip.
- Costs (of V2G, hydrogen production, etc.) are not considered in the contracts or to manage or use the vehicles.
- The electricity consumption in the buildings is considered as the only part of the electricity consumption in the smart city.

Table 3.2: Drivers' results: Average and standard deviation

	UD Scenario	LD Scenario
Plug-in time (h)	3203.8 (±1297)	1903.6 (±831)
V2G energy supplied (kWh)	5105.0 (±2929.1)	5105.0 (±3 188.6)
Start-ups	109.1 (±19.9)	114.9 (±25.0)

3.5.3 Simulation of the CaPP system using agent-based modeling

The properties of the 2300 driver agents are initialized as follows:

- Driving schedule: distribution derived from [19] (average 45 km/day).
- Plug-in profile: 50% of the drivers during work hours, 50% of the drivers during home hours.
- Initial fuel level (kg): random number from a uniform distribution in the interval [3.0,6.5].
- Guaranteed fuel in V2G contract: a minimum level of fuel for individual cars that is not used for V2G power generation.

For the PV, wind, electrolyzers and hydrogen storage, the same capacities as presented in Section 3.3 are used. At the beginning of the simulation, the hydrogen storage system is initialized at 50% of its capacity, and the underground storage is initialized at 50 000 kg. The efficiencies of the fuel cell and electrolyzers, as well as the fuel consumption of the FCEV are also the same as in Section 3.3.

Results

We have run an hourly simulation for a year for two scenarios: 1) Unlimited number of Discharging points (UD scenario) and 2) Limited number of Discharging points (LD scenario). The results in Table 3.2 show the difference in the average (and standard deviation) of the 2300 driver agents' results in terms of plug-in time, V2G power supplied, and number of start-ups at the end of a year.

While the number of discharging points does not influence the aggregate performance of vehicle-to-grid supply in the smart city, the differences between the UD and LD scenario indicate that the choice in the number of dischargers influences the participation of individual drivers, as the use of the dischargers follows a first-come first-serve rule. While more dischargers allow more equal opportunities for drivers, it also leads to a higher number of plug-in hours per driver. As can be seen in Table 3.2, more plug-in hours per driver are not necessary for the operation of the system, as the average V2G supply is the same.

Figure 3.9 shows the distribution of the number of start-ups per driver at the end of the year. In the UD scenario, there are around 2000 drivers with the same

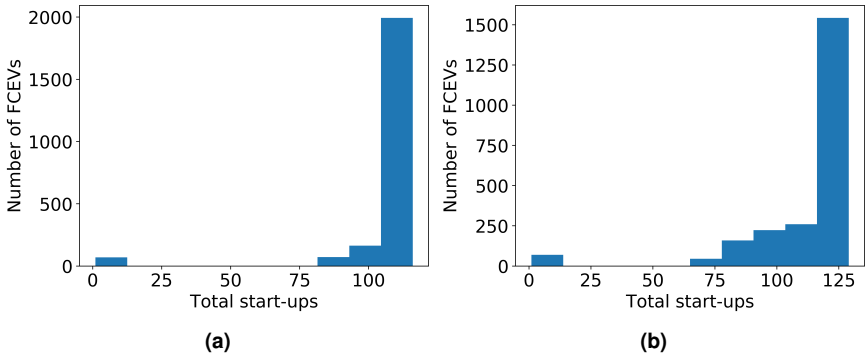

Figure 3.9: Distribution of the total number of start-ups per driver: (a) UD scenario; (b) LD scenario.

number of start-ups, while in the LD scenario the distribution is a bit more skewed. Therefore, while at the system level the performance may be the same, there are differences in the participation of drivers at the individual level. There are more equal opportunities for drivers in the UD scenario to provide V2G, as most of them (around 2000) reach the same number of start-ups at the end of the year. In the LD scenario, there are more drivers that have had fewer opportunities to participate due to the lack of free dischargers. A limited number of discharging points may be appropriate to reduce costs, but additional rules may be needed to provide more fair opportunities for drivers to sell power.

Remark 3.5.1. The results of this section are based on the assumption that the actors are willing to participate based on the agreed contract. However, to implement and make such system operational, policy intervention is required to ensure the fair chances of actors (FCEV owners, grid operators, energy companies, etc.). These policies need to be desinged for infrastructure, energy, and mobility sectors such that they facilitate this system to be technically implementable and to regulate the V2G remuneration.

3.6 Conclusions

In this chapter, we have presented an overview of a hydrogen-based integrated energy and transport system that we call Car as Power Plant (CaPP). Such a complex socio-technical system has a large network of players involved in developing and operating the technical infrastructure and physical components. To illustrate the CaPP system, we designed a 100% renewable integrated energy and transport system for a smart city area based on wind, solar, hydrogen, and fuel cell electric vehicles (FCEVs) inspired by the city of Hamburg in Germany in 2050. Using techno-economic analysis, we have shown that such a design is technically feasi-

ble. However, technical feasibility cannot be guaranteed without taking into account the operation and control of the system. So, the next challenge was to maintain the supply-demand balance as well as to minimize the operational costs of the FCEVs, which we have done by using advanced control techniques. We have also stressed that operation of such an innovative concept should be accompanied by an institutional analysis and designing an organizational system structure. To this end, we have studied the system behavior using different contracts between the system agents, namely the owners of FCEVs and the aggregators.

The future works include performing more extensive case studies to cover different geographical conditions, developing different control strategies for different type of contracts with the owner of the cars, and refining the agent-based simulation to consider the CaPP system with more details.

4

Fuel cell cars in a microgrid for synergies between hydrogen and electricity networks

In the rest of this thesis, we focus more on the control algorithms of the energy management system that is described in Chapter 3. In this chapter, we present an analysis of a community microgrid with photovoltaic systems, wind turbines, and fuel cell electric vehicles that are used to provide vehicle-to-grid power when renewable power generation is scarce. Excess renewable power generation is used to produce hydrogen, which is stored in a refilling station. A central control system is designed to operate the system in such a way that the operational costs are minimized. To this end, a hybrid model for the system is derived, in which both the characteristics of the fuel cell vehicles and their travel schedules are considered. The operational costs of the system are formulated considering the presence of uncertainty in the prediction of the load and renewable energy generation. A robust min-max model predictive control scheme is developed to minimize operational cost and adhere to operational constraints in the presence of such uncertainty. Finally, a case study illustrates the performance of the designed system.

The research presented in this chapter has been published in [3].

4.1 Introduction

The Car as Power Plant (CaPP) concept can be implemented in different settings and for different types of applications. When applied in a parking lot, a large fleet of parked cars can be used to provide power to the grid through an aggregator that sells power on behalf of the drivers. In residential microgrid settings, residents of the neighborhood can use their Fuel Cell Electric Vehicles (FCEVs) to provide power to the local grid at times of low renewable power generation. In buildings with high

electricity and heat demand, such as hospitals, the CaPP system can be implemented not only to use the electricity and heat from vehicles, but also to provide a large back-up capacity to the building.

In the current chapter, we explore the possible synergies between hydrogen and electricity networks using the residential microgrid CaPP case. We consider a residential microgrid with distributed generators that are used to serve local loads and to produce hydrogen, which acts as energy storage medium. This gaseous fuel is used by cars to drive, and additionally, it can be used to generate power when renewable power sources are scarce. This system is studied from the operational control perspective, as operational control is one of the main challenges in the implementation of microgrids [67].

The contributions of this chapter are as follows: a model is developed that describes the power generation of the fuel cell cars while the transportation aspect of the cars is taken into account. Further, a unified model is derived that describes the economic dispatch problem of a microgrid including a fleet of fuel cell cars, a water electrolysis system, and Renewable Energy Sources (RES) in the form of wind turbines and solar Photo Voltaic (PV) systems. A model predictive control scheme is developed to govern the system operation while the uncertainty in the prediction of the electrical load and power generation of RES is taken into account. The min-max optimization problem that arises in model predictive control is converted into a mixed integer linear programming problem. Realistic data for the behavior of drivers based on the survey of the Dutch Ministry of Infrastructure and renewable energy generation based on the Dutch weather data are used to illustrate the behavior of the system.

The rest of this chapter is organized as follows. In Section 4.2, we describe the CaPP microgrid system and the synergies in the CaPP microgrid are described in Section 4.3. In Section 4.4, the system model is developed. Section 4.5 develops an optimization problem for a min-max model predictive control system. In Section 4.6, a case study is simulated and, finally, Section 4.7 concludes the chapter.

4.2 Description of the system

A CaPP microgrid may consist of a group of residential loads, RES such as PV systems and wind turbines, some electrolyzers, and hydrogen storage systems. In this chapter, we consider a specific design of the microgrid as depicted in Figure 4.1. However, the control algorithm of this chapter can be easily adopted to different variations of the CaPP microgrid. In the CaPP microgrid of Figure 4.1, a centralized PV system and also a wind turbine are used to provide electricity to the households. When there is a surplus of renewable power generation, this surplus is used to produce hydrogen via electrolysis of water. The hydrogen produced is compressed and stored in a central storage tank, which is used as a refilling station for FCEVs. The FCEVs are used both for the transportation of residents of the neighborhood and

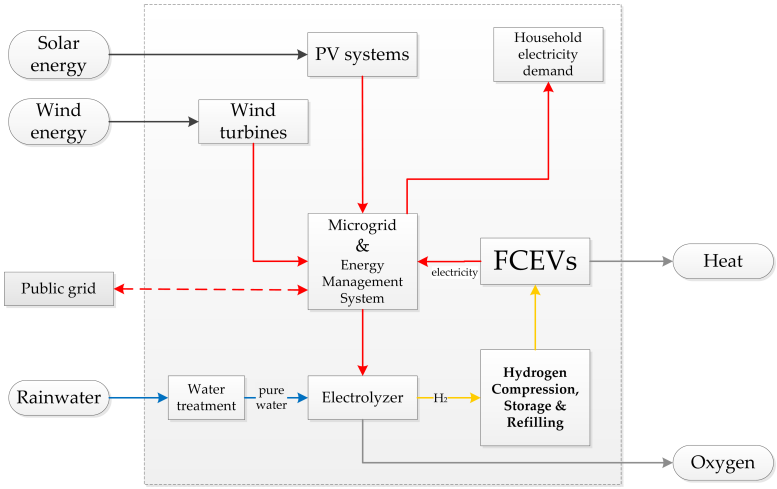

Figure 4.1: Schematic presentation of the CaPP microgrid system. Blue, yellow, and red arrows indicate the flow of water, hydrogen, and electrical power, respectively. The dashed red arrow indicate the bidirectional flow of electrical power between the public grid and the microgrid.

also for generation of electricity inside the neighborhood. The energy management system controls the flows of electricity and the scheduling of FCEVs as power plants.

A side product of generating electricity in each fuel cell stack is heat. In order to keep the temperature of the fuel cell stack inside the desired range, FCEVs are equipped with a relatively big radiator and cooling fans. We assume that in the stationary mode, when the FCEVs are used to generate electricity for the microgrid, the fuel cells are only operated at partial load. In other words, the maximum power generation of a fuel cell in the stationary mode would be a small fraction of its nominal power. As a result, the on-board devices of an FCEV would be still able to regulate the fuel cell's temperature, even at standstill. It is worth mentioning that the use of waste heat from the vehicles can be accommodated by heat exchange equipment as suggested by [52]. Others, like [56], reject this idea given the additional equipment needed and complexity involved, but this could be solved by centralizing the heat exchange system. However, in this chapter, we focus on the electrical power generated by the fuel cells. The use of the heat generated by fuel cells and its corresponding models are considered as topics for future research.

A common feature in most of the RES, such as wind and solar energy, is the variation in power generation due to fluctuations in the weather conditions. The CaPP concept brings the opportunity to create a microgrid system with RES and without wind and solar energy curtailment. We assume that the microgrid is connected to the power grid and that exchange of electrical power may happen in both directions. It is assumed that the cost of power exchange between the microgrid and the power grid is determined by the power grid operator. Based on the load and the generation profile of the other generation units in the power network, the power grid operator

may determine a reward for the microgrid to export power to the grid. However, in some other situations, the power grid operator may discourage the microgrid from exporting the power by determining a cost for the exported power. The presence of the fuel cell cars and of the water electrolysis system creates the flexibility for the microgrid to set the power exchange with the power grid in such a way that the maximum benefit is gained for the microgrid.

4.3 Synergies in the CaPP microgrid

The implementation of the CaPP microgrid system will be beneficial for the transportation system. The CaPP microgrid would provide FCEVs with renewable hydrogen, reducing not only the tailpipe emissions of the transportation system, but also the well-to-wheel emissions. In addition, such a microgrid will benefit from storage of excess renewable generation in the form of hydrogen, increasing the system's flexibility and capturing better the renewable generation potential. Finally, using FCEVs to provide power in the microgrid will increase the system's flexibility in power generation. When FCEVs are operated as power plants using hydrogen that was produced from renewable electricity, the overall carbon emissions linked to the electricity consumption in the microgrid will also be low. Without the vehicles in the microgrid, other dispatchable power plants, demand response, and storage should be used. Alternatively, electricity should be imported from the public grid at times of low or no renewable generation.

4.4 Modeling the CaPP microgrid

In this section, the CaPP microgrid system is modeled. To this end, first we develop a hybrid model that describes the behavior of the fuel cell cars and, next, with a similar approach, a hybrid model of the electrolysis system and of the hydrogen storage tank is developed.

4.4.1 Fuel cell cars model

The fuel cell cars are considered as controllable power generation units. We assume that the total number of cars in the microgrid is equal to N_{veh}. Let $x_{\mathrm{f},i}(k)$ represent the amount of fuel level in car number i at time step k. The inputs of the model consist of a continuous variable, $u_{\mathrm{f},i}(k)$, and two binary variables, $s_{\mathrm{f},i}(k)$ and $s_{\mathrm{r},i}(k)$ for each fuel cell car i. The value of $u_{\mathrm{f},i}(k)$ determines the net power generation of fuel cell car i at time step k. It is assumed that a lower-level control system exists in each fuel cell car that can operate the fuel cell stack of the car in such a way that the net power generation of the car is equal to a given set-point, $u_{\mathrm{f},i}(k)$. The value of the binary variable $s_{\mathrm{f},i}(k)$ determines the operation mode of the fuel cell of car i at time step k. If $s_{\mathrm{f},i}(k) = 1$, the fuel cell is turned on; if $s_{\mathrm{f},i}(k) = 0$, the fuel cell

is turned off. In addition, the refilling process of the cars is determined based on the value of $s_{\mathrm{r},i}(k)$, where $s_{\mathrm{r},i}(k) = 1$ indicates that car i is being refilled at time step k.

The fuel level of car i, when its fuel cell is turned on, can be described by [79, 4]

$$x_{\mathrm{f},i}(k+1) = x_{\mathrm{f},i}(k) - (\alpha_{\mathrm{f},i} u_{\mathrm{f},i}(k) + \beta_{\mathrm{f},i}) T_{\mathrm{s}}, \tag{4.1}$$

where $\alpha_{\mathrm{f},i}$ and $\beta_{\mathrm{f},i}$ are two parameters related to the specifications of each fuel cell stack i. The sampling time interval of the system is presented by T_{s}.

The model presented in this chapter includes both the trip characteristics and the power generation of the cars. Trip characteristics of the cars are the information about the estimated departure and arrival time of each car, in addition to the distance that each car has travelled. The availability of each car in the task of power generation is determined by the trip characteristics. If a car leaves the neighborhood at a specific time, it will not be available in the process of electricity generation until it comes back. In addition, an amount of fuel will be used during the travel of the car. In this chapter, we assume that the trip characteristics of the cars are not controllable, but predictable. Even though the predictions of the departure and arrival time of the cars are not completely accurate, it is possible to determine tight but guaranteed lower bounds for the departure times of each car. Similarly, we can determine tight but guaranteed upper bounds for the arrival times of each car. As a result, there is no uncertainty in the trip characteristics of the cars.

A binary number, $\lambda_{\mathrm{f},i}(k)$, indicates whether fuel cell car i is present in the geographical area of the microgrid at time step k. In addition, the amount of fuel that is used during the travel of car i is denoted by $h_i(k)$. It is assumed that if fuel cell car i leaves the neighborhood and comes back again at the period $\big[(k-1)T_{\mathrm{s}}, kT_{\mathrm{s}}\big)$, the value of $h_i(k)$ represents the amount of fuel that is used for this trip. For all other values of k, we set $h_i(k) = 0$.

The model of fuel cell car i including the refilling process and the trip characteristics of the car is as follows:

$$x_{\mathrm{f},i}(k+1) = \begin{cases} x_{\mathrm{f},i}(k) + R_{\mathrm{f},i} & \text{refilling} \\ x_{\mathrm{f},i}(k) & \text{inactive} \\ x_{\mathrm{f},i}(k) - (\alpha_{\mathrm{f},i} u_{\mathrm{f},i}(k) + \beta_{\mathrm{f},i}) T_{\mathrm{s}} & \text{generation} \\ x_{\mathrm{f},i}(k) & \text{transportation} \\ x_{\mathrm{f},i}(k) - h_i(k) & \text{arrival.} \end{cases} \tag{4.2}$$

The model in (4.2) is a hybrid piecewise affine (PWA) model with five modes. The first mode indicates the refilling process. The system enters this mode when the car is available for power generation and the value of $s_{\mathrm{r},i}(k)$ is set to 1 by the controller. During this mode, the fuel level of the car increases with a constant rate $R_{\mathrm{f},i}$. The second and the third modes belong to the situation when the car is inside the geographical area of the microgrid and it is not refilled. In the second mode, the fuel cell stack is turned off, and hence, the amount of fuel in the car does not change

in time. The third mode represents the system dynamics when the fuel cell stack is turned on and the net power production is equal to $u_{\mathrm{f},i}(k)$. The last two modes in (4.2) belong to the situation where the car is not present in the geographical area of the microgrid. A fuel cell car cannot be refilled or generate electricity when it is not inside the geographical area of the microgrid and, as a result, the fuel level $x_{\mathrm{f},i}(k)$ does not influence the system dynamics in this case. We can assume that the fuel level remains constant during the absence of the car and that one sample time step before arrival of the car in the neighborhood, all the fuel used in the transportation is subtracted from the initial value.

It is assumed that the refilling process and the generation of electricity by a car can be done only when the car is inside the geographical area of the microgrid. In other words,

$$\text{if } \lambda_{\mathrm{f},i}(k) = 0 \text{ then } s_{\mathrm{r},i}(k) = 0. \tag{4.3}$$

$$\text{if } \lambda_{\mathrm{f},i}(k) = 0 \text{ then } s_{\mathrm{f},i}(k) = 0. \tag{4.4}$$

In addition, we assume that during the refilling process, the fuel cell stack should be turned off. Therefore, another constraint in the system is given by:

$$\text{if } s_{\mathrm{r},i}(k) = 1 \text{ then } s_{\mathrm{f},i}(k) = 0. \tag{4.5}$$

Based on the physical limits, an upper bound exists for the generation of electricity in each fuel cell stack. In addition, the rate of power generation is limited to an upper and lower bound as follows:

$$0 \leq u_{\mathrm{f},i}(k) \leq \bar{u}_{\mathrm{f},i} \tag{4.6}$$

$$\Delta\underline{u}_{\mathrm{f},i} \leq \Delta u_{\mathrm{f},i}(k) \leq \Delta\bar{u}_{\mathrm{f},i}, \tag{4.7}$$

where the $\Delta u_{\mathrm{f},i}(k)$ is defined as $u_{\mathrm{f},i}(k) - u_{\mathrm{f},i}(k-1)$. The fuel cell stack cannot generate electricity when it is turned off, i.e.,

$$\text{if } s_{\mathrm{f},i}(k) = 0 \text{ then } u_{\mathrm{f},i}(k) \leq 0. \tag{4.8}$$

The inequality (4.8) combined with (4.6) implies that whenever a fuel cell is turned off, the power generation of that fuel cell has to be equal to zero.

The maximum level of fuel in each car is indicated by $\bar{x}_{\mathrm{f},i}$ and the minimum level of fuel that is necessary for the next travel of car is indicated by $\underline{x}_{\mathrm{f},i}(k)$. Note that the maximum level of fuel in each car, i.e., $\bar{x}_{\mathrm{f},i}$, is a physical constraint and, hence, independent of time. However, we consider $\underline{x}_{\mathrm{f},i}(k)$ as a function of time, because we assume that the owner of car i has the freedom of setting the minimum level of fuel. If the amount of fuel in a car is equal to or lower than this minimum level necessary for the travel purpose, the car is not used in the task of power generation. Therefore,

$$\text{if } x_{\mathrm{f},i}(k) \leq \underline{x}_{\mathrm{f},i}(k) \text{ then } s_{\mathrm{f},i}(k) = 0. \tag{4.9}$$

As a result, the constraints on $x_{\mathrm{f},i}(k)$ can be written as follows:

$$\underline{x}_{\mathrm{f},i}(k)s_{\mathrm{f},i}(k) \leq x_{\mathrm{f},i}(k) \leq \bar{x}_{\mathrm{f},i}. \tag{4.10}$$

4.4.2 Electrolysis system model

A water electrolysis system is responsible for providing the hydrogen needed for the transportation and electricity production in the neighborhood. It is assumed that all the hydrogen produced by the electrolysis system is stored in a reservoir connected to it. The amount of stored hydrogen, $x_{\rm el}(k)$, is a system state. The energy consumption of a typical electrolysis system, $u_{\rm el}(k)$, is a linear function of the produced hydrogen [44]. As a result, the stored hydrogen will increase due to hydrogen production of the electrolysis system with the amount of $\alpha_{\rm el}u_{\rm el}(k)T_{\rm s}$, where $T_{\rm s}$ is the sampling time interval and $\alpha_{\rm el}$ is a constant related to the specifications of the system. Based on the CaPP microgrid scenario, all the fuel cell cars receive their fuel from the water electrolysis system and, hence, the PWA model of the system can be expressed as follows:

$$x_{\rm el}(k+1) = \begin{cases} x_{\rm el}(k) - \sum_{i=1}^{N_{\rm veh}} s_{{\rm r},i}(k) R_{{\rm f},i} & \text{if } s_{\rm el}(k) = 0 \\ x_{\rm el}(k) - \sum_{i=1}^{N_{\rm veh}} s_{{\rm r},i}(k) R_{{\rm f},i} + T_{\rm s}\alpha_{\rm el}u_{\rm el}(k) & \text{if } s_{\rm el}(k) = 1 \end{cases}, \tag{4.11}$$

where $s_{\rm el}(k)$ is the on/off switching signal of the electrolysis system. The physical limitations of the system dictate a bound on the stored hydrogen, consumed electricity, and its rate of change as follows:

$$\underline{u}_{\rm el} \leq u_{\rm el}(k) \leq 0 \tag{4.12}$$

$$\Delta\underline{u}_{\rm el} \leq \Delta u_{\rm el}(k) \leq \Delta\bar{u}_{\rm el} \tag{4.13}$$

$$\underline{x}_{\rm el} \leq x_{\rm el}(k) \leq \bar{x}_{\rm el}. \tag{4.14}$$

The electrolysis system consumes electricity only when it is turned on. Therefore,

$$\text{if } \; s_{\rm el}(k) = 0 \; \text{ then } \; u_{\rm el}(k) \geq 0. \tag{4.15}$$

The inequality (4.15) combined with (4.12) implies that whenever $s_{\rm el}(k) = 0$, then $u_{\rm el}(k) = 0$.

4.4.3 Overall system model

The PWA models of the cars and electrolysis system in (4.2) and (4.11) can be converted into mixed logical dynamical (MLD) models [13] by standard techniques [41]. An MLD model describes the behavior of a hybrid system including continuous and discrete variables.

To derive the MLD model, we define a binary auxiliary variable $\delta_{\rm exp}(k)$ that indicates whether electricity is imported or exported from the microgrid to the power network at time step k. If we define $e_{\rm in}(k)$ as the imported power to the system, the value of $\delta_{\rm exp}(k)$ is determined as follows:

$$e_{\rm in}(k) \leq 0 \Leftrightarrow \delta_{\rm exp}(k) = 1. \tag{4.16}$$

The logical connection (4.16) can be easily translated into a set of affine constraints. We define a lower bound, $\underline{e}_{\text{in}}$, and an upper bound, $\bar{e}_{\text{in}}$, for the imported power to the microgrid, $e_{\text{in}}(k)$. Based on the physical properties of the electrical networks, the amount of imported power to the microgrid is given by:

$$e_{\text{in}}(k) = P_{\text{d}}(k) + \omega(k) - u_{\text{el}}(k) - \sum_{i=1}^{N_{\text{veh}}} u_{\text{f},i}(k). \tag{4.17}$$

Therefore, the following constraint exists in the system:

$$\underline{e}_{\text{in}} \leq P_{\text{d}}(k) + \omega(k) - u_{\text{el}}(k) - \sum_{i=1}^{N_{\text{veh}}} u_{\text{f},i}(k) \leq \bar{e}_{\text{in}}, \tag{4.18}$$

where $P_{\text{d}}(k)$ is the prediction of residual electrical load in the microgrid, which is equal to the total power production of the renewable energy sources subtracted from the load demand in the microgrid. The difference between the prediction of residual electricity demand and its actual realization at time step k is an uncertain value that is denoted by $\omega(k)$.

Using the models (4.2) and (4.11), the overall system model can be written as

$$\mathbf{x}(k+1) = \mathbf{x}(k) + B_1(k)\mathbf{u}(k) + B_3(k)\mathbf{z}(k) + B_4(k), \tag{4.19}$$

where $\mathbf{z}(k)$ contains the continuous auxiliary variables that are used in the MLD models and the system states and inputs are defined as:

$$\mathbf{x}(k) \triangleq \begin{bmatrix} \mathbf{x}_{\text{f}}^T(k) & x_{\text{el}}(k) \end{bmatrix}^T \tag{4.20}$$

$$\mathbf{u}(k) \triangleq \begin{bmatrix} \mathbf{u}_{\text{f}}^T(k) & \mathbf{s}_{\text{r}}^T(k) & \mathbf{s}_{\text{f}}^T(k) & u_{\text{el}}(k) & s_{\text{el}}(k) \end{bmatrix}^T. \tag{4.21}$$

Here, a bold-face variable indicates a vector containing the corresponding variables related to all cars. For example, $\mathbf{x}_{\text{f}}(k) = \begin{bmatrix} x_{\text{f},1}(k) & \dots & x_{\text{f},N_{\text{veh}}}(k) \end{bmatrix}^T$. The matrices $B_1(k)$, $B_3(k)$, and $B_4(k)$ are time-varying, but because we can predict the trip characteristics of the cars, these can be determined over the whole prediction horizon.

All the constraints in the models of the fuel cell cars and the electrolyzer, i.e., (4.3)-(4.10) and (4.12)-(4.15), in addition to the extra constraints (4.16)-(4.18) and the definition of auxiliary variables are affine with respect to the variables $\mathbf{x}(k)$, $\mathbf{u}(k)$, $\delta_{\text{exp}}(k)$, $\mathbf{z}(k)$, and $\omega(k)$. Therefore, for each sample time step we can express the inequalities as:

$$E_1\mathbf{u}(k) + E_4\mathbf{x}(k) + E_{51}(k) + E_{52}\omega(k) \geq E_2\delta_{\text{exp}}(k) + E_3\mathbf{z}(k). \tag{4.22}$$

Using (4.19) and defining $\omega(k)$ as the difference between the prediction of the residual electricity demand and its actual realization at time step k, matrices $G_1(k)$, $G_2(k)$, $G_3(k)$, and $G_4(k)$ can be determined in such a way that all the operational

constraints of the fuel cell cars and the electrolyzer are included in the following inequality:

$$G_1(k)X(k) \leq G_2(k) + G_3(k)\mathbf{x}(k) + G_4(k)\tilde{\omega}(k), \tag{4.23}$$

where $X(k) = \left[\begin{array}{ccc} \tilde{\mathbf{u}}^T(k) & \tilde{\delta}^T_{\exp}(k) & \tilde{\mathbf{z}}^T(k) \end{array} \right]^T$. Here, a variable with a tilde represents the stacked version of that variable in the prediction horizon. For example, $\tilde{\mathbf{u}}(k) = \left[\begin{array}{ccc} \mathbf{u}^T(k) & \dots & \mathbf{u}^T(k+N_{\rm p}-1) \end{array} \right]^T$, where $N_{\rm p}$ indicates the prediction horizon. Equation (4.19) with inequality (4.23) forms the MLD model of the overall system.

4.5 Control system operation

The proposed scenario assumes that, on the one hand, the wind turbine and PV systems are generating maximum power with respect to the weather situation, and on the other hand, the electricity load in the households is not controllable. The connection of the microgrid with the power grid allows the exchange of electricity, but it comes at a cost. An appropriate control system can help the microgrid to use the RES inside the neighborhood as much as possible and avoid unnecessary exchange of electricity. In addition, the physical limits in the transmission lines may cause a power unbalance inside the microgrid at some times. Fortunately, the presence of the fuel cell cars and the electrolysis system makes it possible to still satisfy the power balance; this task is done via a central control system.

We assume that the central control system has access to weather forecast information, predictions of loads and renewable energy sources, predictions of the trip characteristics of the cars, and current values of the system states including the level of hydrogen stored in the electrolysis system and in each fuel cell car. The switching signals of the fuel cell cars and the electrolysis system, in addition to their power generation and consumption, are determined by the control system in such a way that, firstly, the power balance is guaranteed in the system and, secondly, the operational costs of the system are minimized. To this end, a model predictive control (MPC) algorithm is developed. In this algorithm, the operational costs of the system, subject to all constraints, are minimized by determining a sequence of control actions to be implemented in the future. The first control action is applied to the system and, at the next sample time step, the whole procedure is repeated.

The following factors are considered to affect the operational costs:

- The cost of switching the operation mode of the fuel cells and the electrolysis system, $J_{\rm switch}(k)$. This part of the cost function is used to include the strong effect of switching the operation mode of fuel cells and electrolysis systems on their life time. A term $W_{\rm sf}|\Delta s_{{\rm f},i}(k)|$ is considered for each fuel cell car i as the cost of switching at time step k, where $W_{\rm sf}$ is a weight factor to determine the importance of the degradation in the whole operational cost. A similar

term, $W_{\mathrm{sel}}|\Delta s_{\mathrm{el}}(k)|$, is considered for the electrolysis system. The definition of $J_{\mathrm{switch}}(k)$ is as follows:

$$J_{\mathrm{switch}}(k) = \sum_{j=0}^{N_{\mathrm{p}}-1} \left(\sum_{i=1}^{N_{\mathrm{veh}}} W_{\mathrm{sf}} |\Delta s_{\mathrm{f},i}(k+j)| + W_{\mathrm{sel}} |\Delta s_{\mathrm{el}}(k+j)| \right). \quad (4.24)$$

- The cost of power generation of fuel cells and power consumption of the electrolyzer, $J_{\mathrm{power}}(k)$. This term reflects the operational costs, related to the power generation of the fuel cells or the power consumption of the water electrolysis system. The constant coefficient W_{pf} indicates the cost of generating one unit of power during a time step interval by fuel cell cars. The constant coefficient W_{pel} is defined in a similar way for the electrolysis system. The price of hydrogen per kilogram, which is used by the fuel cells or is produced by the electrolysis system, is influencing W_{pf} and W_{pel}. The definition of $J_{\mathrm{power}}(k)$ is as follows:

$$J_{\mathrm{power}}(k) = \sum_{j=0}^{N_{\mathrm{p}}-1} \left(\sum_{i=1}^{N_{\mathrm{veh}}} W_{\mathrm{pf}} u_{\mathrm{f},i}(k+j) + W_{\mathrm{pel}} u_{\mathrm{el}}(k+j) \right). \quad (4.25)$$

- The cost of imported power, $J_{\mathrm{imp}}(k)$. It is assumed that the price of imported electricity should be paid to the power grid operator. As a result, the imported power affects the operational costs of the microgrid. If $C_{\mathrm{e,imp}}(k+j)$ represents the price of electricity at time step $k+j$, the term $\sum_{j=0}^{N_{\mathrm{p}}-1} C_{\mathrm{e,imp}}(k+j) e_{\mathrm{in}}(k+j)(1-\delta_{\mathrm{exp}}(k+j))$ indicates the price of imported power, where $(1-\delta_{\mathrm{exp}}(k+j))$ determines whether the electricity is imported or not. The definition of $J_{\mathrm{imp}}(k)$ is as follows:

$$J_{\mathrm{imp}}(k) = \sum_{j=0}^{N_{\mathrm{p}}-1} C_{\mathrm{e,imp}}(k+j) e_{\mathrm{in}}(k+j)(1-\delta_{\mathrm{exp}}(k+j)). \quad (4.26)$$

- The cost of exported power, $J_{\mathrm{exp}}(k)$. In order to control the total power generation in the power grid, the amount of power injected into the grid should be controlled. When extra power can be used in the power grid, for example the peak demand hours, the grid operator rewards the microgrid to inject electricity into the network. However, in a power grid where the share of RES in total power generation is considerably high, there are time instances that the total power generation of RES is too high for the system. In these cases, the grid operator should discourage the microgrid from injecting power into the network. We assume a variable $C_{\mathrm{e,exp}}(k)$ to indicate the reward or penalty for exporting electricity from the microgrid into the power network at time step k. The definition of $J_{\mathrm{exp}}(k)$ is as follows:

$$J_{\mathrm{exp}}(k) = \sum_{j=0}^{N_{\mathrm{p}}-1} C_{\mathrm{e,exp}}(k+j)(-e_{\mathrm{in}}(k+j))\delta_{\mathrm{exp}}(k+j). \quad (4.27)$$

All the mentioned elements in the operational costs of the system create the total cost function:

$$J(k) = J_{\text{switch}}(k) + J_{\text{power}}(k) + J_{\text{imp}}(k) + J_{\text{exp}}(k). \tag{4.28}$$

By using the MLD model of the system derived in Section 4.4, the cost function can be written in the following form:

$$J(k) = W_{\text{x}}(\tilde{\omega}(k))X(k) + W_{\text{d}}(k)\tilde{\omega}(k) \tag{4.29}$$

The matrices $W_{\text{x}}(\tilde{\omega}(k))$ and $W_{\text{d}}(k)$ can be easily derived from the cost function (4.28) by using the system model. Therefore, the optimization problem that the model predictive controller needs to solve at each time step is of the form:

$$\begin{aligned} &\min_{X(k)} \max_{\tilde{\omega}(k)} \{J(k)\} \\ &\text{subject to } (4.23). \end{aligned} \tag{4.30}$$

The constraint of the optimization problem (4.30) should be satisfied for all possible realizations of $\tilde{\omega}(k)$, and hence, problem (4.30) is hard to solve in general. In order to simplify the problem, the uncertainty in the residual load of the neighborhood is assumed to be bounded and the results of the following lemmas can be taken into account.

Assumption 4.5.1. *There exists a finite bound for the deviation of the predicted residual load from its actual value, $\omega(k)$, at each time step k. Therefore, it is possible to determine $\bar{\omega}$ and $\underline{\omega}$ such that for all k, $\underline{\omega} \leq \omega(k) \leq \bar{\omega}$.*

Lemma 4.5.1. *Defining*

$$\tilde{\omega}_{\min} = \begin{bmatrix} \bar{\omega} & \dots & \bar{\omega} \end{bmatrix}^T_{N_{\text{p}} \times 1} \tag{4.31}$$

$$\tilde{\omega}_{\max} = \begin{bmatrix} \underline{\omega} & \dots & \underline{\omega} \end{bmatrix}^T_{N_{\text{p}} \times 1}, \tag{4.32}$$

the inequality (4.23) holds for all possible disturbances ω satisfying Assumption 4.5.1 if the following two inequalities hold:

$$G_1(k)X(k) \leq G_2(k) + G_3(k)\boldsymbol{x}(k) + G_4(k)\tilde{\omega}_{\min} \tag{4.33}$$

$$G_1(k)X(k) \leq G_2(k) + G_3(k)\boldsymbol{x}(k) + G_4(k)\tilde{\omega}_{\max}. \tag{4.34}$$

Proof: The existence of a maximum and minimum value for ω implies that:

$$\forall \omega \in \mathbb{R}\ \exists \lambda_1, \lambda_2 \in [0,1]\ :\ \lambda_1\underline{\omega} + \lambda_2\bar{\omega} = \omega \text{ and } \lambda_1 + \lambda_2 = 1. \tag{4.35}$$

Now assume an arbitrary realization of $\tilde{\omega}(k)$ as follows:

$$\tilde{\omega}(k) = \begin{bmatrix} \omega(k) & \omega(k+1) & \dots & \omega(k+N_{\text{p}}-1) \end{bmatrix}^T.$$

The inequality constraint (4.23) consists of several inequalities belonging to each time step in the prediction horizon. Considering the structure of G_1, G_2, G_3, and G_4, it can be shown that (4.23) consists of the following inequalities, for $j \in \{0, \ldots, N_\mathrm{p} - 1\}$:

$$G_{1,k+j}(k)X(k) \leq G_{2,k+j}(k) + G_{3,k+j}(k)\mathbf{x}(k) + g_{4,k+j}(k)\omega(k+j) \tag{4.36}$$

where $G_{1,k+j}(k)$, $G_{2,k+j}(k)$, $G_{3,k+j}(k)$, and $g_{4,k+j}(k)$ are the $(j+1)$th row of $G_1(k)$, $G_2(k)$, $G_3(k)$, and $G_4(k)$, respectively. From (4.33) and (4.34), we have:

$$G_{1,k+j}(k)X(k) \leq G_{2,k+j}(k) + G_{3,k+j}(k)\mathbf{x}(k) + g_{4,k+j}(k)\underline{\omega} \tag{4.37}$$

$$G_{1,k+j}(k)X(k) \leq G_{2,k+j}(k) + G_{3,k+j}(k)\mathbf{x}(k) + g_{4,k+j}(k)\bar{\omega}, \tag{4.38}$$

Property (4.35) shows that for any realization of $\omega(k+j)$, there exists a pair $(\lambda_1(k+j), \lambda_2(k+j))$ such that $\lambda_1(k+j)\underline{\omega} + \lambda_2(k+j)\bar{\omega} = \omega(k+j)$ and $\lambda_1(k+j) + \lambda_2(k+j) = 1$. By multiplying these factors to (4.37) and (4.38), it can be seen that (4.36) holds. This reasoning holds for all $j \in \{0, \ldots, N_\mathrm{p} - 1\}$ and, hence, (4.23) holds. □

Lemma 4.5.2. *The maximum of the cost function (4.29) over all the possible realizations of $\tilde{\omega}(k)$, i.e., $\max_{\tilde{\omega}(k)} \{J(k)\}$, always occurs at one of the vectors $\tilde{\omega}_1(k)$, $\tilde{\omega}_2(k)$, …, $\tilde{\omega}_N(k)$ defined as follows:*

$$\begin{aligned}
\tilde{\omega}_1(k) &= \begin{bmatrix} \underline{\omega} & \underline{\omega} & \ldots & \underline{\omega} \end{bmatrix}^T \\
\tilde{\omega}_2(k) &= \begin{bmatrix} \bar{\omega} & \underline{\omega} & \ldots & \underline{\omega} \end{bmatrix}^T \\
&\vdots \\
\tilde{\omega}_N(k) &= \begin{bmatrix} \bar{\omega} & \bar{\omega} & \ldots & \bar{\omega} \end{bmatrix}^T.
\end{aligned}$$

Proof: The first term of the cost function, $W_\mathrm{x}(k)X(k)$, can be written as:

$$W_\mathrm{x}(k)X(k) = W_{\mathrm{x},1}(k)X(k) + W_{\mathrm{x},2}(\tilde{\omega}(k))X(k). \tag{4.39}$$

The first term in (4.39), $W_{\mathrm{x},1}(k)X(k)$, is not affected by $\tilde{\omega}(k)$. The expanded form of the second term, $W_{\mathrm{x},2}(\tilde{\omega}(k))X(k)$, is given by:

$$\sum_{j=0}^{N_\mathrm{p}-1} \Big(C_{\mathrm{e,imp}}(k+j)(1 - \delta_{\exp}(k+j)) - C_{\mathrm{e,exp}}(k+j)\delta_{\exp}(k+j) \Big) \omega(k+j)$$

which is either equal to $C_{\mathrm{e,imp}}(k+j)\omega(k+j)$ or $-C_{\mathrm{e,exp}}(k+j)\omega(k+j)$ at each time step $k+j$, based on the value of $\delta_{\exp}(k+j)$. In these cases, the maximum value of $W_\mathrm{x}(\tilde{\omega}(k))X(k)$ at each time step k for all realizations of $\omega(k+j)$ occurs at $\bar{\omega}$ and $\underline{\omega}$, respectively.

The second term of the cost function, $W_{\mathrm{d}}(k)\tilde{\omega}(k)$, can be written in the form:

$$W_{\mathrm{d}}(k)\tilde{\omega}(k) = \sum_{j=0}^{N_{\mathrm{p}}-1} C_{\mathrm{e,imp}}(k+j)\omega(k+j).$$

It is assumed that the tariff for imported power, $C_{\mathrm{e,imp}}(k)$ is positive, and hence, the maximum value of $W_{\mathrm{d}}(k)\tilde{\omega}(k)$ at each time step k for all realizations of $\omega(k+j)$ occurs at $\bar{\omega}$. The total cost function contains the sum of $W_{\mathrm{x},2}(\tilde{\omega}(k))X(k)$ and $W_{\mathrm{d}}(k)\tilde{\omega}(k)$, and, hence, the maximum of the total cost function at time step $k+j$ occurs at either $\bar{\omega}$ or $\underline{\omega}$. By following the same reasoning for all $j \in \{0, \ldots, N_{\mathrm{p}}-1\}$, we can conclude that the maximum value of the cost, $J(k)$, would be realized when $\tilde{\omega}(k)$ is equal to one of the vectors $\tilde{\omega}_1, \ldots, \tilde{\omega}_N$. □

Lemmas 4.5.1 and 4.5.2 show that the optimization problem (4.30) subject to the constraints (4.23) can be formulated as a number of MILP problems. However, the number of MILP problems to be solved is $N = 2^{N_{\mathrm{p}}}$. In this case, an increase in the prediction horizon will create an exponential increase in the computation time needed for the controller, which is not desired. In order to reduce the number of MILP problems that need to be solved at each time step and therewith to reduce the computational burden of the proposed control strategy, we consider the following additional assumption.

Assumption 4.5.2. *In the optimization problem (4.30), the value of $\delta_{\mathrm{exp}}(k+j)$ is the same for all $j \in \{0, \ldots, N_{\mathrm{p}}-1\}$.*

Assumption 4.5.2 is a restriction on the import or export of electricity in the future. It means that the control actions are determined based on the assumption of either exporting or importing electricity during the entire prediction period $[kT_{\mathrm{s}}, kT_{\mathrm{s}} + N_{\mathrm{p}}T_{\mathrm{s}})$, but not a combination of them. This assumption may decrease the system performance, but it is used due to its significant influence on the reduction of the computational burden. Lemma 4.5.2 indicates that the optimal point of the cost function (4.29) is located at one of the N realizations of the uncertainty that are mentioned in Lemma 4.5.2. The following lemma indicates that if Assumption 4.5.2 holds, the optimal point is located at one of the two realizations of the uncertainty indicated by $\tilde{\omega}_{\min}$ and $\tilde{\omega}_{\max}$ defined in (4.31) and (4.32).

Lemma 4.5.3. *Considering Assumption 4.5.2, the maximum of the cost function (4.29) over all the possible realizations of $\tilde{\omega}(k)$, i.e., $\max_{\tilde{\omega}(k)}\{J(k)\}$, always occurs at one of the vectors $\tilde{\omega}_{\min}$ or $\tilde{\omega}_{\max}$ defined in (4.31) and (4.32).*

Proof: Assumption 4.5.2 allow us to consider $\delta_{\mathrm{exp}}(k)$ instead of $\delta_{\mathrm{exp}}(k+j)$ for all $i \in \{1, \ldots, N_{\mathrm{p}}-1\}$. Therefore, we have the following term for the cost function that is related to $\tilde{\omega}(k)$:

$$\sum_{j=0}^{N_{\mathrm{p}}-1} \Big(C_{\mathrm{e,imp}}(k+j)(1-\delta_{\mathrm{exp}}(k)) - C_{\mathrm{e,exp}}(k+j)\delta_{\mathrm{exp}}(k) \Big)\omega(k+j)$$

which is either equal to $\sum_{j=0}^{N_\mathrm{p}-1} C_{\mathrm{e,imp}}(k+j)\omega(k+j)$ or $\sum_{j=0}^{N_\mathrm{p}-1} -C_{\mathrm{e,exp}}(k+j)\omega(k+j)$, based on the value of $\delta_{\mathrm{exp}}(k)$. In both cases, the maximum value for all realizations of $\omega(k+j)$ for $j \in \{0,\dots,N_\mathrm{p}-1\}$ occurs for an extreme value of ω for the entire prediction period. In the first case, this extreme case is $\bar{\omega}$ and in the second case, $\underline{\omega}$. Therefore, the maximum value of the cost, $J(k)$, would be realized when $\tilde{\omega}(k)$ is equal to either $\tilde{\omega}_{\max}$ or $\tilde{\omega}_{\min}$. □

Lemma 4.5.1 and 4.5.3 show that the optimization problem (4.30) subject to the constraints (4.23) can be formulated as an MILP problem as follows:

$$\min_{X(k)}\{\max\{W_\mathrm{x}(\tilde{\omega}_{\min}(k))X(k)+W_\mathrm{d}(k)\tilde{\omega}_{\min}(k), \\ W_\mathrm{x}(\tilde{\omega}_{\max}(k))X(k)+W_\mathrm{d}(k)\tilde{\omega}_{\max}(k)\}\} \tag{4.40}$$

subject to

$$G_1(k)X(k) \le G_2(k)+G_3(k)\mathbf{x}(k)+G_4(k)\tilde{\omega}_{\min} \tag{4.41}$$

$$G_1(k)X(k) \le G_2(k)+G_3(k)\mathbf{x}(k)+G_4(k)\tilde{\omega}_{\max}, \tag{4.42}$$

which can be solved by a variety of MILP solvers, such as GLPK [34], CPLEX [23], or Gurobi [39]. The conversion of the optimization problem (4.30) into (4.40) reduces the complexity of the problem and as a result, the computation time in the model predictive controller is decreased significantly.

4.6 Simulation of a CaPP microgrid

In this section, the CaPP microgrid system described in Section 4.2 is simulated. A central controller is assumed to operate the system as described in Section 4.5. We consider 200 households inside the neighborhood. In order to simulate the electricity demand of the households, standard demand curves corresponding to 2014 are extracted from [29]. Using the standardized power fractions for each 15-min period of the year, we calculated the hourly demand by assuming a yearly consumption of 3400 kWh/year [89]. Photovoltaic systems and wind turbines are the available RES in the system. It is assumed that the RES units generate the maximum electrical power that is possible given weather conditions. To simulate the power generation of the wind turbine, data from one of the measuring stations of the Dutch Institute of Meteorology is used [80]. Since the wind turbine is assumed to be inside the geographical area of the microgrid, a small turbine of 130kW is considered [86]. Given the turbine size, a measuring station in a coastal area is chosen to better capture the wind's energy [62]. Using the hourly wind speed data measured at Hoek van Holland in 2014, the hourly wind power generation is calculated for a 130kW turbine.

To simulate the power generation of solar photovoltaic systems, the PV Watts tool [63] is used. For the Netherlands, Amsterdam is the only location available in PV Watts. Hourly power generation of a 10 kWp PV system is calculated. The

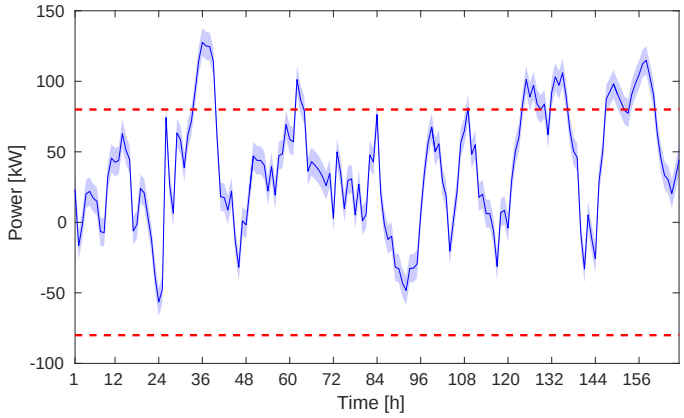

Figure 4.2: Residual load of the microgrid; the shaded area indicates the uncertainty and the red lines are the limits on the power exchange between the microgrid and the power network.

historical data show that the total RES capacity installed generates as much as 90% of the yearly electricity consumption in the microgrid.

As mentioned in Section 4.5, the residual load of the microgrid is assumed to be equal to the electricity load in the microgrid minus the power production of renewable energy sources. Figure 4.2 depicts the prediction of the residual load in the microgrid in a sample week. It is assumed that the prediction of the residual load contains uncertainty up to around 10 percent of its peak value. Here we assume that $\bar{\omega} = -\underline{\omega} = 10$ kW. The electrical connection between the microgrid and the power network are assumed to have a capacity of power exchange equal to 80 kW, i.e. $\bar{e}_{\rm in} = -\underline{e}_{\rm in} = 80$.

The number of the fuel cell cars in the neighborhood is assumed to be 50. In order to derive the trip characteristics of the cars, the traveling behavior of the Dutch drivers for the year 2014 [19] is used. About 13700 data points were used to derive the distribution of the departure and arrival times of the cars, and also the daily distance driven. The driving behaviors of the 50 cars are determined using these distributions. The resulting average daily distance traveled per car is 53 km. It is assumed that all the fuel cell cars consume 1 kg of hydrogen per 100 km driving distance. In addition, in the model of fuel cell stacks, the results of [79] are used to determine the required parameters. Therefore, the parameters $\alpha_{{\rm f},i}$ and $\beta_{{\rm f},i}$ for all the cars are selected to be 0.06 kg/kWh and 0.11 kg/h, respectively. The refilling speed of the cars, $R_{{\rm f},i}$, is assumed to be equal to 2 kg/h for all the cars. The maximum power generation of the fuel cells, $\bar{u}_{{\rm f},i}$, is set to 15 kW. Because the nominal power generation of a typical fuel cell car is around 100 kW, the fuel cell is operated at partial load. The coefficient of the power generation of fuel cell cars, $W_{\rm pf}$, and power consumption of the electrolysis system, $W_{\rm pel}$, in the cost function are assumed to be equal to 0.6 €/kW and 0.15 €/kW, respectively.

A water electrolysis system with a maximum power consumption of 100 kW

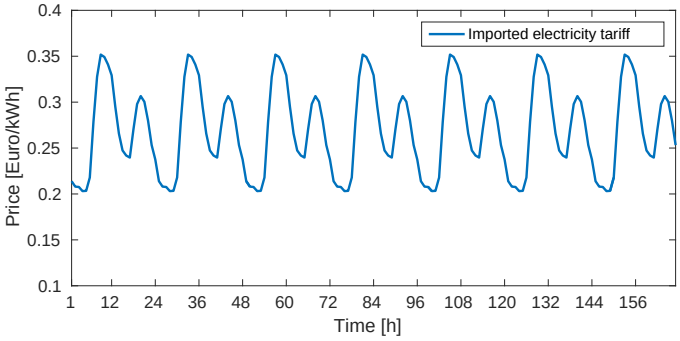

Figure 4.3: Price of importing electricity to the microgrid based on the APX market.

and a hydrogen storage tank with the capacity of 500 kg are assumed to be available inside the neighborhood. The limits of the hydrogen level in the storage tank are $\underline{x}_{\text{el}} = 10$ kg and $\bar{x}_{\text{el}} = 500$ kg. For the water electrolysis system we assume an efficiency, $\eta_{\text{el}} = 70\%$. Considering that the high heating value of hydrogen, h_{el}, is 39.4 kWh/kg [44], α_{el} is equal to $\eta_{\text{el}}/h_{\text{el}} \approx 0.02$ kg/kWh.

The price of importing electricity is assumed to be equal to the price of the Amsterdam Power Exchange (APX) market in a day of April 2016 [7] and it is shown in Figure 4.3. In addition, we have considered a constant cost for the system, 0.2 €/kWh, to be paid to the grid operator in case of exporting electricity from the microgrid to the power network between 11 P.M. and 7 A.M. In this period of the time, the load of the power grid is low and exporting electricity from the microgrid to the power grid is discouraged.

Based on the system model developed in Section 4.4 and the control algorithm of Section 4.5, the system is simulated for an entire year. Figure 4.4 illustrates the resulting hydrogen level in the storage tank during a year. The use of hydrogen for transportation and electricity generation by the fuel cell cars causes the hydrogen level in the storage tank to fluctuate, but it stays inside the predefined minimum and maximum of 10 and 500 kg, respectively.

If the RES in the microgrid are operated with their maximum power generation capacity, the residual load of the microgrid would not always be in the range -80 to 80 kW, i.e., the range in which exchange of power between the microgrid and the power network is possible. In our simulation, we consider a price for exporting electricity from microgrid into the power network in order to discourage the microgrid from exporting electricity. The result of the simulation on the imported power to the microgrid in Figure 4.5(a) shows that the microgrid barely exports power to the power network. The residual load of the microgrid, depicted in Figure 4.2, indicates that in the absence of a water electrolysis system and in the case of avoiding the curtailment of the RES generation, the microgrid inevitably exports electricity to the power grid. However, Figure 4.5(a) shows that by using the fuel cell cars and the water electrolysis system, the imported power to the microgrid always remains

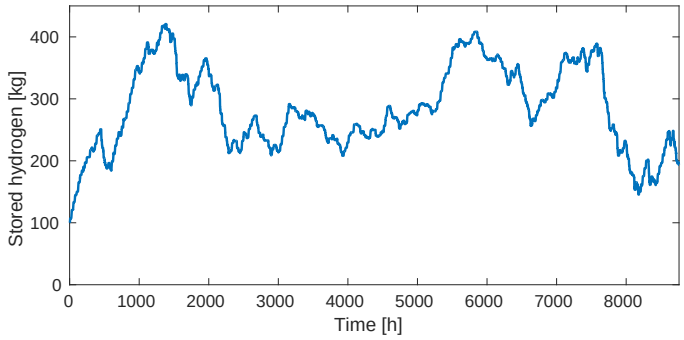

Figure 4.4: Level of hydrogen stored in the storage tank.

inside the predefined bounds. Figure 4.5(b) represents the power consumption of the water electrolysis system in a sample week. The imported power to the microgrid is also influenced by the total power generation of the fuel cell cars. Figure 4.5(c) shows the total power generation of the fuel cell cars inside the microgrid. Note that during several ours per day, fuel cell cars do not generate any power. However, the generated power by fuel cell cars results in satisfying the system constraint on the maximum power imported into the microgrid. For example, by comparing Figures 4.2 and 4.5 at the hour 36, we observe that the power imported into the microgrid is below its upper limit because of the power generation of the fuel cell cars at this time.

In order to check the sufficiency of the produced hydrogen by the water electrolysis system, the simulation of the microgrid is now extended to an entire year while we consider the seasonal variation in RES power generation. The resulting energy flows in the microgrid are listed in Table 4.1. It can be inferred from Table 4.1 that around 70% of the total consumed energy of the microgrid is delivered via the renewable energy sources, while the share of fuel cell cars in generation of the electrical energy of the microgrid is only 3%. Even though the fuel cell cars generate only a small portion of the total energy in the microgrid, they play an important role in decreasing the required capacity of the electrical connection between the power grid and the microgrid. The residual load of the microgrid has a peak power demand of around 170 kW and it repeatedly exceeds 150 kW. If the optimization problem of the min-max MPC algorithm is feasible, we can conclude that even in the presence of uncertainty in the load and in the RES generation, the power imported into the microgrid does not exceed 80 kW. The reduction of the peak load in the microgrid is done using the fuel cell cars. Therefore, the presence of fuel cell cars plays an important role in reducing the peak of the imported power to the microgrid.

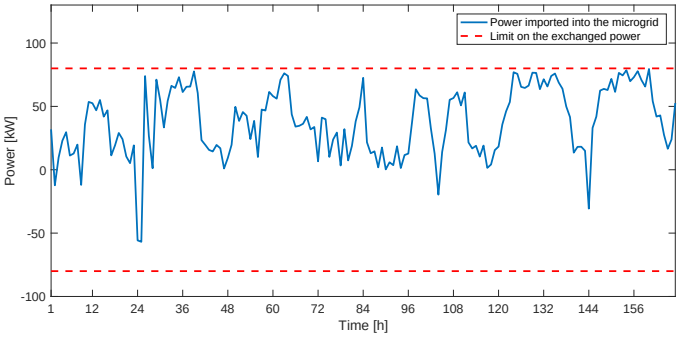

(a): Power imported into the microgrid from the power grid. The red dashed lines indicate the limits on the exchanged power between the power grid and the microgrid.

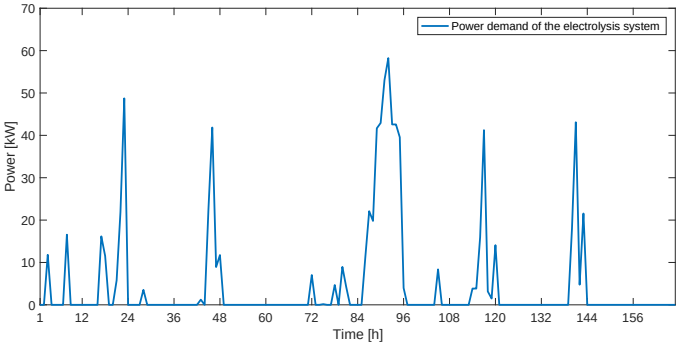

(b): Electrical power usage of the water electrolysis system.

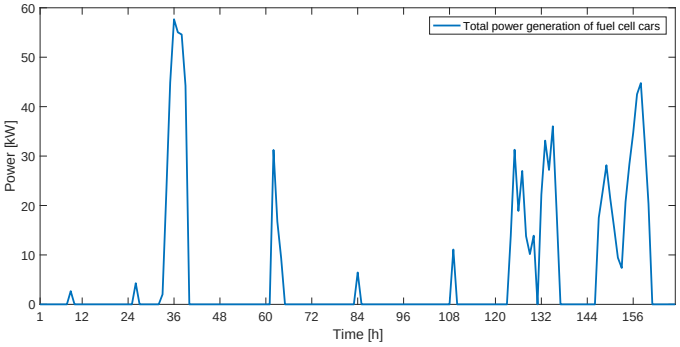

(c): Total power generation of the fuel cell cars.

Figure 4.5: Operation of the control system during a week.

Table 4.1: Electrical energy generation and consumption in one year

Electrical energy load/source	Generation [MWh]	Consumption [MWh]
Power grid	227	74
Households	0	680
Renewable energy sources	607	0
Fuel cell cars	24	0
Water electrolysis system	0	103

4.7 Conclusions

The presence of the FCEVs and the water electrolysis system in a microgrid creates the flexibility for the microgrid to store energy in the form of hydrogen and to regenerate electricity from the stored hydrogen. In the scenario developed in this chapter, hydrogen is the storage form of energy and it is used both for the transportation of the cars and for the generation of electricity. Our assumption is that RES can generate electricity with their maximum capacity and the fast variation in the power generation of RES is compensated inside the microgrid. As a result, the problem of congestion in the power network and fast variation in the power generation profile of the conventional power plants can be solved without curtailment in the RES generation. The tariff on power exchange between the microgrid and the power network influences the decision of the microgrid controller to export or import power from the power network. The influence of the power exchange tariff on the performance of the microgrid is a topic for future research. The simulation of the CaPP microgrid system illustrates the effectiveness of the developed control system.

In the system presented in this chapter, surplus renewable generation in the microgrid is stored in the form of hydrogen. Therefore, in the formulated scenario, i.e., when the RES power generation may exceed the total load of the system, the microgrid does not cause additional problems to the larger grid by injecting extra power into the grid. By making this hydrogen available for transportation purposes and for power generation by fuel cells, the use of FCEVs can reduce the well-to-wheel emissions in the transportation system as well as the carbon emissions related to power generation within the neighborhood.

5

Power Scheduling of Fuel Cell Cars in an Islanded Mode Microgrid with Private Driving Patterns

In this chapter, we consider a microgrid in the islanded mode, where the considered microgrid is not connected to the power network. The objective of the proposed control system is to minimize the operational cost of the system, subject to the physical and operational constraints of the system. In order to maintain the power balance of a microgrid in the islanded mode, the power generation of fuel cell cars should change according to the actual load of the microgrid and because the prediction of the load has some uncertainty, the actual power generation of the fuel cell cars also has some uncertainty. This chapter develops two model predictive control methods, namely, min-max control and disturbance feedback min-max control, for the power scheduling of the fuel cell cars inside the microgrid. Furthermore, three distributed control strategies are proposed for the min-max and the disturbance feedback min-max methods that require less computation time compared to the central control strategy. We show that by using these distributed strategies, the driving patterns of the fuel cell cars can be kept private. In other words, no privacy sensitive data on the usage of the cars is collected by a central control agent. Numerical case studies are presented to demonstrate the excellent performance of the proposed control methods.

The research presented in this chapter has been published in [5] and [6].

5.1 Introduction

In the considered islanded-mode microgrid of this chapter, a fleet of fuel cell cars is responsible for the power balance of the microgrid. Even though we assume that

the microgrid's load can be predicted, the uncertainty in the realization of the load enforces the fuel cell cars to deviate their power generation from the scheduled value for the sake of power balance. As a result, the power generation of the fuel cell cars deviates from the scheduled value with an uncertain value.

To understand the reason of this deviation, we need to take a look at different levels of control in a power system. Traditionally, three control levels exist in power systems, namely tertiary, secondary, and primary control. In tertiary control [38], set points for the amount of power generation are determined for each generator. The objective of this control level is to set the power generation profile of each generator in such a way that the power generation will be equal to the load of the power network. The operational cost of each generator and the system constraints, such as the maximum power generation of each generator, are also considered at this level. Model Predictive Control (MPC) is commonly used in tertiary control or power scheduling [69, 78, 61] and the control methods in this chapter are all based on MPC and designed for tertiary control. After solving the power scheduling problem, each generator receives a power generation profile from the tertiary controller. In an ideal power network, where the actual load is exactly equal to the predicted load, if all the generators follow their respective power generation profiles, the generated power will be equal to the load and, hence, the voltage and frequency of the system will remain in a specific value. However, the inaccuracy in the prediction of the load necessitates two other control levels for the generators that are called secondary and primary control levels. The objective of the secondary and primary controllers of each generator is to keep the voltage and frequency of the power system at a specific value for any realization of the load [82, 83, 49]. By assuming that the secondary and primary controllers are functional, regulation of the voltage and frequency still comes with the cost of deviating the actual power generation from the scheduled power generation that is determined by the tertiary controller. In this chapter, we show how this deviation can be taken into account while designing a control algorithm for the tertiary control level.

The rest of this chapter is organized as follows. The problem is formulated in Section 5.2. Model predictive control of the system with a centralized architecture is introduced in Section 5.3. The three distributed control methods are developed in Section 5.4 and the results of illustrative case studies are presented in Section 5.5.

5.2 Problem formulation

5.2.1 System description

We consider a problem setting in which a fleet of fuel cell cars is acting as the power generation source of a microgrid. Besides the fuel cell cars, wind turbines, solar photo voltaic cells, and diesel generators are the other sources of power generation. It is assumed that the microgrid is operated in the islanded mode, where there is not any electrical connection to the power grid, and there is no control over the load of the

microgrid. So the power balance should be maintained via the control of generation units. The goal of the microgrid's operator is, first, to allow the renewable energy sources to generate as much power as possible based on the weather conditions and, second, to penalize the use of the diesel generators. With these requirements, the power balance of microgrid should be realized by a suitable power scheduling of the fuel cell cars.

The objective of the control method proposed in this chapter is similar to a traditional tertiary control algorithm in the sense that the objective of the control algorithm is also to minimize the operational cost of the system while considering system constraints. However, a fleet of fuel cell cars in an islanded mode microgrid has some unique features that further challenge the controller design. In particular, the fuel cell cars are used both for power generation and transportation, the amount of fuel is limited, and refilling the cars takes time. These unique features necessitate a new design for the control system. The goal of the control system is to determine a power generation profile for each fuel cell car in such a way that the power balance of the microgrid is satisfied. In addition, the central control system should exclude from the power generation units those cars of which the owners intend to use them for transportation.

From an energy management point of view, the functioning of the primary and secondary control levels affects the power generation of the generator and, as a result, the generated power typically deviates from the scheduled power generation profile. Here, we assume that the primary and secondary control levels are present in each power generation unit and, as a result, the scheduled and the actual power generation are not necessarily equal to each other. The mismatch between the scheduled and the actual power generation is considered as an uncertain disturbance in the model of the system. With this abstraction of the influence of the primary and secondary control levels, we focus on the power scheduling problem at the tertiary level.

In the scenario considered here, the communication between different agents of a system is considered to be ideal. So, no delay, packet loss, nor cost is considered in the communication process. All the cars are connected to the microgrid whenever these are not used for transportation or refueling. In addition, each car is equipped with a computer that can operate the fuel cell of the car and exchange information with the central control system.

5.2.2 Mixed logical dynamical model of the system

One of the most significant features of the considered microgrid is that the fuel cell cars are used for two purposes: transportation and power generation. In addition, the fuel stored in each car is limited and refueling each car takes time. In this section, with inspiration from Chapter 4, a mixed logical dynamical model is developed for the system. Note that the model developed in this chapter is different from the one of Chapter 4, because in this chapter, we consider an islanded-mode microgrid, while in Chapter 4, we assumed that the microgrid is connected to the power grid.

We consider the remaining fuel in each car as a system state. Therefore, the system states can change both in the transportation and the power generation mode. The transportation mode of each car is determined by the driving pattern of the car owner. We assume that by studying the behavior of each driver, it is possible to determine the driving pattern of each driver for a finite horizon in the future from time step k to $k+N_{\rm p}$, where $N_{\rm p}$ is the prediction horizon. By defining $\mathcal{P}=\{0,1,\ldots,N_{\rm p}-1\}$ and $\mathcal{I}=\{1,\ldots,N_{\rm veh}\}$ with $N_{\rm veh}$ the total number of cars in the system, we can model the availability of a car $i\in\mathcal{I}$ for power generation at time steps $k+j$, for all $j\in\mathcal{P}$, with a sequence of binary variables $\lambda_{{\rm f},i}(k+j)$ for $i\in\mathcal{I}$ and $j\in\mathcal{P}$: if fuel cell car i is in the transportation mode at time step $k+j$, then $\lambda_{{\rm f},i}(k+j)$ is equal to 1, and otherwise it is 0. In addition, we assume that if a car arrives at the geographical area of the microgrid in the period $\big[(k-1)T_{\rm s},kT_{\rm s}\big)$, the amount of fuel that is used for that trip is predictable and described by $h_{{\rm f},i}(k)$. Therefore, we can assume that if a car is in the transportation mode, the fuel level remains the same, and at the time step k, i.e., the next time step after the arrival, it will be reduced with the amount $h_{{\rm f},i}(k)$. We also consider a specific mode for refilling a car where the fuel level is increased by $R_{{\rm f},i}$ at each time step. Note that as a microgrid can span a wide geographical region, and the fuel cell cars can be parked at different locations, we assume that hydrogen would be available only at a few spots. This is the main reason that we need to refill the hydrogen tank of fuel cell cars.

By considering the relation between the fuel consumption and the net power generation of a fuel cell [79], we can derive the following equation for the evolution of the fuel level of car $i\in\mathcal{I}$ in the power generation mode:

$$x_{{\rm f},i}(k+1)=x_{{\rm f},i}(k)-(\alpha_{{\rm f},i}u^*_{{\rm f},i}(k)+\beta_{{\rm f},i})T_{\rm s}, \tag{5.1}$$

where $\alpha_{{\rm f},i}$ and $\beta_{{\rm f},i}$ are parameters related to the fuel cell i and $T_{\rm s}$ is the sampling time interval. The actual power generation of fuel cell i at time step k is indicated by $u^*_{{\rm f},i}(k)$. Considering that the primary and secondary controllers may induce actual power generation levels that deviate from the scheduled level, we have:

$$u^*_{{\rm f},i}(k)=u_{{\rm f},i}(k)+\omega_i(k),\ \forall k, \tag{5.2}$$

where $u_{{\rm f},i}(k)$ indicates the scheduled power generation of fuel cell $i\in\mathcal{I}$ at time step k and $\omega_i(k)$ is an unknown time-varying deviation from the scheduled value.

By gathering all the operational modes of fuel cell car $i\in\mathcal{I}$, the following piecewise affine model describes the system dynamics:

$$x_{{\rm f},i}(k+1)=\begin{cases}x_{{\rm f},i}(k)+R_{{\rm f},i} & \text{refilling}\\ x_{{\rm f},i}(k) & \text{inactive}\\ x_{{\rm f},i}(k)-(\alpha_{{\rm f},i}u^*_{{\rm f},i}(k)+\beta_{{\rm f},i})T_{\rm s} & \text{generation}\\ x_{{\rm f},i}(k) & \text{transportation}\\ x_{{\rm f},i}(k)-h_{{\rm f},i}(k) & \text{arrival.}\end{cases} \tag{5.3}$$

The motivation behind this model has been discussed in more detail in Chapter 4. Note that a car in the driving mode influences the control system only by changing the remaining fuel in its tank. As the car is not used for the power generation until it returns to the microgrid's area, only the amount of remaining fuel at the arrival time is important. Therefore, the loss of communication when the car is out of range is not a problem.

To indicate the operational mode of fuel cell car $i \in \mathcal{I}$, we use two binary variables $s_{\mathrm{f},i}$ and $s_{\mathrm{r},i}$. The refilling mode at time step k is indicated by $s_{\mathrm{r},i}(k) = 1$; in other modes, we have $s_{\mathrm{r},i}(k) = 0$. The power generation mode corresponds to $s_{\mathrm{f},i}(k) = 1$ and, if $s_{\mathrm{f},i}(k) = 0$, the fuel cell i is turned off. It is assumed that while a fuel cell car is in the driving mode, it can neither generate power for the microgrid nor be refilled. These constraints can be represented by:

$$\begin{aligned} &\text{if } \lambda_{\mathrm{f},i}(k) = 1 \text{ then } s_{\mathrm{r},i}(k) = 0, \\ &\text{if } \lambda_{\mathrm{f},i}(k) = 1 \text{ then } s_{\mathrm{f},i}(k) = 0. \end{aligned}$$

We assume that if a fuel cell is being refilled, it cannot generate power. Other constraints in the operation of a fuel cell include the maximum level of power generation and the maximum fuel level. Moreover, a fuel cell can generate power only when the fuel level of the car is above a certain minimum level. These constraints can be represented as follows:

$$\begin{aligned} &\text{if } s_{\mathrm{r},i}(k) = 1 \text{ then } s_{\mathrm{f},i}(k) = 0, \\ &0 \leq u_{\mathrm{f},i}(k) \leq \bar{u}_{\mathrm{f},i}, \\ &\underline{x}_{\mathrm{f},i} s_{\mathrm{f},i}(k) \leq x_{\mathrm{f},i}(k) \leq \bar{x}_{\mathrm{f},i}. \end{aligned}$$

The equivalent MLD model [13] of the system in (5.3) with the constraints as explained above is given by:

$$\begin{aligned} &x(k+1) = x(k) + B_1(\omega(k))u(k) + B_3(k)z(k) + B_4(k), \\ &E_1 u(k) + E_4 x(k) + E_5(k) \geq E_3 z(k), \end{aligned} \tag{5.4}$$

where the vectors x, u, and z are defined as:

$$\begin{aligned} x &= \begin{bmatrix} x_{\mathrm{f},1}(k) & \dots & x_{\mathrm{f},N_{\mathrm{veh}}}(k) \end{bmatrix}^T, \\ u &= \begin{bmatrix} u_{\mathrm{f},1}(k) & s_{\mathrm{r},1}(k) & s_{\mathrm{f},1}(k) & \dots & u_{\mathrm{f},N_{\mathrm{veh}}}(k) & s_{\mathrm{r},N_{\mathrm{veh}}}(k) & s_{\mathrm{f},N_{\mathrm{veh}}}(k) \end{bmatrix}^T, \\ z &= \begin{bmatrix} z_{\mathrm{f},1}(k) & \dots & z_{\mathrm{f},N_{\mathrm{veh}}}(k) \end{bmatrix}^T. \end{aligned} \tag{5.5}$$

The continuous auxiliary variables $z_{\mathrm{f},i}$ are defined as $z_{\mathrm{f},i}(k) \triangleq s_{\mathrm{f},i}(k) u_{\mathrm{f},i}(k)$, for all $i \in \mathcal{I}$ and k. With defining $\mathrm{diag}\{.\}$ as a block diagonal matrix with the arguments as diagonal blocks, we can define matrices $B_1(k)$, $B_3(k)$, and $B_4(k)$ in (5.4) as

follows:

$$
\begin{aligned}
B_1(k) &= \mathrm{diag}\{b_1^1(k),\ \ldots,\ b_1^{N_{\mathrm{veh}}}(k)\},\\
B_3(k) &= \mathrm{diag}\{b_3^1(k),\ \ldots,\ b_3^{N_{\mathrm{veh}}}(k)\},\\
B_4(k) &= \begin{bmatrix} -\lambda_{\mathrm{f},1}(k)h_{\mathrm{f},1}(k) & \ldots & -\lambda_{\mathrm{f},N_{\mathrm{veh}}}(k)h_{\mathrm{f},N_{\mathrm{veh}}}(k) \end{bmatrix}^T,
\end{aligned}
$$

where $b_1^i(k) = \begin{bmatrix} 0 & R_{\mathrm{f},i} & (1-\lambda_{\mathrm{f},i}(k))\,T_{\mathrm{s}}(\beta_{\mathrm{f},i}+\alpha_{\mathrm{f},i}\omega_i(k)) \end{bmatrix}$ and $b_3^i = (1-\lambda_{\mathrm{f},i}(k))T_{\mathrm{s}}\alpha_{\mathrm{f},i}$, for $i \in \mathcal{I}$.

5.3 Centralized robust control for a CaPP system

The power scheduling problem of the considered microgrid can be solved by designing a central control system for the whole microgrid. In this scenario, a control center gathers all the relevant information from the devices in the microgrid, determines a power scheduling profile for each fuel cell car, and sends these profiles to each car. To determine the power scheduling profiles, the operational cost of the system over a finite horizon is minimized subject to the system constraints. In this section, two centralized MPC approaches are developed by considering the specific features of the system, such as the presence of some fuel cell stacks that are used both for power generation and for transportation.

5.3.1 Min-max control method

In the framework of model predictive control, the operational cost of the system is minimized over a finite time window with respect to the system constraints. The model for the system developed in Section 5.2.2 contains an uncertain variable, ω, see (5.2), and to deal with this uncertainty, a min-max control method is proposed in Chapter 4. In the min-max control method, the operational cost of the system is minimized for the worst-case realization of the uncertainty. In addition, by satisfying the system constraints for the worst-case uncertainty, the min-max control method guarantees the satisfaction of the constraints for any realization of the uncertainty.

We can define the following cost function for the system [3]:

$$
\begin{aligned}
J(k) = \sum_{j\in\mathcal{P}}\sum_{i\in\mathcal{I}} \big[& W_{\mathrm{p},i}u_{\mathrm{f},i}^2(k+j) + W_{\mathrm{s},i}|\Delta s_{\mathrm{f},i}(k+j)| \\
& + C_{\mathrm{e}}(k+j)\omega_i(k+j)\big],
\end{aligned} \tag{5.6}
$$

where $\Delta s_{\mathrm{f},i}(k+j)$ is defined as $s_{\mathrm{f},i}(k+j) - s_{\mathrm{f},i}(k+j-1)$. The two parameters, $W_{\mathrm{p},i}$ and $W_{\mathrm{s},i}$, determine the cost of power generation and the cost of switching the operational mode of a fuel cell. The value of $\omega_i(k+j)$ indicates the deviation from the scheduled power generation of fuel cell $i \in \mathcal{I}$ at time step $k+j$. This deviation is the result of an effort for stabilizing the microgrid. In order to encourage the fuel cell cars to stabilize the microgrid, we assume that each fuel cell $i \in \mathcal{I}$ gets a reward

equal to $C_{\mathrm{e}}(k+j)\omega_i(k+j)$ at time step $k+j$ for the willingness to deviate its actual power generation from the scheduled one by the amount of $\omega_i(k+j)$. This reward for fuel cell cars is an additional cost for the microgrid operator. We consider a predetermined value for this additional cost for each unit of power generation and hence the last term of (5.6) has a linear form with respect to the deviation ω_i. Note that the quadratic part of the cost function (5.6), i.e., $W_{\mathrm{p},i}u_{\mathrm{f},i}^2(k)$, is mainly the result of the degradation of the fuel cells due to the power generation. This part of the cost is defined in a quadratic way because by increasing the net power generation of a fuel cell, some auxiliary devices such as the fuel cell cooling system and the air compressor will be activated, which result in an increase in the operational cost.

By defining:

$$\tilde{\omega}_i(k) = \begin{bmatrix} \omega_i(k) & \dots & \omega_i(k+N_{\mathrm{p}}-1) \end{bmatrix}^T,$$

the operational cost of the system can be rewritten as:

$$J(k) = \sum_{i\in\mathcal{I}} \big(\tilde{V}_i^T(k)W_{\mathrm{q},i}(k)\tilde{V}_i(k) + W_{\mathrm{v},i}(k)\tilde{V}_i(k) + W_{\mathrm{d},i}(k)\tilde{\omega}_i(k)\big), \tag{5.7}$$

where $W_{\mathrm{q},i}$, $W_{\mathrm{v},i}$, and $W_{\mathrm{d},i}$ can be determined for all $i \in \mathcal{I}$ based on the values of $W_{\mathrm{p},i}$, $W_{\mathrm{s},i}$, and C_{e}, respectively. The vector of optimization variables, $\tilde{V}(k)$, is defined as:

$$\tilde{V}(k) = \begin{bmatrix} \tilde{V}_1^T(k) & \dots & \tilde{V}_{N_{\mathrm{veh}}}^T(k) \end{bmatrix}^T, \tag{5.8}$$

where $\tilde{V}_i(k)$ is the vector of optimization variables related to fuel cell $i \in \mathcal{I}$:

$$\tilde{V}_i(k) = \begin{bmatrix} \tilde{u}_i^T(k) & \tilde{z}_i^T(k) \end{bmatrix}^T. \tag{5.9}$$

The vectors $\tilde{u}_i$ and $\tilde{z}_i$ in (5.9) are the stacked version of u_i and z_i over time steps k to $k+N_{\mathrm{p}}-1$:

$$\tilde{u}_i(k) = \begin{bmatrix} u_i(k) & \dots & u_i(k+N_{\mathrm{p}}-1) \end{bmatrix}$$
$$\tilde{z}_i(k) = \begin{bmatrix} z_i(k) & \dots & z_i(k+N_{\mathrm{p}}-1) \end{bmatrix},$$

where

$$u_i(k) = \begin{bmatrix} u_{\mathrm{f},i}(k) & s_{\mathrm{r},i}(k) & s_{\mathrm{f},i}(k) \end{bmatrix}^T,$$
$$z_i(k) = s_{\mathrm{f},i}(k)u_{\mathrm{f},i}(k).$$

By extending the system constraints in (5.4) to all the time steps in the prediction window, we can determine matrices $G_{1,i}$, $G_{2,i}$, and $G_{3,i}$ such that the following inequalities describe the system constraints in the whole prediction window:

$$G_{1,i}(\tilde{\omega}(k))\tilde{V}_i(k) \le G_{2,i}(k) + G_{3,i}(k)x_i(k),\ \forall i \in \mathcal{I}. \tag{5.10}$$

The power balance condition is:

$$\sum_{i\in\mathcal{I}} u_{\mathrm{f},i}(k+j) = P_{\mathrm{d}}(k+j),\ \forall j \in \mathcal{P}, \tag{5.11}$$

where $P_{\mathrm{d}}(k+j)$ is the residual load of the microgrid at time step $k+j$, i.e., the microgrid's load minus the generated power by the renewable energy sources. The inequalities (5.10) and equalities (5.11) include all the operational constraints of the system.

We have separated the system constraints into two categories, (5.10) and (5.11), because each inequality in the first category is related to a single fuel cell car while the equality constraints in the second category involve all the cars. In a centralized architecture, both of the categories can be included in the optimization problem of the MPC controller. However, in a distributed architecture, the first part of constraints in (5.10), can be satisfied by individual cars, but to satisfy the second part in (5.11), a communication process between different agents is necessary. The specific communication process for the developed distributed methods will be explained in detail in Section 5.4.

In the min-max approach, the aim is to minimize the operational cost of the system for the worst-case uncertainty, while the system constraints are satisfied for any realization of the uncertainty. So, the following optimization problem should be solved at each time step k:

$$\begin{aligned}\min_{\{\tilde{V}_i(k)\}_{i\in\mathcal{I}}} \max_{\{\tilde{\omega}_i(k)\}_{i\in\mathcal{I}}} \sum_{i\in\mathcal{I}} \big(&\tilde{V}_i^T(k) W_{\mathrm{q},i}(k)\tilde{V}_i(k) + W_{\mathrm{v},i}(k)\tilde{V}_i(k) \\ &+ W_{\mathrm{d},i}(k)\tilde{\omega}_i(k)\big) \\ \text{subject to (5.10), (5.11), for all } \tilde{\omega}_i &\text{ where } i \in \mathcal{I}.\end{aligned} \tag{5.12}$$

We assume that the uncertainties are always realized within given bounds as follows:

$$\underline{\omega}_i \le \omega_i(k) \le \bar{\omega}_i, \text{ for all } i \in \mathcal{I} \text{ and } k. \tag{5.13}$$

The source of uncertainty is the errors in the prediction of the residual load, which contain the errors in the prediction of RES power generation and the microgrid's load. Note that because the microgrid is operated in the islanded-mode, the total power generation of fuel cell cars is equal to the residual load and, hence, the inaccuracy in the prediction of the residual load results in the presence of the uncertain parameters $\omega_i(k)$ for $i \in \mathcal{I}$. An extensive review on the different methods of forecasting the load is presented in [36] and based on this reference, a common forecasting method can be written in the form $p(t) = f(t) + v(t)$, where $p(t)$ is the predicted load, $f(t)$ is the value of a predetermined function, and $v(t)$ is a bounded noise at time t. Because the uncertain variables $\omega_i(k)$ for all $i \in \mathcal{I}$ are proportionally related to the error in the total load of the microgrid, we can define a minimum and a maximum level for realization of each $\omega_i(k)$.

As a result of (5.13), we can define the set Ω such that $[\tilde{\omega}_1^T(k)\ \dots\ \tilde{\omega}_{N_{\mathrm{veh}}}^T(k)]^T \in \Omega$, where for all $i \in \mathcal{I}$, all the elements of $\tilde{\omega}_i(k)$ comply with the inequalities in (5.13).

Lemma 5.3.1. *Define:*

$$\begin{aligned}
\hat{\omega}_{1,i}(k) &= \begin{bmatrix} \underline{\omega}_i(k) & \underline{\omega}_i(k+1) & \dots & \underline{\omega}_i(k+N_{\mathrm{p}}-1) \end{bmatrix}^T \\
\hat{\omega}_{2,i}(k) &= \begin{bmatrix} \underline{\omega}_i(k) & \underline{\omega}_i(k+1) & \dots & \bar{\omega}_i(k+N_{\mathrm{p}}-1) \end{bmatrix}^T \\
&\vdots \\
\hat{\omega}_{N,i}(k) &= \begin{bmatrix} \bar{\omega}_i(k) & \bar{\omega}_i(k+1) & \dots & \bar{\omega}_i(k+N_{\mathrm{p}}-1) \end{bmatrix}^T .
\end{aligned}$$

Given assumption (5.13)*, the following inequalities guarantee that inequality* (5.10) *is satisfied for any realization of* $\tilde{\omega}(k) \in \Omega$*:*

$$\begin{aligned}
& G_{1,i}(\hat{\omega}_{1,i}(k))\tilde{V}_i(k) \leq G_{2,i}(k) + G_{3,i}(k)x_i(k),\ \forall i \in \mathcal{I} \\
& \vdots \\
& G_{1,i}(\hat{\omega}_{N,i}(k))\tilde{V}_i(k) \leq G_{2,i}(k) + G_{3,i}(k)x_i(k),\ \forall i \in \mathcal{I},
\end{aligned} \tag{5.14}$$

Proof: Considering the structure of $G_{1,i}(\tilde{\omega}(k))$, $G_{2,i}(k)$, and $G_{3,i}(k)$, each row of inequality (5.10) can be written in the form:

$$\gamma_1\omega_i(k) + \gamma_2\omega_i(k+1) + \cdots + \gamma_{N_{\mathrm{p}}}\omega_i(k+N_{\mathrm{p}}-1) \leq a, \tag{5.15}$$

where $a \in \mathbb{R}$ and $\gamma_i \in \mathbb{R}$ for all i. The maximum value of the left-hand side of (5.15) will be realized at a specific realization of the uncertainty $\tilde{\omega}_i^*(k) = \begin{bmatrix}\omega_i^*(k) & \dots & \omega_i^*(k+N_{\mathrm{p}}-1)\end{bmatrix}^T$. The left-hand side of (5.15) is linear with respect to ω_i; moreover, $\underline{\omega}_i \leq \omega_i(k+j) \leq \bar{\omega}_i$ for all j. Therefore, there exists an n inside the set $\{1,\dots,N\}$ such that the value of $\tilde{\omega}_i^*(k)$ is equal to $\hat{\omega}_{n,i}(k)$ defined in Lemma 5.3.1. Based on (5.14), we know that (5.15) holds for $\hat{\omega}_{n,i}$ for all $n \in \{1,\dots,N\}$. Therefore, (5.15) holds for any realization of $\tilde{\omega}_i(k)$ that satisfies (5.13).

Equation (5.10) consists of several rows, all in the form of (5.15) and we have shown that (5.14) is a sufficient condition for the validity of (5.15). Therefore, the satisfaction of (5.14) implies the satisfaction of (5.10). □

By using the results of Lemma 5.3.1, the optimization problem (5.12) can be rewritten as follows:

$$\begin{aligned}
\min_{\tilde{V}_i(k), i\in\mathcal{I}} \ \max_{p\in\{1,\dots,N\}} & \textstyle\sum_{i\in\mathcal{I}} \big(\tilde{V}_i^T(k)W_{\mathrm{q},i}(k)\tilde{V}_i(k) \\
& + W_{\mathrm{v},i}(k)\tilde{V}_i(k) + W_{\mathrm{d},i}(k)\hat{\omega}_{p,i}(k)\big) \\
\text{subject to } & (5.14) \text{ and } (5.11).
\end{aligned} \tag{5.16}$$

The problem (5.16) is a mixed integer quadratic programming (MIQP) problem and can be solved by a standard solver such as Gurobi [39].

5.3.2 Disturbance feedback min-max control method

The min-max control method of Section 5.3.1 guarantees that the system constraints are satisfied for any realization of the disturbance. However, the level of conservatism in the min-max method may be considerable. In this section, an alternative

method, called disturbance feedback min-max control, is developed by using the idea of [87]. Even though the realized value of the disturbance is unknown to the controller, the presence of a disturbance feedback mechanism prevents the expansion of possible state trajectories in the prediction horizon. As a result, the disturbance feedback min-max controller is less conservative compared to the regular min-max controller of Section 5.3.1.

In the disturbance feedback min-max approach, a control law is considered for the sequence of future control inputs of fuel cell cars. For each time step $k+j$, the control input of fuel cell car i is determined as follows:

$$u_{\mathrm{f},i}(k+j) = v_{\mathrm{f},i}(k+j) + K_{\mathrm{f},i}(k+j)\omega_i(k+j-1),\ \forall i \in \mathcal{I} \tag{5.17}$$

where $v_{\mathrm{f},i}(k+j)$ and $K_{\mathrm{f},i}(k+j)$ are, respectively, the deterministic part of the scheduled power generation and the disturbance feedback gain for fuel cell car $i \in \mathcal{I}$ at time step $k+j$. The value of $\omega_i(k+j-1)$ is unknown before time step $k+j$ but after that, it can be determined by subtracting the actual power generation, $u^*_{\mathrm{f},i}(k+j-1)$, from the scheduled power generation, $u_{\mathrm{f},i}(k+j-1)$. Note that in the disturbance feedback method, the scheduled power generation, $u_{\mathrm{f},i}(k+j)$, at time step $k+j$ for $j \geq 1$ consists of two parts: a deterministic part, i.e., $v_{\mathrm{f},i}(k+j)$, and an unknown part, i.e., $K_{\mathrm{f},i}\omega_i(k+j-1)$. The value of the deterministic part of the scheduled power generation, $v_{\mathrm{f},i}$, and the feedback gain, $K_{\mathrm{f},i}$, are determined via solving an optimization problem for all $i \in \mathcal{I}$.

Using (5.17), the actual power generation of fuel cell cars can be still represented by (5.2). In addition, the model of fuel cell cars will remain the same. However, the matrices B_3 and E_1 in (5.4) will become functions of $\omega(k-1)$. The resulting MLD model is:

$$\begin{aligned} &x(k+1) = x(k) + B_1(w(k))u(k) + B_3(w(k-1))z(k) + B_4(k) \\ &E_1(w(k-1))u(k) + E_4x(k) + E_5(k) \geq E_3z(k), \end{aligned} \tag{5.18}$$

where the definition of x remains the same as in (5.5). The new definition of u and z is as follows:

$$\begin{aligned} &u(k) = \\ &[v_{\mathrm{f},1}(k)\ s_{\mathrm{r},1}(k)\ s_{\mathrm{f},1}(k)\ K_{\mathrm{f},1}(k)\ \ldots\ v_{\mathrm{f},N_{\mathrm{veh}}}(k)\ s_{\mathrm{r},N_{\mathrm{veh}}}(k)\ s_{\mathrm{f},N_{\mathrm{veh}}}(k)\ K_{\mathrm{f},N_{\mathrm{veh}}}(k)]^T \\ &z(k) = [z_{\mathrm{f},1}(k)\ z_{\mathrm{k},1}(k)\ \ldots\ z_{\mathrm{f},N_{\mathrm{veh}}}(k)\ z_{\mathrm{k},N_{\mathrm{veh}}}(k)]^T. \end{aligned} \tag{5.19}$$

The variable $K_{\mathrm{f},i}(k)$ represents the disturbance feedback gain for fuel cell car i at time step k and the new auxiliary variables are defined as $z_{\mathrm{k},i}(k) := K_{\mathrm{f},i}(k)s_{\mathrm{f},i}(k)$ for all $i \in \mathcal{I}$. By extending the inequality constraints in (5.18) over the prediction horizon we get:

$$G^{\mathrm{DF}}_{1,i}(\tilde{\omega}_i(k))\tilde{V}^{\mathrm{DF}}_i(k) \leq G^{\mathrm{DF}}_{2,i}(k) + G^{\mathrm{DF}}_{3,i}(k)x_i(k), \tag{5.20}$$

where $\tilde{V}_i^{\mathrm{DF}}(k)$ has the same definition as (5.9). The matrices $G_{1,i}^{\mathrm{DF}}$, $G_{2,i}^{\mathrm{DF}}$, and $G_{3,i}^{\mathrm{DF}}$ are different from the min-max approach, but the format given in (5.15) still applies to it. As a result, by following a similar approach as in the proof of Lemma 5.3.1, we can show that (5.20) will be satisfied if the following inequalities are satisfied:

$$\begin{aligned} & G_{1,i}^{\mathrm{DF}}(\hat{\omega}_{1,i}(k))\tilde{V}_i^{\mathrm{DF}}(k) \leq G_{2,i}^{\mathrm{DF}}(k) + G_{3,i}^{\mathrm{DF}}(k)x_i(k),\ \forall i \in \mathcal{I} \\ & \vdots \\ & G_{1,i}^{\mathrm{DF}}(\hat{\omega}_{N,i}(k))\tilde{V}_i^{\mathrm{DF}}(k) \leq G_{2,i}^{\mathrm{DF}}(k) + G_{3,i}^{\mathrm{DF}}(k)x_i(k),\ \forall i \in \mathcal{I}. \end{aligned} \tag{5.21}$$

The power balance constraint in the disturbance feedback min-max method can be expressed as:

$$\begin{cases} \sum_{i\in\mathcal{I}} u_{\mathrm{f},i}(k) = P_{\mathrm{d}}(k), \\ \sum_{i\in\mathcal{I}} v_{\mathrm{f},i}(k+j) = P_{\mathrm{d}}(k+j),\ j \in \{1,\ldots,N_{\mathrm{p}}-1\}. \end{cases} \tag{5.22}$$

The optimization problem of the model predictive controller at time step k can be written as:

$$\begin{aligned} \min_{\tilde{V}_i^{\mathrm{DF}}(k), i\in\mathcal{I}} \ \max_{p\in\{1,\ldots,N\}} \sum_{i\in\mathcal{I}} \Big(& (\tilde{V}_i^{\mathrm{DF}})^T(k) W_{\mathrm{q},i}^{\mathrm{DF}}(k) \tilde{V}_i^{\mathrm{DF}}(k) \\ & + W_{\mathrm{v},i}^{\mathrm{DF}}(k)\tilde{V}_i^{\mathrm{DF}}(k) + W_{\mathrm{d},i}^{\mathrm{DF}}(k)\hat{\omega}_{p,i}(k) \Big) \\ \text{subject to (5.21) and (5.22)}, & \end{aligned} \tag{5.23}$$

where $W_{\mathrm{q},i}^{\mathrm{DF}}(k)$, $W_{\mathrm{v},i}^{\mathrm{DF}}(k)$, and $W_{\mathrm{d},i}^{\mathrm{DF}}(k)$ are defined based on the cost function (5.6). Any standard MIQP solver, such as CPLEX [23] or Gurobi [39], can be used in order to solve the optimization problem (5.23).

The min-max and the disturbance feedback min-max methods are able to determine a power schedule for the fuel cell cars such that the system constraints are satisfied. In the disturbance feedback min-max approach, a feedback law on the future disturbances prevents the expansion of the possible state trajectories inside the predicted period and, as a result, the level of conservatism is lower compared to the min-max method [5]. However, in order to implement these methods, the driving patterns of all the fuel cell cars should be shared with a central controller. To increase the privacy level of the car owners, three distributed control methods are developed in the next section.

5.4 Distributed robust control for a CaPP system

In this section, three distributed control strategies based on the dual decomposition, the alternating direction method of multipliers (ADMM), and the proximal ADMM (PADMM) are developed in order to support the min-max and the disturbance feedback min-max approaches in a distributed fashion. In the developed methods, the

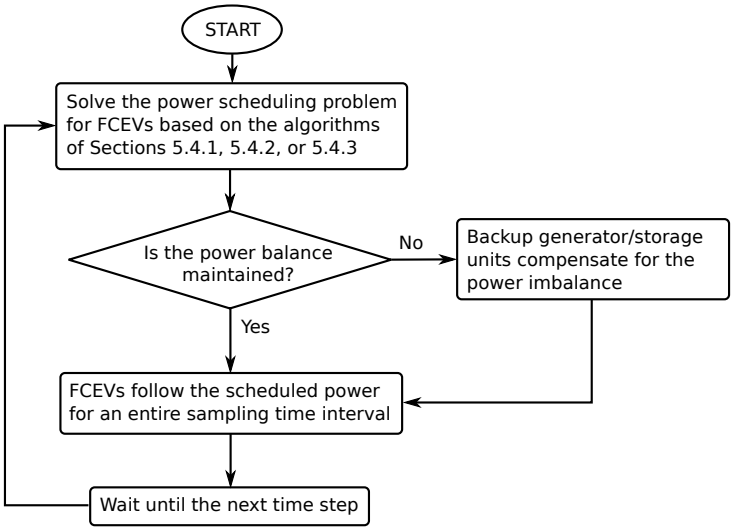

Figure 5.1: Workflow for the power scheduling.

driving patterns of the cars are kept private, i.e., there is no need to share the information about the departure or arrival time of the cars with any other agent.

The generic distributed control strategies employed in this section were originally developed for convex programming problems [15, 16, 27]. The presence of binary variables makes the optimization problems (5.16) and (5.23) non-convex and, hence, the developed algorithms might not converge at all or they might converge to a non-optimal point. The lack of convergence in the power scheduling process will result in an imbalance in the power generation and usage in the microgrid. However, the use of some diesel generators as backup generation units and some batteries to store energy can still guarantee the power balance condition of the microgrid. To decrease the usage of fossil fuels or batteries, we assume that the correction of power scheduling using backup generation and storage units is much more expensive compared to the generated power of a fuel cell. Therefore, an efficient control system minimizes the use of the backup generation or storage units to decrease the operational cost of the system.

The developed methods are based on iterations, i.e., an information exchange process between a coordinator and the cars. At the end of each iteration, the control system reaches a specific power schedule. If the power balance is satisfied or a maximum number of iterations is reached, the iteration process is terminated by the coordinator and the fuel cell cars generate the amount of power scheduled in the last iteration point; otherwise, the coordinator starts a new iteration. The backup generation and storage units are used when the iteration process is terminated while the power balance condition is not yet reached. This specific workflow for the power scheduling is depicted in Figure 5.1.

5.4.1 Dual decomposition method

In the dual decomposition approach, a new optimization problem, called the dual problem, is constructed based on the original problem, i.e., the primal problem, e.g., (5.16) or (5.23). In some cases, the structure of the dual problem allows us to solve it in a distributed fashion. As will be explained below, the dual problems of (5.16) and (5.23) can be separated across all the cars.

In the dual decomposition method, the dual problem is solved in a distributed fashion. Because the optimization problems are not convex, the optimum value of the dual problem might be smaller than that of the primal problem. In other words, there might be a duality gap [15]. The presence of a duality gap means that the power scheduling process has not reached the balance condition yet; in this case, the backup generation and storage units will be used to guarantee the power balance condition.

The min-max problem (5.16) consists of N MIQP problems, where the pth MIQP (primal) problem is formulated as:

$$\begin{aligned} \mathrm{P}: \quad \min_{\tilde{V}_i(k), i\in\mathcal{I}} \sum_{i\in\mathcal{I}} \big(\tilde{V}_i^T(k) W_{\mathrm{q},i}(k)\tilde{V}_i(k) + W_{\mathrm{v},i}(k)\tilde{V}_i(k) \\ + W_{\mathrm{d},i}(k)\hat{\omega}_{p,i}(k)\big) \\ \text{subject to (5.11) and (5.14)}, \end{aligned} \tag{5.24}$$

and its dual problem can be written as:

$$\begin{aligned} \mathrm{D}: \quad \max_{\lambda(k)\in\mathbb{R}^{N_\mathrm{p}}} \min_{\tilde{V}_i(k), i\in\mathcal{I}} \sum_{i\in\mathcal{I}} \big(\tilde{V}_i^T(k) W_{\mathrm{q},i}(k)\tilde{V}_i(k) \\ + W_{\mathrm{v},i}(k)\tilde{V}_i(k) + W_{\mathrm{d},i}(k)\hat{\omega}_{p,i}(k)\big) \\ + \lambda^T(k)\big(\tilde{u}_\mathrm{t}(k) - \tilde{P}_\mathrm{d}(k)\big) \\ \text{subject to (5.14)}, \end{aligned} \tag{5.25}$$

where $\tilde{u}_\mathrm{t}(k)$ and $\tilde{P}_\mathrm{d}(k)$ are the stacked versions of u_t and P_d over time steps k to $k+N_\mathrm{p}$, i.e.,

$$\begin{aligned} \tilde{u}_\mathrm{t}(k) &= \begin{bmatrix} u_\mathrm{t}(k) & \dots & u_\mathrm{t}(k+N_\mathrm{p}-1) \end{bmatrix}^T \\ \tilde{P}_\mathrm{d}(k) &= \begin{bmatrix} P_\mathrm{d}(k) & \dots & P_\mathrm{d}(k+N_\mathrm{p}-1) \end{bmatrix}^T. \end{aligned}$$

The variable $u_\mathrm{t}(k)$ represents the total power generation of fuel cell cars at time step k: $u_\mathrm{t}(k) = \sum_{i\in\mathcal{I}} u_{\mathrm{f},i}(k)$.

With a given value for $\lambda(k)$, the minimization part of (5.25) can be separated, i.e., distributed, between the cars. For fuel cell car number $i \in \mathcal{I}$, the following problem should be solved:

$$\begin{aligned} \tilde{V}_i^*(k) = \quad \arg\min_{\tilde{V}_i(k)} \big(\tilde{V}_i^T(k) W_{\mathrm{q},i}(k)\tilde{V}_i(k) + W_{\mathrm{v},i}(k)\tilde{V}_i(k) \\ + W_{\mathrm{d},i}(k)\hat{\omega}_{p,i}(k)\big) + \lambda^T(k)\tilde{u}_{\mathrm{f},i}(k)\big), \end{aligned} \tag{5.26}$$

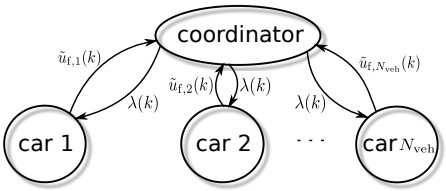

Figure 5.2: Information exchanged between the coordinator and the fuel cell cars during one iteration at time step k using the dual decomposition approach.

subject to:

$$\begin{aligned} &G_{1,i}(\hat{\omega}_{1,i}(k))\tilde{V}_i(k) \leq G_{2,i}(k) + G_{3,i}(k)x_i(k) \\ &\vdots \\ &G_{1,i}(\hat{\omega}_{N,i}(k))\tilde{V}_i(k) \leq G_{2,i}(k) + G_{3,i}(k)x_i(k). \end{aligned} \tag{5.27}$$

All the optimization variables in (5.26) belong to a single car and the problem can be solved without any dependencies on other fuel cell cars. The solution of (5.26) and (5.27), $\tilde{V}_i^*(k)$, is in fact a function of $\lambda(k)$, where $\lambda(k+j)$ for $j \in \mathcal{P}$ can be interpreted as a signal to determine the need for power generation in different time steps. A lower value for $\lambda(k)$ indicates more need for power generation at time step k. The maximization part of (5.25) is called the master problem and can be written in the following form:

$$\max_{\lambda(k)\in\mathbb{R}^{N_{\mathrm{p}}}} \sum_{i\in\mathcal{I}} \tilde{V}_i^*(\lambda(k)). \tag{5.28}$$

Note that $\sum_{i\in\mathcal{I}} \tilde{V}_i^*(\lambda(k))$ is a concave function of $\lambda(k)$, because it is the minimum of a collection of linear functions in $\lambda(k)$. So, (5.28) can be solved by a gradient ascent algorithm. We consider a coordinator to solve the master problem (5.28). Note that only the variables related to the power generation, $u_{\mathrm{f},i}(k+j)$, for $i \in \mathcal{I}$ and $j \in \mathcal{P}$, are involved in the master problem (5.28) and, hence, driving patterns of the cars, i.e., $\lambda_{\mathrm{f},i}(k+j)$, for $i \in \mathcal{I}$ and $j \in \mathcal{P}$, are not required for solving the master problem. Therefore, no privacy-sensitive data on usage of the cars needs to be shared between the fuel cell cars and a central coordinator. The information exchanged between the coordinator and the fuel cell cars is demonstrated in Figure 5.2.

The optimization problem (5.25) can be solved by using a specific protocol for the coordinator and the fuel cell cars, respectively described in Algorithms 5.1 and 5.2. The proposed algorithm solves the dual problem (5.25) first, and in the case that the duality gap does not exist, the power scheduling task is completed until the next time step. Otherwise, the backup generation units are scheduled in order to provide the power balance condition in the microgrid.

Algorithm 5.1 Workflow of the coordinator in the dual decompostion approach.

procedure
initialization:
  update k as the current time step
  update the prediction $\tilde{P}_{\mathrm{d}}(k)$ of the residual load
  $\lambda(k) \leftarrow \mathbf{0}$
  $i \leftarrow 0$
loop:
  send a message to all the cars to announce the value of $\lambda(k)$
  wait until all the messages of the cars regarding $u_{\mathrm{f},i}(k+j)$ for $i \in \mathcal{I}$ and $j \in \mathcal{P}$ are received (see Algorithm 5.2)
  if power balance is reached, **then**
    goto *implementation*
  end if
  update $\lambda(k)$ by solving (5.28)
  $i \leftarrow i + 1$
  if i has reached the maximum number of iterations, **then**
    goto *compensation*
  end if
  goto *loop*.
compensation for power unbalance:
  $\tilde{e}(k) \leftarrow \tilde{P}_{\mathrm{d}}(k) - \tilde{u}_{\mathrm{t}}(k)$
  set the power schedule of backup resources as $\tilde{e}(k)$
  goto *implementation*
implementation:
  send a message to all the cars to announce the completion of power scheduling
  wait until the next time step, then **goto** *initialization*
end procedure

5.4.2 ADMM method

In the method of Alternating Direction Method of Multipliers (ADMM), the dual problem is constructed based on an augmented Lagrangian function, L_ρ [16]. By considering the definition of the cost function in (5.7) and the power balance constraint, the augmented Lagrangian function is of the form:

$$\begin{aligned} L_\rho(\tilde{u}(k), \tilde{z}(k), \lambda) = J(k) + \lambda^T(\tilde{u}_{\mathrm{t}}(k) - \tilde{P}_{\mathrm{d}}(k)) \\ + \tfrac{\rho}{2}||\tilde{u}_{\mathrm{t}}(k) - \tilde{P}_{\mathrm{d}}(k)||_2^2 \ , \end{aligned} \tag{5.29}$$

where ρ is a penalty parameter. The dual problem is then:

$$\begin{aligned} \mathrm{D}: \ & \max_{\lambda \in \mathbb{R}^{N_{\mathrm{P}}}} \ \min_{\tilde{u}(k), \tilde{z}(k)} \ L_\rho(\tilde{u}(k), \tilde{z}(k), \lambda) \\ & \text{subject to (5.14).} \end{aligned} \tag{5.30}$$

Algorithm 5.2 Workflow of fuel cell car i in the dual decompostion approach.

procedure
initialization:
  update k as the current time step
  update the driving pattern and the fuel level
listen:
  listen to the coordinator until a message m arrives
  if m is an update about $\lambda(k)$ **then**
    goto *optimization*
  else if m is the announcement of implementation **then**
    goto *implementation*
  end if
optimization
  solve (5.26) with the given $\lambda(k)$ and determine $\tilde{V}_i^*(k)$
  send $\tilde{u}_{\mathrm{f},i}(k)$ to the coordinator
implementation:
  operate the fuel cell based on $\tilde{V}_i^*(k)$ for a period of T_s
  goto *initialization*
end procedure

Based on the ADMM approach, in order to solve (5.30), each fuel cell requires to solve the following optimization problem:

$$\begin{aligned} &\min_{\tilde{u}_i(k),\tilde{z}_i(k)} \; L_{\rho,i}(\tilde{u}_i(k), \tilde{z}_i(k), \tilde{u}_{\mathrm{r},i}(k), \lambda) \\ &\text{subject to (5.27)}, \end{aligned} \tag{5.31}$$

where $L_{\rho,i}$ and $\tilde{u}_{\mathrm{r},i}(k)$ are defined as follows:

$$\begin{aligned} L_{\rho,i}(k,\lambda) &= J_i(k) + \lambda^T(\tilde{u}_{\mathrm{f},i}(k) + \tilde{u}_{\mathrm{r},i}(k) - \tilde{P}_\mathrm{d}(k)) \\ &\quad + \tfrac{\rho}{2}||\tilde{u}_{\mathrm{f},i}(k) + \tilde{u}_{\mathrm{r},i}(k) - \tilde{P}_\mathrm{d}(k)||_2^2 \\ \tilde{u}_{\mathrm{r},i}(k) &= \begin{bmatrix} u_{\mathrm{r},i}(k) & \dots & u_{\mathrm{r},i}(k+N_\mathrm{p}-1) \end{bmatrix}^T. \end{aligned}$$

In the above definition, $J_i(k)$ is a part of the cost function (5.6) related to fuel cell i and $u_{\mathrm{r},i}(k)$ is the total power generation of all the fuel cells except fuel cell i at time step k as follows:

$$\begin{aligned} J_i(k) &= \sum_{j\in\mathcal{P}} \big(W_{\mathrm{p},i} u_{\mathrm{f},i}^2(k+j) + W_{\mathrm{s},i}|\Delta s_{\mathrm{f},i}(k+j)| \\ &\quad + C_\mathrm{e}(k+j)\omega_i(k+j)\big), \\ u_{\mathrm{r},i}(k) &= \sum_{n\in\mathcal{I}} u_{\mathrm{f},n}(k) - u_{\mathrm{f},i}(k). \end{aligned}$$

If the value of $\tilde{u}_{\mathrm{r},i}(k)$ is known for fuel cell i, (5.31) can be written as an MIQP problem:

$$\min_{\tilde{V}_i(k)} \tilde{V}_i^T(k) M_{\mathrm{q},i}(k) \tilde{V}_i(k) + M_{\mathrm{v},i}(k) \tilde{V}_i(k)$$
$$\text{subject to (5.27)}, \tag{5.32}$$

where $M_{\mathrm{q},i}(k)$ and $M_{\mathrm{v},i}(k)$ can be determined based on the model and driving pattern of fuel cell car i.

In the ADMM method, different agents solve their minimization problem one after another. In fact, each agent minimizes the augmented Lagrangian function by assuming that all the other agents have already made their decision. The determined solution, or the decision of the agent, will be shared with the next agent and the same procedure will be repeated until the last agent. After solving the last optimization problem, the coordinator will be informed about the decisions of all the agents. The coordinator executes a gradient ascent algorithm and as a result, new values for the Lagrangian multipliers will be determined. The coordinator propagates these updated values among all the agents. In our problem formulation, only the power generation profiles of the fuel cells are involved in the global constraint. Therefore, there is no need to share all the optimization variables with other agents. It is worth mentioning that the driving patterns of the cars can also be kept private, as they are not directly involved in the global constraint.

To solve the optimization problem (5.30) in a distributed fashion using the ADMM method, the following algorithm is executed at each time step k. First, the coordinator propagates an initial value for $\lambda(k)$ and all the fuel cell cars update the value of $\lambda(k)$ accordingly. Then, $\tilde{u}_{\mathrm{t}}(k)$ is set to a zero vector of appropriate size and its value is transmitted to fuel cell car 1 to solve a minimization problem of the form (5.32) with $i = 1$. This agent later updates $\tilde{u}_{\mathrm{t}}(k)$ according to the determined values for the optimization variables and passes it to the next agent. The same procedure is followed for each agent. The last agent sends back the updated value of $\tilde{u}_{\mathrm{t}}(k)$ to the coordinator. Based on a gradient ascent algorithm and the new value of $\tilde{u}_{\mathrm{t}}(k)$, the coordinator updates the value of $\lambda(k)$. At this point, the first iteration is completed. In the next iteration, the coordinator propagates $\lambda(k)$ to all the agents and sends the latest value of $\tilde{u}_{\mathrm{t}}(k)$ to the first agent. The next iterations are similar to the first one, except that each agent with number i subtracts the latest determined value for $\tilde{u}_{\mathrm{f},i}(k)$ from $\tilde{u}_{\mathrm{t}}(k)$ in order to determine the value of $\tilde{u}_{\mathrm{r},i}(k)$. At the end of each iteration, the coordinator decides whether another iteration is required. The iterations are terminated in two cases: the current power schedule satisfies the power balance or the maximum number of iterations is reached. In the latter case, similar to the dual decomposition approach in Section 5.4.1, the backup generation and storage units are used to compensate the error in the scheduled power. In any case, after termination of the iterations, all fuel cell cars pursue the power schedule determined at the last iteration until the next sampling time instant.

Figure 5.3 demonstrates the exchange of information between the coordinator

and the cars. Algorithm 5.3 describes the procedure for the coordinator in the ADMM approach and this algorithm differs from the one described in Algorithm 5.1 only in two points; the first difference is that a new variable, $\tilde{u}_{\mathrm{t}}(k)$ is initialized with a zero vector. The second difference is that at line 10 of this algorithm, the coordinator sends $\tilde{u}_{\mathrm{t}}(k)$ to the first car and waits until receiving the updated value of $\tilde{u}_{\mathrm{t}}(k)$ from the last car. Algorithm 5.4 indicates the procedure that each fuel cell car executes in the ADMM approach.

Algorithm 5.3 Workflow of the coordinator in the ADMM approach.

1: **procedure**
2: *initialization*:
3: update k as the current time step
4: update the prediction $\tilde{P}_{\mathrm{d}}(k)$ of the residual load
5: $\lambda(k) \leftarrow \mathbf{0}$
6: $\tilde{u}_{\mathrm{t}} \leftarrow \mathbf{0}$
7: $i \leftarrow 0$
8: *loop*:
9: send a message to all the cars to announce the value of $\lambda(k)$
10: send a message to fuel cell car 1 to announce the value of $\tilde{u}_{\mathrm{t}}(k)$
11: wait until a message from fuel cell car N_{veh} is received regarding an update for $\tilde{u}_{\mathrm{t}}(k)$ (see Algorithm 5.4)
12: **if** power balance is reached, **then**
13: **goto** *implementation*
14: **end if**
15: update $\lambda(k)$ by solving (5.28)
16: $i \leftarrow i + 1$
17: **if** i has reached the maximum number of iterations, **then**
18: **goto** *compensation for power unbalance*
19: **end if**
20: **goto** *loop*.
21: *compensation for power unbalance*:
22: $\tilde{e}(k) \leftarrow \tilde{P}_{\mathrm{d}}(k) - \tilde{u}_{\mathrm{t}}(k)$
23: set the power schedule of backup resources as $\tilde{e}(k)$
24: **goto** *implementation*
25: *implementation*:
26: send a message to all the cars to announce the completion of power scheduling
27: wait until the next time step, then **goto** *initialization*
28: **end procedure**

5.4.3 PADMM method

In the Proximal Alternating Direction Method of Multipliers (PADMM) [27], the coordinator and all the cars are following the same procedure as described in Section 5.4.2. However, the optimization problem that is solved in the fuel cell cars is

Algorithm 5.4 Workflow of fuel cell car i in the ADMM approach.

procedure
initialization:
  update k as the current time step
  update the driving pattern and the fuel level
listen:
  wait for an incoming message, m
  if m is an update about $\lambda(k)$ and $\tilde{u}_{\mathrm{t}}(k)$ **then**
    goto *optimization*
  else if m is the announcement of implementation **then**
    goto *implementation*
  end if
optimization
  solve (5.32) with the given $(\lambda(k), \tilde{u}_{\mathrm{t}}(k))$ and determine $\tilde{V}_i^*(k)$
  update $\tilde{u}_{\mathrm{t}}(k)$ based on the new value of $\tilde{V}_i^*(k)$
  if i is equal to N_{veh} **then**
    send $\tilde{u}_{\mathrm{t}}(k)$ to the coordinator
  else
    send $\tilde{u}_{\mathrm{t}}(k)$ to the next agent
  end if
  goto *listen*
implementation:
  operate the fuel cell based on $\tilde{V}_i^*(k)$ for a period of T_{s}
  goto *initialization*
end procedure

different because a proximal term is added to the objective function. So, rather than solving (5.32), fuel cell i solves the following problem during each iteration for time step k:

$$\begin{aligned}&\min_{\tilde{V}_i(k)} \tilde{V}_i^T(k) M_{\mathrm{q},i}(k) \tilde{V}_i(k) + M_{\mathrm{v},i}(k) \tilde{V}_i(k) \\ &\quad + \tfrac{1}{2}(\tilde{V}_i(k) - V_i^{\mathrm{prev}}(k))^T Q_i (\tilde{V}_i(k) - V_i^{\mathrm{prev}}(k)) \\ &\text{subject to (5.27)},\end{aligned} \tag{5.33}$$

where $V_i^{\mathrm{prev}}(k)$ indicates the vector of optimization variables related to agent i determined at the previous iteration. At the first iteration, we assume that $V_i^{\mathrm{prev}}(k) = 0$. The matrix Q_i is a weight factor. The purpose of adding the proximal term to the objective function of each agent is to achieve a faster convergence compared to the ADMM method [27, 93]. Note that (5.33) is still an MIQP problem.

5.5 Illustrative case studies

In this section, the results of simulating the developed control methods in different microgrids are reported. The total number of fuel cell cars, N_{veh}, in the microgrid is

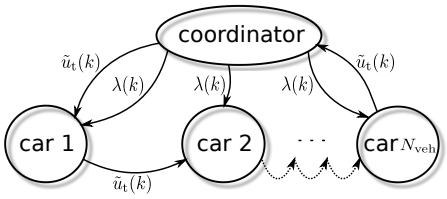

Figure 5.3: Information exchanged between the coordinator and the fuel cell cars during one iteration at time step k using the ADMM approach.

variable among different simulation scenarios. In line with [79], the characteristics of fuel cell i are given by $\alpha_{{\rm f},i} = 0.05 + 0.001i + \gamma_{\alpha,i}$ and $\beta_{{\rm f},i} = 0.09 + 0.0001i + \gamma_{\beta,i}$; so note that the characteristics are different for each fuel cell. The parameters $\gamma_{\alpha,i}$ and $\gamma_{\beta,i}$ represent the difference between the simulation model of the plant and the model that is used in the controller. Their values are set to zero in the control model, while in the simulation, we selected random real numbers in the range [-0.001, 0.001] for $\gamma_{\alpha,i}$ and [-0.002, 0.002] for $\gamma_{\beta,i}$. The maximum power generation of any fuel cell, $\bar{u}_{{\rm f},i}$, is assumed to be 15 kW and the fuel tank of any car has a capacity $\bar{x}_{{\rm f},i}$ of 5 kg for all $i \in \mathcal{I}$. In order to preserve some fuel for transportation purposes, we consider $\underline{x}_{{\rm f},i} = 2$ kg as the minimum level of fuel in each car. The time interval between two consecutive time steps, $T_{\rm s}$, is 15 minutes.

The values of $W_{{\rm p},i}$ and $W_{{\rm s},i}$ in the cost function (5.6) are $0.5 + 0.005i$ and $1.5 + 0.005i$, respectively. We consider a number of cars, $N_{\rm veh}$, that varies from 4 to 50. Following the standard tuning rule in MPC [33], we have selected the prediction horizon in such a way that during the prediction horizon window, the most important dynamics of the system can be covered. For example, $N_{\rm p} = 6$ can cover the refilling process and power generation of a car in the future. Any prediction horizon around this number is suitable for our application and we use $N_{\rm p}$ = 4, 6, and 8 to show that the improvement of the performance by using disturbance feedback min-max approach is not dependent on the specific selection of the control horizon.

The upper and lower bounds on the uncertainty of power generation of each fuel cell are assumed to have equal magnitude, but different signs, i.e., $\bar{\omega}_i = -\underline{\omega}_i$. The value of $\bar{\omega}_i$ varies from 0.5 kW to 2 kW for all $i \in \mathcal{I}$ in different simulations, but we assume that in each simulation $\bar{\omega}_i$ is the same for all $i \in \mathcal{I}$. Figure 5.4 depicts the residual load, $P_{\rm d}(k)$, of a microgrid that contains 4 fuel cell cars during the 10 hours of our simulation. In the rest of our case studies, the residual load will increase in direct proportion to the number of the cars. In order to obtain a comparison between the systems with different sizes, we consider that the fuel cell cars do not leave the microgrid. The refilling rate of all cars, $R_{{\rm f},i}$ for all i, is considered to be 2 kg per time step.

The value of 0.1 is selected for the penalty parameter, ρ, in the ADMM and PADMM methods. In order to solve the optimization problems of the PADMM

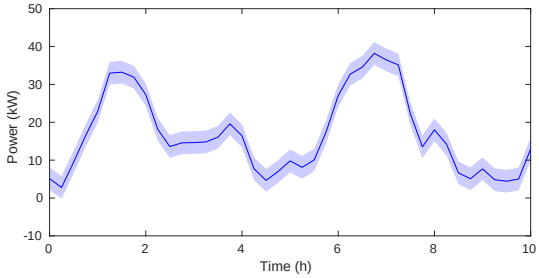

Figure 5.4: Residual load of the microgrid, $P_{\mathrm{d}}(k)$, with 4 fuel cell cars. The solid line indicates the predicted value, while the actual residual load will be realized inside the shaded area.

method fast, the weight factor Q_i is determined to have a diagonal form $Q_i = \mathrm{diag}\{W_{\mathrm{s},i}\mathbf{I}_{3N_{\mathrm{veh}}\times 3N_{\mathrm{veh}}}, \mathbf{0}_{N_{\mathrm{veh}}\times N_{\mathrm{veh}}}\}$ for the min-max method. In the disturbance feedback min-max method, the structure of Q_i remains the same, while the size of the diagonal blocks changes with respect to the changes in the size of $\tilde{u}_i(k)$ and $\tilde{z}_i(k)$.

Table 5.1 lists the performance of the two developed centralized approaches, i.e., the min-max approach and the disturbance feedback min-max approach, for a microgrid containing 4 fuel cell cars. The results show that for different values of the prediction horizon, N_{p}, and the disturbance bound, $\bar{\omega}_i$, the disturbance feedback min-max approach outperforms the min-max approach. These results are as expected, because the level of conservatism in the disturbance feedback approach is less than in the min-max approach.

In order to compare the performance of the three distributed control approaches, the system is first simulated with a central control system. Then, the operational cost of each distributed control approach is compared to the centralized solution in order to determine a measure for the loss of performance induced by the distributed solution. For example, if the operational cost of the system using the dual decomposition system is determined by J_{dd} and the centralized MPC cost is J_{c}, we define the performance loss, e_{dd}, as follows:

$$e_{\mathrm{dd}} \triangleq \left| \frac{J_{\mathrm{dd}} - J_{\mathrm{c}}}{J_{\mathrm{c}}} \right| \cdot 100\%.$$

A lower value for e_{dd} indicates that the performance of the dual decomposition approach is closer to the centralized solution. Similarly, we define two other measures for the performance loss, e_{admm} and e_{padmm}, related to the ADMM and PADMM approaches. Figure 5.5 depicts the performance loss of each distributed control method when the number of fuel cell cars is changing, for $N_{\mathrm{p}} = 6$, and $\bar{\omega}_i = 1$. For the ADMM and PADMM methods, the performance loss drops significantly when the number of fuel cell cars in the system increases. In fact, when the number of fuel cell cars in the system increases, the influence of a single fuel cell car on the total power generation decreases. So, the influence of binary variables $s_{\mathrm{f},i}$

Table 5.1: Operational cost of a microgrid with a centralized control architecture using the disturbance feedback min-max (DF) approach and the min-max (MM) approach.

N_{p}	4		6		8	
$\bar{\omega}_i$	MM	DF	MM	DF	MM	DF
0.5	2064.20	1818.91	2082.39	1876.21	2079.55	1900.61
1	2068.44	1761.74	2086.53	1754.12	2084.05	1851.52
1.5	2094.26	1698.76	2098.83	1508.34	2093.41	1482.97
2	2114.67	1453.71	2119.25	1511.26	2114.81	1552.50

and $s_{\mathrm{r},i}$ for $i \in \mathcal{I}$, on the total power generation decreases when the number of fuel cell cars in the system increases. As a result, the optimization problem becomes similar to a convex programming problem with the same form, but with continuous variables. We also know that in a convex programming problem the solution of primal and dual problems are identical. This fact explains the decrease of performance loss in ADMM and PADMM when the number of fuel cell cars in the system increases. For a system with a small number of fuel cell cars, compared to the other distributed methods using the disturbance feedback min-max approach, the performance of PADMM is the closest to the one of the centralized solution.

In general, the reason for the performance loss in all the distributed methods is that in some time steps the power balance is achieved by using the auxiliary generator/batteries. In the distributed control architectures, two types of power generators/storage are used. The first type is the fleet of fuel cell cars and the second type is auxiliary generator/batteries. In the case that the power balance is not maintained by the fuel cell car, the auxiliary generator/battery is used to maintain the power balance. As this auxiliary equipment is much more expensive to operate compared to fuel cell cars, in the case that there is a mismatch between the power generation of fuel cell cars and the residual load of the microgrid, the power balance is maintained by using the auxiliary equipment and, hence, the operational cost increases. The large performance loss of dual decomposition method is mainly the result of a relatively high level of power imbalance after scheduling the power generation profile of all the fuel cell cars.

In order to show the satisfactory performance of the distributed ADMM and PADMM approaches when the number of fuel cell cars is high enough, we have simulated different scenarios by considering different levels of the disturbance and different values for the prediction horizon. Tables 5.2 and 5.3 indicate the results of this set of simulations and, as a result, we can check that for different values of N_{p} and $\bar{\omega}_i$, the performance loss of the two distributed approaches with respect to the centralized approach remains small.

In the two centralized control methods, i.e., the centralized min-max method and the centralized disturbance feedback min-max method, the driving patterns of the cars are shared with a centralized controller. In the rest of the methods, i.e., all the distributed methods, the driving patterns are kept private. Figure 5.5 shows a

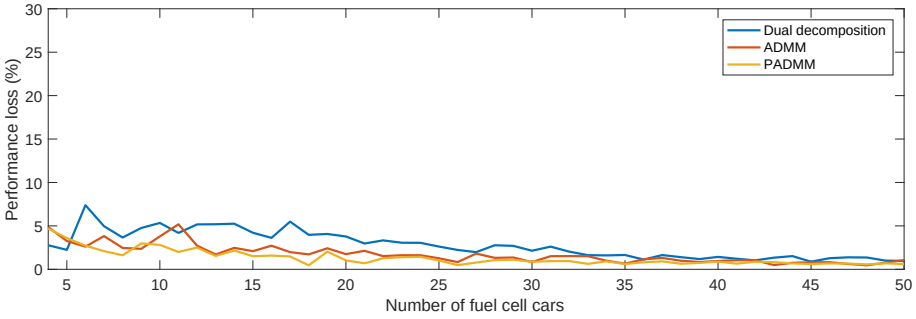

(a)

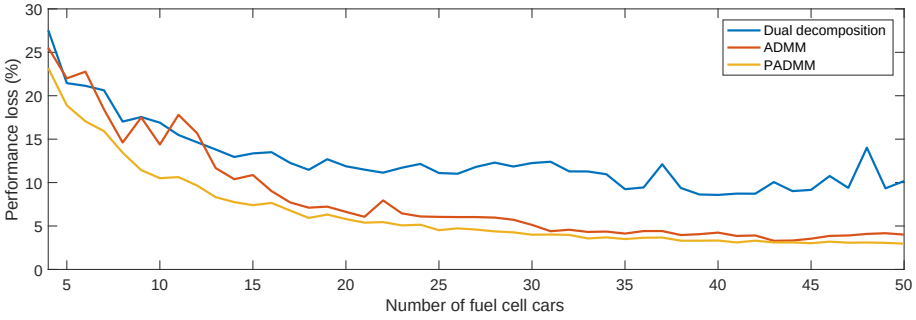

(b)

Figure 5.5: Performance loss of distributed control systems, e_{dd}, e_{admm}, and e_{padmm}, with respect to the number of fuel cell cars inside the system for (a) the min-max approach and (b) the disturbance feedback min-max approach.

Table 5.2: Percentage of performance loss of ADMM and PADMM in a microgrid with 50 fuel cell cars and for different values of N_{p} and $\bar{\omega}_i$, using the min-max approach.

N_{p}	4		6		8	
$\bar{\omega}_i$	e_{admm}	e_{padmm}	e_{admm}	e_{padmm}	e_{admm}	e_{padmm}
0.5	0.02	0.40	0.03	0.61	0.04	0.40
1	0.68	0.48	1.02	0.57	1.64	0.49
1.5	0.52	0.64	1.26	0.78	1.80	1.06
2	1.20	0.93	1.94	1.05	2.87	1.09

Table 5.3: Percentage of performance loss of ADMM and PADMM in a microgrid with 50 fuel cell cars and for different values of N_{p} and $\bar{\omega}_i$, using the disturbance feedback min-max approach.

N_{p}	4		6		8	
$\bar{\omega}_i$	e_{admm}	e_{padmm}	e_{admm}	e_{padmm}	e_{admm}	e_{padmm}
0.5	10.26	1.12	5.93	1.35	4.56	1.55
1	4.03	2.66	3.53	2.63	4.57	3.49
1.5	3.53	2.67	5.05	3.89	4.97	3.68
2	6.42	5.25	5.35	4.24	7.07	5.45

comparison between the centralized methods, i.e., the methods in which the driving patterns have to be shared, and the distributed methods, i.e., the methods that keep the driving patterns private. In general, the centralized methods have the best performance, because the controller can determine the optimal control input. In the distributed methods, the performance decreases. However, Figure 5.5 indicates that for a system with more than 30 fuel cell cars, the performance loss of the ADMM and PADMM methods is negligible.

Figure 5.6 shows a comparison between the total optimization time of different control strategies, while the CaPP system is simulated for 10 hours, or equivalently, for 40 sampling time steps. From this figure, we can conclude that the optimization problems of distributed control methods can be solved significantly faster than those of the centralized methods. Here, the communication process between different agents and between each agent and the coordinator is not taken into account and the sole purpose of Figure 5.6 is the comparison in the computation time required to solve the optimization problems. All the simulations are run on a Linux machine with 16 GB of RAM and an Intel Xeon CPU with 8 cores and 3.7 GHz clock speed. The solver Gurobi is used in all the simulations. Note that the optimization problems of different cars are solved in parallel in the dual decomposition approach. As a result, increasing the number of cars does not influence the computation time of this method. We have used an example of serial implementation of the ADMM and PADMM methods, see, e.g., [93]. In a serial implementation of the ADMM, agents solve their respective optimization problems consecutively. In other words, the optimization problems are solved serially and the result is that increasing the number of agents in the system increases the total computation time. However, compared to the centralized control architecture, ADMM and PADMM methods still require much less computation time. Considering that a branch and bound technique is used to solve the optimization problem, finding the optimal solution requires the creation of lots of branches of the problem in memory. Even if we find a feasible solution, the optimality of that solution is not certain until all the other branches are explored or bounded by the branch and bound algorithm. In order to prevent the shortage of memory, we have set a limit, equal to 100 seconds, on the computation time of each optimization problem. If the optimization time reaches this limit, the best known feasible solution is considered as the solution. The computation times of the distributed methods are all less than this bound and as a result, the total computation time of any distributed method is not influenced by this limit. However, by increasing the number of cars, the computation time of the centralized architecture becomes more than this limit. The reason that the computation time of the centralized control architecture in Figure 5.6 does not grow exponentially after around 10 fuel cell cars is in fact the limit that is set in the solver. Note that even though we still have a feasible solution with terminating the branch and bound algorithm prematurely, the solution is not optimal and, hence, the system performance decreases. Table 5.4 lists the computation time of different control methods by using different prediction horizons. This table shows that increasing the prediction horizon results in a

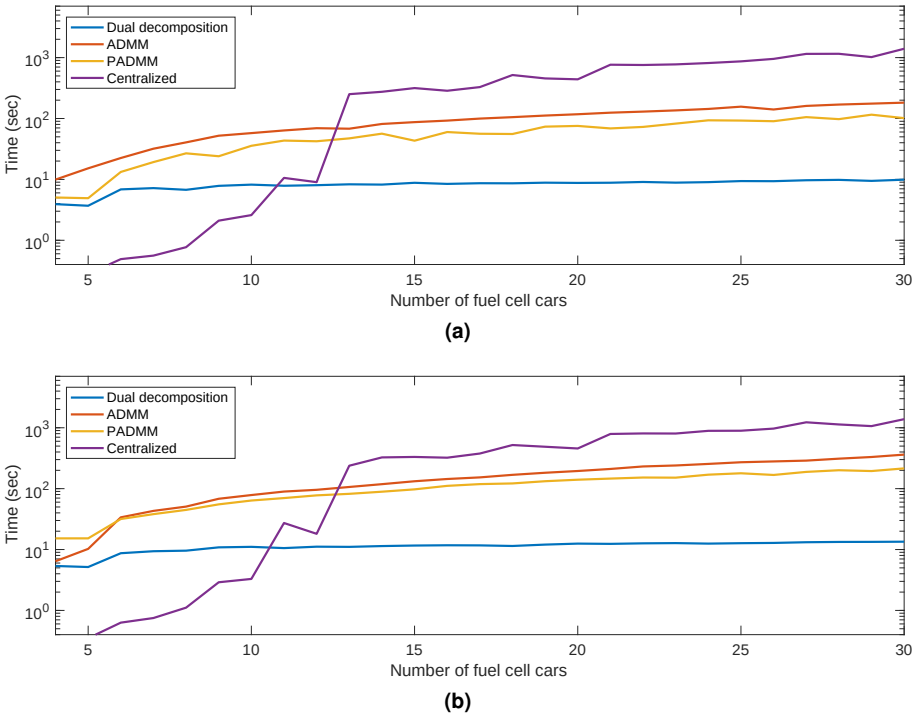

Figure 5.6: Computation time of different control strategies with respect to the number of fuel cell cars using (a) the min-max approach and (b) the disturbance feedback min-max approach.

considerable increase in the optimization time of all the methods.

The results of our simulations show that in all cases, the ADMM and the PADMM control methods require less computation time compared to the central control method, while the performance loss of these methods is negligible with respect to the centralized method for a CaPP system with a large number of cars. Therefore, the ADMM and the PADMM methods can be considered as suitable control methods for control of a CaPP system.

5.6 Conclusions

A fleet of fuel cell cars can be considered as a distributed power generation system inside an islanded mode microgrid and an appropriate power scheduling of the fuel cells can maintain the power balance of the microgrid. We have shown that the min-max and the disturbance feedback min-max methods are able to schedule the power generation of fuel cell cars by minimizing the operational cost of the system with respect to the physical and operational cost of the system. Both control methods can deal with uncertainty in the prediction of the residual load of the microgrid. A centralized architecture to implement min-max and disturbance feedback min-max

Table 5.4: Computation time (in seconds) of different control strategies for a microgrid with 50 fuel cell cars, $\bar{\omega}_i = 0.5$, and for different values of N_{p}, using the min-max (MM) and the disturbance feedback min-max (DF) approaches.

Method \ N_{p}	4	6	8
Centralized MM	1214.67	1608.43	2105.31
Dual Decomposition MM	6.22	10.99	18.63
ADMM MM	187.55	346.65	607.10
PADMM MM	77.47	110.75	214.27
Centralized DF	1237.07	1620.16	2105.75
Dual Decomposition DF	8.59	15.26	25.06
ADMM DF	421.05	701.53	1083.42
PADMM DF	188.58	300.80	503.46

methods is disadvantageous because the privacy of the car owner, with respect to driving patterns, cannot be respected in such centralized setting. However, in the proposed distributed control methods, the driving pattern of any car is kept private and not shared with any other agent. Another advantage of the proposed distributed methods is their scalability and applicability in large-scale systems by reducing the computational burden of the solution of the optimization problems. The mentioned advantages of the distributed control methods come at the cost of losing a certain level of performance in the operation of the system. However, the case studies show that the performance loss is related to the number of fuel cell cars in the system and becomes smaller for large vehicle numbers, which would be the case in envisioned practical scenarios. Among the three distributed control methods, the proximal ADMM has the least loss of performance when the number of cars is small. When the number of cars in the system grows, the performance of the ADMM and the proximal ADMM methods becomes closer to the performance of a centralized control architecture.

Topics for future research include the development of a distributed control architecture for the operation of a microgrid in the grid-connected mode, optimal for of clustering the fuel cell cars in the ADMM method, and extending the current control methods to deal with more complex models of the system.

6

Min-Max and Min-Max-Regret Model Predictive Control for Power Scheduling of Parking Lots

In this chapter, we consider several parking lots in a microgrid, where in each parking lot, fuel cell cars are connected to the microgrid and are able to generate power. The aim of this chapter is to develop power scheduling profiles for each parking lot inside the microgrid. To deal with the uncertainty in the prediction of the number of cars inside each parking lot, we develop three different model predictive control (MPC) methods, namely nominal, min-max, and min-max-regret methods for such optimal power scheduling. By using the specific structure of the associated optimization problems, the computational complexity of the min-max and min-max regret methods are reduced. We also present a case study to demonstrate the system performance by using the developed methods.

6.1 Introduction

In the specific problem formulation of this chapter, the number of cars inside a parking lot influences the operational cost of the system. We assume that by using historical data about the number of cars inside each parking, it is possible to predict this number for the future. However, we need to deal with the inaccuracy of such prediction. As discussed earlier in Chapter 4, one way to deal with the uncertainty is to use a min-max model predictive control approach. An alternative approach is the regret minimization technique that is discussed in more detail in Chapter 2.

In this chapter, we formulate the power scheduling problem of all the fuel cell cars in a microgrid in such a way that the central control system needs to determine the total power generation of each parking lot. Note that in Chapters 4 and 5, individual fuel cell cars were considered as the units of power generation inside the CaPP

system. However, in this chapter, we consider parking lots as the power generation units. Because each parking lot may contain hundreds of fuel cell cars, the control system can schedule the power generation of hundreds or even thousands of fuel cell cars. To deal with the uncertainty in the prediction of the number of cars inside each parking lot, we develop three different MPC approaches, namely, nominal, min-max, and min-max regret approaches. The main contributions of this chapter, other than formulating the power scheduling problem of fuel cell cars in a modular way, are the development of two methods to reduce the complexity of the min-max and the min-max-regret approaches for the CaPP problem. These two methods allow us to identify a relatively small region inside the search space where the optimal point is located. As a result, the optimization problems of the mentioned approaches become tractable. Finally, these approaches are applied to a CaPP scenario, to illustrate their relative benefits.

The rest of this chapter is organized as follows. Section 6.2 formulates the CaPP microgrid control problem in a modular way, where each parking lot for fuel cell cars is considered as a unit of power generation. Three different approaches to solve this problem are developed in Sections 6.3, 6.4, and 6.5. Finally, the performance of each approach is demonstrated via a case study in Section 6.6. Section 6.7 closes with conclusions.

6.2 Problem formulation

We consider a microgrid in the islanded mode, with some renewable energy sources, such as wind turbines and solar photo voltaic panels inside the microgrid. We assume that the renewable energy sources generate as much power as possible based on the weather conditions, while the load of the microgrid is not controllable. The aggregated load of the microgrid is defined as the difference between the microgrid's load and the power generation of renewable energy sources (RES). If the load is more than the RES' power generation, then the aggregated load has a positive sign. Conversely, a negative sign for the aggregated load indicates that the load is less than the RES' power generation.

The microgrid also includes a water electrolysis system that is able to produce hydrogen by electrolyzing water. The produced hydrogen is stored in an underground reservoir for later use for refueling fuel cell cars. The electrolysis process requires power and we assume that whenever the aggregated load has a negative sign, the electrolyzer will be activated. In this case, the amount of consumed power by the electrolyzer is the same as the absolute value of the aggregated load. As a result, whenever the aggregated load is lower than zero, the power balance of the microgrid is maintained by adjusting the power consumption of the electrolyzer.

In order to maintain the power balance of the microgrid for the case that the aggregated load is larger than zero, we consider the presence of a car as power plant setup [65]. As discussed earlier in Chapter 2, the fleet of fuel cell cars can be

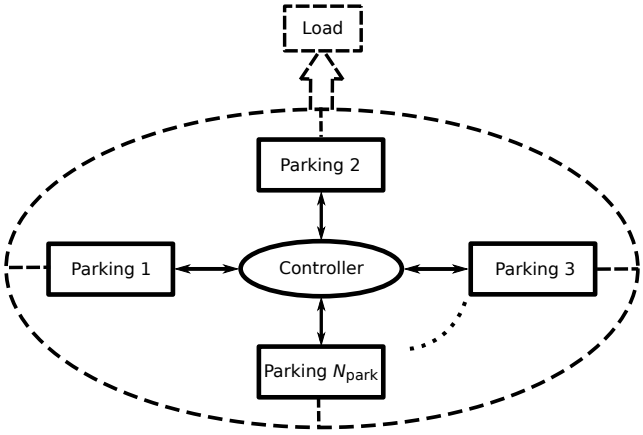

Figure 6.1: Schematic representation of the system.

considered as a power plant that is able to maintain the power balance of a microgrid. In the considered scenario, whenever the aggregated load is larger than zero, the power generation of all fuel cell cars should in total equal the aggregated load.

We consider N_{park} parking lots for the fuel cell cars inside the microgrid, where each parking lot is designed for vehicle to grid (V2G) operation. In other words, the fuel cell stacks of the cars that are parked inside the parking lot are used to generate electricity and inject it into the microgrid. Therefore, a parking lot can be considered as an electrical power generator. A central control unit is considered in order to determine the power generation profile of each parking lot inside the microgrid. A schematic representation of the system is depicted in Figure 6.1. The objective of the controller is, firstly, to maintain the power balance of the microgrid by setting the total power generation of fuel cell cars equal to the residual load whenever the residual load is larger than zero. Therefore, by defining $u_p(k+j)$ as the total power generation of parking lot p at time step $k+j$, the following power balance condition should hold for a prediction time window with the length N_{p}:

$$\sum_{p\in\mathcal{P}} u_p(k+j) = P_{\text{d}}(k+j), \quad \forall j \in \mathcal{J}. \tag{6.1}$$

where $\mathcal{J} = \{0,\dots,N_{\text{p}}-1\}$, $\mathcal{P} = \{1,\dots,N_{\text{park}}\}$ is the index set of all the parking lots inside the microgrid, and $P_{\text{d}}(k+j) \triangleq \max\{0, P_{\text{res}}(k+j)\}$ indicates the residual load of the microgrid if the residual load, $P_{\text{res}}(k+j)$, has a positive sign. Otherwise, i.e., if $P_{\text{res}}(k+j) < 0$, then $P_{\text{d}}(k+j)$ is equal to zero.

Another objective of the controller is to minimize the operational cost of the system, which mainly consists of the sum of the operational costs of individual cars. If we let $\mathcal{I}_p$ denote the index set of all the fuel cell cars inside parking lot $p \in \mathcal{P}$, the operational cost of fuel cell car $i \in \mathcal{I}_p$ for the prediction window starting at time

step k can be written as follows:

$$J_{p,i}(k) = \sum_{j \in \mathcal{J}} W_{2,i} u_{p,i}^2(k+j) + W_{1,i} u_{p,i}(k+j) + W_{0,i}, \tag{6.2}$$

where $u_{p,i}(k)$ indicates the power generation of the fuel cell car i at time step k, and $W_{2,i}$, $W_{1,i}$, $W_{0,i}$ are constant coefficients related to the specifications of the fuel cell stack of car i. The quadratic form of the operational cost in (6.2) is chosen mainly because of the quadratic relation between fuel consumption and the net power generation of a fuel cell stack [85, 43]; the degradation of a fuel cell is another part of the operational cost and we assume that this part can also be expressed as a quadratic function of the net power generation. Therefore, the cost function (6.2) includes both the fuel consumption and the degradation of fuel cells.

Considering (6.2) as the operational cost of one fuel cell car at time step k, the operational cost of parking lot $p \in \mathcal{P}$ for the prediction window starting at time step k can be written as

$$J_p(k) = \sum_{i \in \mathcal{I}_p} \sum_{j \in \mathcal{J}} W_{2,p,i} u_{p,i}^2(k+j) + W_{1,p,i} u_{p,i}(k+j) + W_{0,p,i}. \tag{6.3}$$

We assume that in each parking lot, the power generation is evenly distributed over all the fuel cell cars inside that parking lot. As a result, for all $i \in \mathcal{I}_p$, all $p \in \mathcal{P}$, and all k we have

$$u_{p,i}(k) = \frac{u_p(k)}{n_p(k)}, \tag{6.4}$$

where $n_p(k)$ is the number of cars inside parking lot p at time step k. Note that by evenly distributing the power generation of a parking lot among all the fuel cell cars, we eliminate the need for another control system inside parking lots in order to determine the power generation for each individual car. As a result, the overall system becomes simpler. Another possibility is to consider a control system inside each parking lot for the operation of the parking lot, see, e.g., Chapters 4 and 5. However, for the sake of simplicity, here we consider an even distribution of the power generation inside each parking over the available cars.

Another assumption adopted in this chapter is to consider a scenario that the constant coefficients $W_{2,p,i}$, $W_{1,p,i}$, and $W_{0,p,i}$ in (6.3) are the same for fuel cell cars. In other words, for all $i \in \mathcal{I}_p$ and for all $p \in \mathcal{P}$, we have $W_{2,p,i} = W_2$, $W_{1,p,i} = W_1$, and $W_{0,p,i} = W_0$. Because the power generation of all the cars inside each parking lot is the same, selecting W_2, W_1, and W_0 as the mean value of the respected parameters results in a good approximation of the total cost function. As a result, by using (6.4) the operational cost of parking lot $p \in \mathcal{P}$ for the prediction window starting at time step k in (6.3) can be rewritten as:

$$J_p(k) = \sum_{j \in \mathcal{J}} W_2 \frac{u_p^2(k+j)}{n_p(k+j)} + W_1 u_p(k+j) + W_0 n_p(k+j). \tag{6.5}$$

Based on the driving patterns of the cars, a prediction, $\hat{n}_p(k+j)$, for the value $n_p(k+j)$, for $j \in \mathcal{J}$, is assumed to be available. However, there is generally some uncertainty in the realization of $n_p(k+j)$ due to the inaccuracy of such a prediction. As a result, we have that

$$n_p(k+j) = \hat{n}_p(k+j) + \omega_p(k+j) \quad \forall j \in \mathcal{J}, \forall p \in \mathcal{P}, \tag{6.6}$$

where $\hat{n}_p(k+j)$ is the predicted value of $n_p(k+j)$ and $\omega_p(k+j)$ is an uncertain variable. We define the uncertainty set Ω_p as the set of integer numbers within a closed interval such that all the possible realizations of $\omega_p(k+j)$ for all $j \in \mathcal{J}$ are inside this set. Using (6.5) and (6.6), the operational cost of the system for the prediction window can be written as follows:

$$\begin{aligned} J_p(k) = \sum_{j \in \mathcal{J}} W_2 \frac{u_p^2(k+j)}{\hat{n}_p(k+j) + \omega_p(k+j)} + W_1 u_p(k+j) \\ + W_0 \left(\hat{n}_p(k+j) + \omega_p(k+j)\right) \quad \forall p \in \mathcal{P}. \end{aligned} \tag{6.7}$$

By considering (6.7) as the operational cost of parking lot p, the operational cost of the whole system for the prediction window can be written as:

$$J(k) = \sum_{p \in \mathcal{P}} J_p(k). \tag{6.8}$$

The objective of designing a controller for the microgrid is to determine power generation profiles for each parking lot, in other words, to determine $u_p(k+j)$ for all $p \in \mathcal{P}$ and $j \in \mathcal{J}$, such that the cost in (6.8) is minimized, while adhering to the power balance constraint in (6.1). In the presence of uncertainty in the cost function, this problem may be considered from different perspectives. In the rest of this chapter, we develop three different MPC approaches, namely nominal, min-max, and min-max-regret approaches, where each approach is developed from such a different perspective.

In the first approach, i.e., the nominal approach, the uncertainty is simply neglected and the MPC controller minimizes the operational cost for the nominal model of the system. In the second approach, i.e., the min-max approach, the maximum possible operational cost of the system is minimized while in the last approach, i.e., the min-max-regret approach, the maximum possible regret of a decision maker in the CaPP system is minimized.

6.3 Nominal approach

In the nominal approach, we define an estimate, $\hat{J}(k)$, for the operational cost by neglecting the presence of uncertainty in the cost function (6.7). As a result, by

defining

$$\hat{J}_p(k) = \sum_{j\in\mathcal{J}} W_2 \frac{u_p^2(k+j)}{\hat{n}_p(k+j)} + W_1 u_p(k+j) + W_0 \hat{n}_p(k+j),$$
$$\hat{J}(k) = \sum_{p\in\mathcal{P}} \hat{J}_p(k),$$

the MPC optimization problem using the nominal approach is given by

$$\min_{\tilde{u}(k)} \hat{J}(k) \quad \text{subject to (6.1).} \tag{6.9}$$

In (6.9), we have $\tilde{u}(k) \triangleq \left[\tilde{u}_1^T(k) \dots \tilde{u}_{N_{\text{park}}}^T(k)\right]^T$, where $\tilde{u}_p(k) \triangleq [u_p(k) \ \dots \ u_p(k+N_{\text{p}}-1)]^T$ for all $p \in \mathcal{P}$. The optimization problem (6.9) is in the form of a quadratic programming problem and is solvable by a variety of solvers, such as CPLEX [23] or Gurobi [39].

6.4 Min-max approach

Let us now consider a robust control approach in which the uncertainty in (6.6) is taken into account. The value of the cost function in (6.7) is related to the realization $\omega_p(k+j)$ for different $p \in \mathcal{P}$ and $j \in \mathcal{J}$. For the rest of this chapter, we adopt the following assumptions on the uncertainty sets Ω_p.

Assumption 6.4.1. *For any $p \in \mathcal{P}$, $j \in \mathcal{J}$, and all k, $\omega_p(k+j)$ is an integer number in the set $[\underline{\omega}, \bar{\omega}]$, where $\underline{\omega}$ and $\bar{\omega}$ are two known integer numbers.*

Note that $\underline{\omega}$ and $\bar{\omega}$ in the above assumption can also be negative integer numbers.

Assumption 6.4.2. *For any $p \in \mathcal{P}$, $j \in \mathcal{J}$, and all k, $\hat{n}_{\text{p}}(k+j) + \underline{\omega} > 0$.*

The above assumption is valid in the case that the prediction about the number of cars is always bigger than $\underline{\omega}$. For a large parking lot, with high number of cars at any given time, the above assumption is not restrictive.

Assumption 6.4.3. *The realization of $\omega_{p_1}(k+j_1)$ is independent from the realization of $\omega_{p_2}(k+j_2)$ if $p_1 \neq p_2$ or $j_1 \neq j_2$.*

The above assumption is valid in the case that the parking lots are spread across a city and each parking lot is located in an area with a specific behavior of the car owners. For example, if the system has three parking lots, these could be located in a residential area, an industrial area, and a marketplace.

In the min-max approach, the highest possible value of $J(k)$ (i.e., the worst-case cost given the uncertainty characterization given above) is minimized at each time

step k and as a result of this minimization, the control inputs, i.e., $u_p(k+j)$ for all $p \in \mathcal{P}$ and $j \in \mathcal{J}$, are determined.

By defining

$$\tilde{\omega}(k) \triangleq \left[\tilde{\omega}_1^T(k) \ \dots \ \tilde{\omega}_{N_{\text{park}}}^T(k)\right]^T$$
$$\tilde{\omega}_p(k) \triangleq \left[\omega_p(k) \ \dots \ \omega_p(k+N_{\text{p}}-1)\right]^T,$$

the optimization problem characterizing the min-max approach can be written as follows:

$$\min_{\tilde{u}(k)} \max_{\tilde{\omega}(k)\in\Omega} J(k)$$
$$\text{subject to (6.1)}, \tag{6.10}$$

where Ω is a set that consists of all realizations of uncertainties that correspond to Assumptions 6.4.1 , 6.4.2, and 6.4.3 for all parking lots $p \in \mathcal{P}$. The cost function $J(k)$ is in fact a function of $\tilde{u}(k)$ and $\tilde{\omega}(k)$ and can be written as $J\left(\tilde{u}(k), \tilde{\omega}(k)\right)$. In order to solve (6.10), one can solve a two-level optimization problem, where the inner problem is the maximization of $J\left(\tilde{u}(k), \tilde{\omega}(k)\right)$ over $\tilde{\omega}(k)$ for a given $\tilde{u}(k)$, while the outer problem is the minimization of $J_{\max}(\tilde{u}(k))$ over $\tilde{u}(k)$, where

$$J_{\max}(\tilde{u}(k)) \triangleq \max_{\tilde{\omega}(k)\in\Omega} J(k). \tag{6.11}$$

The outer level of the two-level optimization problem (6.10), can be solved by using a gradient descent algorithm [9]. Considering the structure of $J_p(k)$ in (6.7), we can conclude that $J\left(\tilde{u}(k), \tilde{\omega}(k)\right)$ is[1] convex in $\tilde{u}(k)$. Therefore, the maximization part of (6.10), i.e., (6.11), is convex in $\tilde{u}(k)$, because it is a point-wise maximization of a finite number of convex functions. As a result, an arbitrary single starting point is enough to find the minimum of (6.11) over $\tilde{u}(k)$ if we solve the problem using a convex optimization method or a gradient descent method.

The convexity of $J_{\max}(\tilde{u}(k))$ simplifies the outer optimization problem in (6.10). However, the inner optimization problem of (6.10) determined in (6.11) requires the evaluation of $J\left(\tilde{u}(k), \tilde{\omega}(k)\right)$ in $N_\omega^{N_{\text{p}}N_{\text{park}}}$ points, where $N_\omega \triangleq \bar{\omega} - \underline{\omega} + 1$. Therefore, solving the inner optimization by evaluating the cost function for all possible realizations of the uncertainty is time-consuming and inefficient in practice. However, by using the following lemma, we can find the value of $J_{\max}(\tilde{u}(k))$ for a given $\tilde{u}(k)$ by evaluating the cost function $J(k)$ in only $2N_{\text{p}}N_{\text{park}}$ points.

Lemma 6.4.1. *Let Assumptions 6.4.1-6.4.3 hold. Let us define:*

$$\tilde{\omega}^*(k) \triangleq \arg\max_{\tilde{\omega}(k)\in\Omega} J\left(\tilde{u}(k), \tilde{\omega}(k)\right), \quad \text{for given } \tilde{u}(k).$$

[1] Note that J is a function of $\tilde{u}(k)$ and $\tilde{\omega}(k)$. Therefore, it can be written as $J(\tilde{u}(k), \tilde{\omega}(k))$ or, alternatively, as $J(k)$.

The vector $\tilde{\omega}^*(k)$ is unique and if we denote the $[(p-1)N_{\rm park}+1+j]$th element of this vector by $\omega_p^*(k+j)$, then $\omega_p^*(k+j)$ is either $\underline{\omega}$ or $\bar{\omega}$ and maximizes $J_p^0(k+j)$, where

$$J_p^0(k+j) \triangleq W_2 \frac{u_p^2(k+j)}{\hat{n}_p(k+j)+\omega_p(k+j)} + W_1 u_p(k+j) + W_0\left(\hat{n}_p(k+j)+\omega_p(k+j)\right). \tag{6.12}$$

Proof: Considering the definition of $J_p^0(k+j)$ in (6.12), we have:

$$\max_{\tilde{\omega}(k)\in\Omega} J\left(\tilde{u}(k),\tilde{\omega}(k)\right) = \max_{\tilde{\omega}(k)\in\Omega} \sum_{p\in\mathcal{P}}\sum_{j\in\mathcal{J}} J_p^0(k+j).$$

Because the value of $\omega_{p_0}(k+j_0)$ is independent from the value of $\omega_p(k+j)$ for all $p \neq p_0$ or $j \neq j_0$, we have that

$$\max_{\tilde{\omega}(k)\in\Omega} \sum_{p\in\mathcal{P}}\sum_{j\in\mathcal{J}} J_p^0(k+j) = \sum_{p\in\mathcal{P}}\sum_{j\in\mathcal{J}} \max_{\omega_p(k+j)\in\Omega_p} J_p^0(k+j).$$

As a result, we can conclude that for any $p\in\mathcal{P}$ and $j\in\mathcal{J}$, the function $J_p^0(k+j)$ has its maximum at $\omega_p^*(k+j)$. Therefore, the last part of the lemma is true.

Considering Assumption 6.4.2, we have that $\hat{n}_{\rm p}(k+j)+\omega_p(k+j)>0$ for all k and $j\in\mathcal{J}$. Therefore, $J_p^0(k+j)$ is a convex function of $\omega_p(k+j)$. As a result, $\tilde{\omega}^*(k)$ is unique and the maximum of $J_p^0(k+j)$ over $\omega_p(k+j)$ is realized on the boundaries of $\omega_p(k+j)$. As a result, by considering Assumption 6.4.1, for all $p\in\mathcal{P}$ and $j\in\mathcal{J}$, $\omega_p^*(k+j)$ is either $\underline{\omega}$ or $\bar{\omega}$. □

By using the results of Lemma 6.4.1, we can conclude that in order to solve the inner optimization problem for any given $\tilde{u}(k)$, i.e., in order to find the value of $\tilde{\omega}^*(k)$, it is sufficient to find the argument of the maximum of each part of the cost function individually. In other words, the $(p-1)N_{\rm park}+1+j$th element of $\tilde{\omega}^*(k)$ maximizes $J_p^0(k+j)$. Therefore, we can reduce the number of evaluations of the cost function from $N_\omega^{N_{\rm p}N_{\rm park}}$, i.e., from all possible realizations of uncertainty, to only $2N_{\rm p}N_{\rm park}$ points. This reduction in the number of evaluations of the cost function results in a more efficient solution of the optimization problem (6.10).

6.5 Min-max-regret approach

In the min-max-regret approach, we minimize the maximum possible regret of a decision maker [12, 20]. In other words, a decision maker determines the control actions, i.e., $\tilde{u}(k)$, by solving the following optimization problem:

$$\min_{\tilde{u}(k)} \max_{\tilde{\omega}(k)\in\Omega} R\left(\tilde{u}(k),\tilde{\omega}(k)\right)$$
$$\text{subject to (6.1)}, \tag{6.13}$$

where the regret function, $R(.)$, is defined as follows:

$$R\left(\tilde{u}(k),\tilde{\omega}(k)\right) \triangleq J(\tilde{u}(k),\tilde{\omega}(k)) - J(\tilde{u}^*(k,\tilde{\omega}(k)),\tilde{\omega}(k)). \tag{6.14}$$

The first part of the regret function in (6.14) indicates the realized operational cost caused by the control input $\tilde{u}(k)$ and uncertainty $\tilde{\omega}(k)$, while the second part indicates the lowest operational cost of the system for a given uncertainty $\tilde{\omega}(k)$. In other words, for a given $\tilde{\omega}(k)$, the value of $\tilde{u}^*(k,\tilde{\omega}(k))$ is defined in such a way that the cost function, J, is minimized, i.e., in (6.14), the value of $\tilde{u}^*(k,\tilde{\omega}(k))$ is determined by solving the following optimization problem for a given $\tilde{\omega}(k)$:

$$\begin{aligned}\tilde{u}^*(k,\tilde{\omega}(k)) = &\arg\min_{\tilde{u}(k)} J(\tilde{u}(k),\tilde{\omega}(k))\\ &\text{subject to (6.1).}\end{aligned} \tag{6.15}$$

Note that if the value of $\tilde{\omega}(k)$ was known in advance, a wise decision maker would select $\tilde{u}^*(k,\tilde{\omega}(k))$. However, the selected control input by a decision maker, $\tilde{u}(k)$, is not necessarily equal to $\tilde{u}^*(k,\tilde{\omega}(k))$, because the value of $\tilde{\omega}(k)$ is uncertain at the time of making the decision. Only after a decision has been made and applied to the system, we can observe the realization of $\tilde{\omega}(k)$, which was once uncertain. At this point, the decision maker finds out how much the operational cost could have been decreased by choosing $\tilde{u}^*(k,\tilde{\omega}(k))$. This potential increase in the outcome of the system is very similar to what we call "regret" in daily life and, in fact, this similarity is the reason of calling R the regret function.

To solve the optimization problem (6.13), one can solve a two-level optimization problem, where in the outer level, a minimization problem with respect to $\tilde{u}(k)$ should be solved. Considering the structure of $J(\tilde{u}(k),\tilde{\omega}(k))$ defined in (6.8), this minimization problem is convex and, hence, can be solved by a standard algorithm for convex problems using an arbitrary single starting point. Note that the cost function in this minimization problem is defined by the following optimization problem:

$$\max_{\tilde{\omega}(k)\in\Omega} R(\tilde{u}(k),\tilde{\omega}(k)). \tag{6.16}$$

One way to find the solution of (6.16), i.e., the inner level optimization problem of the two-level optimization problem (6.13), is to evaluate the regret function for all possible realizations of uncertainty. In this way, the regret function should be determined for $N_\omega^{N_{\rm p}N_{\rm park}}$ points. However, by using the results of Lemma 6.5.1 below, we know that the maximum of regret is located on a vertex of the uncertainty set Ω. Therefore, if we find the maximum of the regret function over the vertexes of the uncertainty set Ω, i.e., over $2^{N_{\rm p}N_{\rm park}}$ points, we have found the solution of (6.16). Algorithm 6.1 indicates the procedure of finding the solution of the optimization problem (6.16).

Lemma 6.5.1. *Adopt Assumptions 6.4.1-6.4.3. Define the set:*

$$\Gamma(k) \triangleq \arg\max_{\tilde{\omega}(k)\in\Omega} R(\tilde{u}(k),\tilde{\omega}(k)). \tag{6.17}$$

There exists a vertex $\tilde{\omega}^*(k)$ of the polytopic set Ω such that $\tilde{\omega}^*(k) \in \Gamma(k)$. In other words, if we denote the $[(p-1)N_{\text{park}} + 1 + j]$th element of the vector $\tilde{\omega}^*(k)$ by $\omega_p^*(k+j)$, then for all $p \in \mathcal{P}$ and $j \in \mathcal{J}$, $\omega_p^*(k+j)$ is equal to either $\underline{\omega}$ or $\bar{\omega}$.

Proof: Define

$$u^*(k, \tilde{\omega}^*(k)) \triangleq \arg\min_{\tilde{u}(k)} \sum_{p\in\mathcal{P}} \sum_{j\in\mathcal{J}} J_p^0(u_p(k+j), \omega_p^*(k+j))$$
$$u^{\#}(k, \tilde{\omega}^{\#}(k)) \triangleq \arg\min_{\tilde{u}(k)} \sum_{p\in\mathcal{P}} \sum_{j\in\mathcal{J}} J_p^0(u_p(k+j), \omega_p^{\#}(k+j)),$$

where $\tilde{\omega}^*(k) \in \Gamma(k)$ and $\tilde{\omega}^{\#}(k)$ is an arbitrary vector inside the set Ω. From the above definitions we have:

$$\sum_{p\in\mathcal{P}} \sum_{j\in\mathcal{J}} J_p^0 \left(u_p^{\#}(k+j, \tilde{\omega}^{\#}(k)), \omega_p^{\#}(k+j)\right) \leq$$
$$\sum_{p\in\mathcal{P}} \sum_{j\in\mathcal{J}} J_p^0 \left(u_p^*(k+j, \tilde{\omega}^*(k)), \omega_p^{\#}(k+j)\right),$$

and as a result:

$$\sum_{p\in\mathcal{P}} \sum_{j\in\mathcal{J}} \left(\frac{W_2 u_p^{\#^2}(k+j, \tilde{\omega}^{\#}(k))}{\hat{n}_p(k+j) + \omega_p^{\#}(k+j)} + W_1 u_p^{\#}(k+j, \tilde{\omega}^{\#}(k)) \right)$$
$$\leq \sum_{p\in\mathcal{P}} \sum_{j\in\mathcal{J}} \left(\frac{W_2 u_p^{*^2}(k+j, \tilde{\omega}^*(k))}{\hat{n}_p(k+j) + \omega_p^{\#}(k+j)} + W_1 u_p^*(k+j, \tilde{\omega}^*(k)) \right). \tag{6.18}$$

Now consider rewriting the regret function as in (6.14) in the following form:

$$R(\tilde{u}(k), \tilde{\omega}^*(k)) = \sum_{p\in\mathcal{P}} \sum_{j\in\mathcal{J}} \Big(\frac{W_2 \left(u_p^2(k+j) - u_p^{*^2}(k+j, \tilde{\omega}^*(k))\right)}{\hat{n}_p(k+j) + \omega_p^*(k+j)}$$
$$+ W_1 \left(u_p(k+j) - u_p^*(k+j, \tilde{\omega}^*(k))\right) \Big).$$

Assume that $\tilde{\omega}^{\#}(k)$ is selected based on the following rule:

- If $u_p^2(k+j) - u_p^{*^2}(k+j, \tilde{\omega}^*(k)) > 0$, then $\omega_p^{\#}(k+j) = \underline{\omega}$.
- If $u_p^2(k+j) - u_p^{*^2}(k+j, \tilde{\omega}^*(k)) \leq 0$, then $\omega_p^{\#}(k+j) = \bar{\omega}$.

Based on the above selection rule for $\tilde{\omega}^{\#}(k)$, we can conclude that $\tilde{\omega}^{\#}(k)$ is a vertex

of Ω and the following inequality is always true:

$$\begin{aligned} R(\tilde{u}(k),\tilde{\omega}^*(k)) \quad &\leq \sum_{p\in\mathcal{P}}\sum_{j\in\mathcal{J}}\Big(\frac{W_2\left(u_p^2(k+j)-{u_p^*}^2(k+j,\tilde{\omega}^*(k))\right)}{\hat{n}_p(k+j)+\omega_p^{\#}(k+j)} \\ &\qquad +W_1\left(u_p(k+j)-u_p^*(k+j,\tilde{\omega}^*(k))\right)\Big) \\ &= \sum_{p\in\mathcal{P}}\sum_{j\in\mathcal{J}}\Big(\frac{W_2u_p^2(k+j)}{\hat{n}_p(k+j)+\omega_p^{\#}(k+j)}+W_1u_p(k+j)\Big) \\ &+ \sum_{p\in\mathcal{P}}\sum_{j\in\mathcal{J}}\Big(\frac{-W_2{u_p^*}^2(k+j,\tilde{\omega}^*(k))}{\hat{n}_p(k+j)+\omega_p^{\#}(k+j)}-W_1u_p^*(k+j,\tilde{\omega}^*(k))\Big)\ . \end{aligned}$$

By using (6.18), we have:

$$\begin{aligned} R(\tilde{u}(k),\tilde{\omega}^*(k)) \quad &\leq \\ &\sum_{p\in\mathcal{P}}\sum_{j\in\mathcal{J}}\Big(\frac{W_2u_p^2(k+j)}{\hat{n}_p(k+j)+\omega_p^{\#}(k+j)}+W_1u_p(k+j)\Big) \\ &+ \sum_{p\in\mathcal{P}}\sum_{j\in\mathcal{J}}\Big(\frac{-W_2{u_p^{\#}}^2\left(k+j,\tilde{\omega}^{\#}(k)\right)}{\hat{n}_p(k+j)+\omega_p^{\#}(k+j)}-W_1u_p^{\#}\left(k+j,\tilde{\omega}^{\#}(k)\right)\Big) \\ &= \sum_{p\in\mathcal{P}}\sum_{j\in\mathcal{J}}\Big(\frac{W_2\left(u_p^2(k+j)-{u_p^{\#}}^2\left(k+j,\tilde{\omega}^{\#}(k)\right)\right)}{\hat{n}_p(k+j)+\omega_p^{\#}(k+j)} \\ &\qquad +W_1\left(u_p(k+j)-u_p^{\#}\left(k+j,\tilde{\omega}^{\#}(k)\right)\right)\Big) \\ &= R(\tilde{u}(k),\tilde{\omega}^{\#}(k)). \end{aligned}$$

So, if we select $\tilde{\omega}^{\#}(k)$ based on the previously mentioned rule, we have:

$$R(\tilde{u}(k),\tilde{\omega}^*(k)) \leq R(\tilde{u}(k),\tilde{\omega}^{\#}(k)). \tag{6.19}$$

Considering that $\tilde{\omega}^*(k) \in \Gamma(k)$, we can conclude that $\tilde{\omega}^{\#}(k)$, i.e., a vertex of the polytopic set Ω, is inside the set $\Gamma(k)$ and the lemma is proved. □

Algorithm 6.1 Efficient solution of the optimization problem (6.16) for the min-max-regret approach

```
procedure
    R̄ ← 0
    for each vertex of Ω such as ω̃_i do
        Find ũ*_i(k, ω̃_i(k)) defined in (6.15).
        if R(ũ*_i(k), ω̃_i(k)) > R̄ then
            R̄ ← R(ũ*_i(k), ω̃_i(k))
            ũ*(k) ← ũ*_i(k)
            ω̃*(k) ← ω̃_i(k)
        end if
    end for
end procedure
```

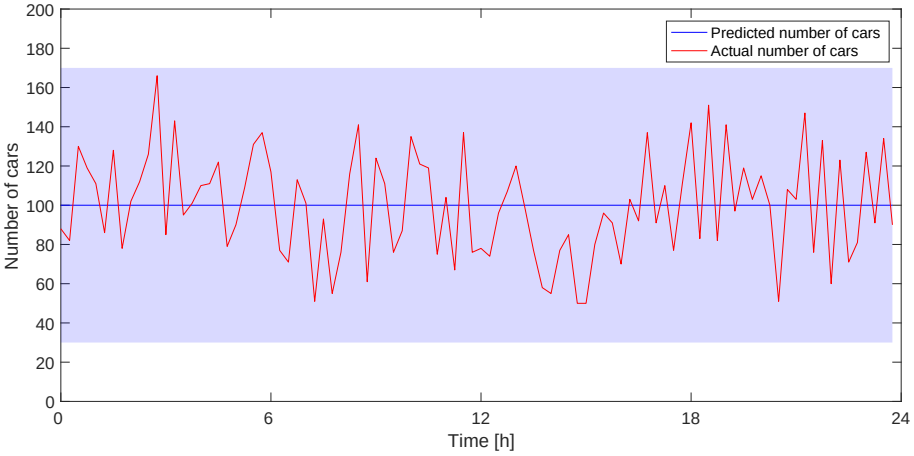

Figure 6.2: Number of cars inside the first parking lot. The blue line indicates the predicted number of cars, while the shaded area indicates the range of possible realizations of the number of cars. The red line shows an actual realization of number of cars. in a case that the probability distribution of the uncertainty has a zero mean value, with the probability distribution function indicated in the third case of Figure 6.3.

6.6 CaPP microgrid case study

In this section, we present the results of a case study, where a CaPP microgrid including three parking lots, i.e., $N_{\text{park}} = 3$, is considered. The coefficients of the cost function (6.5) are selected as $W_2 = 1$, $W_1 = 0.6$, and $W_0 = 1.2$. The predictions of the number of cars inside the parking lots are assumed to be constant and equal to 100, 120, and 90 cars. The maximum inaccuracy in the prediction of the number of cars, in other words, the uncertainty in its prediction, is assumed to be 70, i.e. $\bar{\omega} = -\underline{\omega} = 70$. The shaded area in Figure 6.2 indicates the set of possible realizations of the number of cars in the future for the first parking lot.

The considered sample time in the case studies is assumed to be 1 hour and the system is simulated for 100 sampling intervals by using the three control approaches of Sections 6.3, 6.4, and 6.5. In our simulation, we have considered four different probability distribution functions with bounded support for the uncertainty, as indicated in Figure 6.3. The prediction horizon, N_{p}, is selected equal to 4, because this prediction horizon is large enough to cover the essential time scales in the time-varying number of cars in the parking lots.

Table 6.1 shows the results of our simulations, where the total a posteriori closed-loop operational cost is calculated for each method. Figure 6.4 depicts the results of our simulations in a graphical way. Note that the performance of each method depends on the probability distribution of the uncertain parameter. The min-max-regret method achieves the best performance for the cases 1 and 3 of Figure 6.3, while the min-max method achieves its best performance for case 3 of Figure 6.3. The best

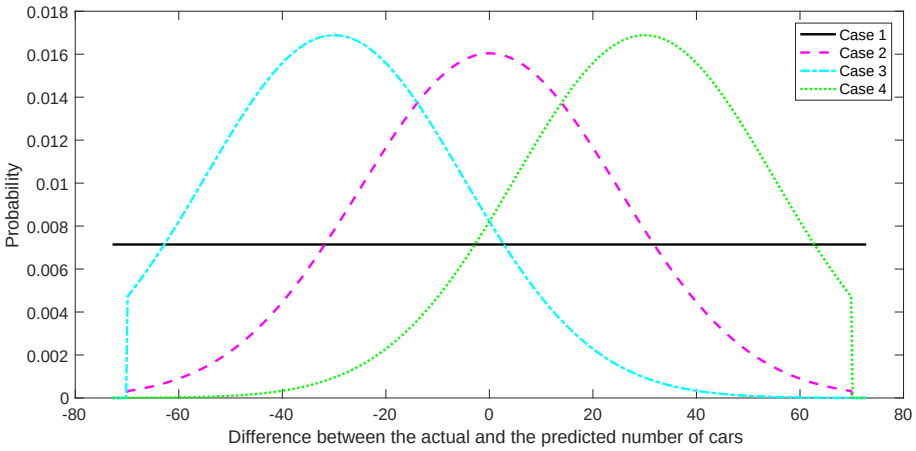

Figure 6.3: Four different probability distribution functions with bounded support for the uncertain parameter ω.

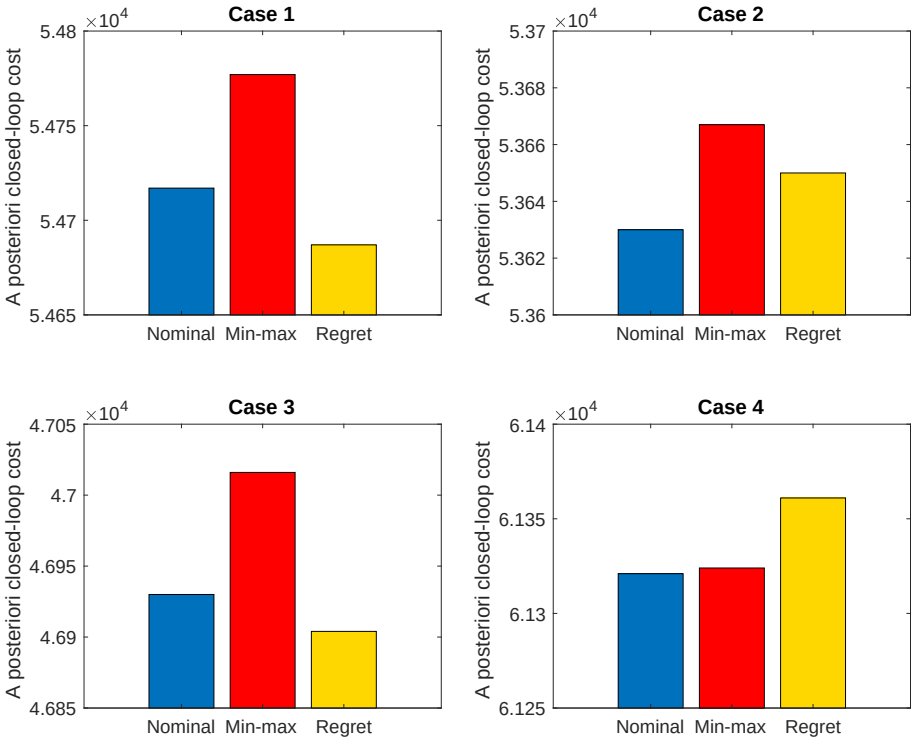

Figure 6.4: The total a posteriori closed-loop operational cost of the nominal, min-max, and min-max-regret approach for four different cases of the uncertainty depicted in Figure 6.3.

Table 6.1: The total a posteriori closed-loop operational cost of the nominal, min-max, and min-max-regret approach for the four cases of the uncertainty depicted in Figure 6.3. The last two columns of this table indicate the average and the standard deviation (SD) of the results.

		Experiment											
Case	Method	1	2	3	4	5	6	7	8	9	10	Average	SD
1	Nominal	55385	55344	53910	54096	55281	54901	54050	54849	55048	54306	54717	574
	Min-Max	55425	55349	53961	54190	55376	54965	54086	54912	55115	54390	54777	569
	Min-Max-Regret	55374	55328	53873	54052	55230	54783	54123	54786	54985	54336	54687	557
2	Nominal	53330	53937	54075	53458	53794	53460	53745	52981	53313	54205	53630	385
	Min-Max	53377	53962	54120	53494	53806	53494	53784	53040	53356	54232	53667	377
	Min-Max-Regret	53320	53957	54098	53468	53828	53507	53747	53005	53321	54249	53650	392
3	Nominal	46731	47066	46823	46968	46932	46630	46785	47405	47347	46618	46930	275
	Min-Max	46817	47167	46915	47050	47037	46691	46872	47489	47439	46684	47016	281
	Min-Max-Regret	46708	47066	46784	46943	46832	46643	46727	47383	47323	46630	46904	272
4	Nominal	61220	62168	61044	61608	61244	61633	61091	60744	61157	61302	61321	395
	Min-Max	61211	62177	61058	61612	61243	61637	61094	60745	61156	61308	61324	396
	Min-Max-Regret	61276	62223	61081	61653	61262	61663	61140	60787	61194	61332	61361	398

performance of the nominal method can be seen in case 2 of Figure 6.3, where the probability distribution function of the uncertainty is a normal distribution function with a zero mean value. In this case, we also expect that the nominal approach gives the best performance, because there is a relatively high chance that the actual number of cars in each parking lot is almost the same as the predicted number of cars.

6.7 Conclusions

We have formulated the optimization problem of an MPC controller that can be used for power scheduling of parking lots inside a CaPP-based microgrid. As each parking lot may contain hundreds of fuel cell cars, the developed control system is able to schedule the power generation of hundreds or thousands of fuel cell cars. We assumed that there exists a prediction for the number of cars inside each parking lot. However, the inherent inaccuracy of this prediction results in an uncertain parameter in the cost function of the MPC controller. To deal with this uncertainty, three different methods, namely nominal, min-max, and min-max-regret methods have been developed. We have also proposed methods to improve the computational efficiency of the latter two methods. Note that in the min-max-regret method, the regret of a human operator of the CaPP system is formulated and the controller minimizes the possible maximum regret of the human operator. Via a CaPP microgrid case study, the performance of these methods has been compared, where the results show that the nominal and the min-max-regret methods have a better a posteriori closed-loop performance compared to the min-max method.

Future works related to this chapter include the development of a distributed control architecture for the min-max-regret approach. As we have shown earlier in Chapter 5, distributed control architecture can result in reducing the computational complexity of the MPC optimization problem. Therefore, the distributed version of the min-max-regret MPC approach has the advantages of scalability, due to reducing the complexity of the optimization problem, and high performance of the min-max-regret approach.

7 Conclusions

In this chapter, the main results of this thesis are summarized and some recommendations for future research are mentioned.

7.1 Conclusions

In this thesis, we have considered a car as power plant (CaPP) system, in which a fleet of fuel cell cars is used to generate electricity inside a microgrid. The energy management system of the CaPP is able to schedule the power generation of these fuel cell cars and it is expected that this system maintains the power balance of the microgrid while there are uncertainties in the prediction of the microgrid's load or the number of cars connected to the microgrid. To meet this expectation, we have developed model predictive control (MPC) methods for the CaPP system in the presence of uncertainty. A min-max MPC method has been designed to guarantee the power balance of the system while the operational cost of the system is minimized. In addition, we have developed three distributed MPC methods to increase the privacy of the car owners regarding the driving patterns of the cars. In the last part of the thesis, we have developed another control strategy, min-max-regret MPC, in which the controller optimizes the same objective as the one that a human operator would try to optimize.

The main contributions of this thesis are as follows:

- **Development of a disturbance feedback min-max MPC strategy for the CaPP system**

  The advantage of a min-max MPC strategy is to minimize the operational cost of a system for the worst case uncertainty. However, high level of con-

servatism is a bottleneck for min-max MPC strategies. In this thesis, a disturbance feedback min-max MPC strategy has been developed for the CaPP system, that not only has the mentioned advantage of min-max MPC, but the level of conservatism is considerably lower compared to the normal min-max MPC strategy. The reason of this improvement in the performance of the disturbance min-max MPC strategy is that by using a feedback law on the future disturbance, possible state trajectories will remain closer together compared to the case where a normal min-max MPC is used.

- **Improving the privacy of the car owners in the CaPP system by using distributed MPC strategies**

  We have developed distributed control strategies for a CaPP system which, firstly, ensures that the control approach is scalable and applicable for a large fleet of fuel cell cars, and, secondly, ensures that the fuel cell car owners benefit from a better privacy regarding their driving patterns. In other words, by using the distributed control strategies developed in this thesis no the privacy sensitive data on the usage of the cars is collected by the control system.

- **Development of a control strategy for the CaPP system by mimicking the decision behavior of humans**

  Minimizing the maximum regret of a choice is a natural decision process for humans. Inspired by this decision behavior, we have developed a min-max-regret control strategy for the CaPP system in which the maximum regret of the decision maker is minimized. The min-max-regret MPC strategy not only lowers the maximum regret of the decision maker in the CaPP system, but it can also outperform the normal min-max MPC strategy in several cases.

7.2 Recommendations for future research

In this section, some recommendations for the possible directions of future research are given as follows:

- **Means of communication**

  In this thesis, we have assumed that there exist ideal communication channels between different agents of the CaPP system in such a way that there is not any delay or packet loss in the communication process. However, further research on the means of communication in a CaPP system is required in order to analyze such communication channels and to determine the effect of imperfect communication on the control system.

- **Security of communication**

As the CaPP system is an important element in maintaining the power balance of a microgrid, its proper functioning is critical. Therefore, the communication between the controller and the fuel cell cars inside the system should be immune to any possible attack of a malicious agent. An extensive research on the security of the communication process in the CaPP system is necessary before the implementing such a system in the real world.

- **Minimizing the investment budget for realization of the first CaPP system**

  The real-life implementation of the system is of great importance and minimizing the investment budget for realization of the first CaPP system is an important element for a successful real-life implementation. The investment costs of different devices such as the DC to AC power converters, communication devices, and parking lots, should be analyzed.

- **Non-cooperative approach for distributed control**

  In the developed distributed control methods, we have assumed that all the agents, i.e., fuel cell cars, inside the system are cooperating with a coordinator. This assumption is not always true and there might be some special cases in which one or more agents are not cooperating with the coordinator. A control method should be developed for a CaPP system that can guarantee the power balance condition of the system in presence of such non-cooperative agents.

- **Market-based control**

  If we consider the non-cooperative behavior of the agents in the extreme case, i.e., when every agent is selfish and prefers the self benefit over the systems' performance, market-based control is a good candidate for the control system. A possible direction for the future research is the design of a market-based control algorithm for the CaPP system by considering the hard constraint of the power balance and the specific features of fuel cell cars such as a high level of cost for switching the fuel cell on or off, the limited fuel in each car, and the transportation mode of the cars.

- **Primary and secondary control levels**

  In this thesis, we have designed control algorithms for the power scheduling of fuel cell cars inside a CaPP system. In other words, we have developed control algorithms for the tertiary control level by assuming that the primary and secondary control levels are functioning properly in a CaPP system. The development of a suitable primary and secondary controllers for the CaPP system is a critical step before actual implementation of the CaPP system.

- **Event-driven control approach**

  The sample time of the MPC control approaches developed in this thesis is assumed to be predetermined and with equal time intervals between any two

consecutive time steps. However, by implementing an event-driven approach, one may reduce the amount of information that has to be exchanged between the central controller and the fuel cell cars and as a result, the burden on the medium of communication in the CaPP system will be reduced.

- **Hydrogen-based energy system**

  Electricity is one of the most important forms of energy that we use today. Currently, there are several ways of generating electricity from renewable and non-renewable energy sources. As the CaPP concept links the power network with hydrogen, analyzing a hydrogen-based energy system, a system in which hydrogen is the main carrier and storage from of energy, is a further step toward realization of a fully renewable and clean energy system.

- **Adapting the developed control methods for the application of water management**

  The developed control methods in this thesis are able to minimize the operational cost of a CaPP system while the power balance of the microgrid is maintained. Similar to the power balance concept of a microgrid, the input and output volumes of water in a network of canals and water reservoirs should be equal to achieve a constant level of water in all places. Considering this similarity between the form of the problems in a microgrid and a water network, we can adapt the control methods of this thesis for the application of water management systems.

References

[1] Aebischer, B., Catenazzi, G., and Jakob, M. (2007). Impact of climate change on thermal comfort, heating and cooling energy demand in Europe. In *Proceedings of European Council for an Energy Efficient Economy (ECEEE)*, pages 23–26.

[2] Aissi, H., Bazgan, C., and Vanderpooten, D. (2009). Min-max and min-max regret versions of combinatorial optimization problems: A survey. *European Journal of Operational Research*, 197:427–438.

[3] Alavi, F., Park Lee, E., van de Wouw, N., De Schutter, B., and Lukszo, Z. (2017a). Fuel cell cars in a microgrid for synergies between hydrogen and electricity networks. *Applied Energy*, 192:296–304.

[4] Alavi, F., van de Wouw, N., and De Schutter, B. (2016). Min-max control of fuel-cell-car-based smart energy systems. In *European Control Conference*, pages 1223–1228, Aalborg, Denmark.

[5] Alavi, F., van de Wouw, N., and De Schutter, B. (2017b). Power scheduling in islanded-mode microgrids using fuel cell vehicles. In *56th IEEE Conference on Decision and Control*, pages 5056–5061, Melbourne, Australia.

[6] Alavi, F., van de Wouw, N., and De Schutter, B. (2018). Power scheduling of fuel cell cars in an islanded mode microgrid with private driving patterns. *Submitted to IEEE Transactions on Control Systems and Technology*.

[7] Amsterdam Power Exchange (2016). APX Market Results - APX Power NL Day Ahead .

[8] Andrews, J. and Shabani, B. (2012). Re-envisioning the role of hydrogen in a sustainable energy economy. *International Journal of Hydrogen Energy*, 37:1184–1203.

[9] Antoniou, A. and Lu, W. S. (2007). *Practical Optimization - Algorithms and Engineering Applications*. Springer.

[10] Arnold, M., Negenborn, R. R., Andersson, G., and De Schutter, B. (2009). Multi-area predictive control for combined electricity and natural gas systems. In *European Control Conference (ECC)*, pages 1408–1413.

[11] Battistelli, C. (2013). Generalized microgrid-to-smart grid interface models for vehicle-to-grid. In *PES Innovative Smart Grid Technologies Conference*, pages 1–6.

[12] Bell, D. E. (1982). Regret in decision making under uncertainty. *Operations Research*, 30(5):961–981.

[13] Bemporad, A. and Morari, M. (1999). Control of systems integrating logic, dynamics, and constraints. *Automatica*, 35(3):407–427.

[14] Bertismas, D., Litvinov, E., Sun, X. A., Zhao, J., and Zheng, T. (2013). Adaptive robust optimization for the security constrained unit commitment problem. *IEEE Transaction on Power Systems*, 28(1):52–63.

[15] Bertsekas, D. P. (1999). *Nonlinear Programming*. Athena Scientific.

[16] Boyd, S., Parikh, N., Chu, E., Peleato, B., and Eckstein, J. (2011). Distributed optimization and statistical learning via the alternating direction method of multipliers. *Foundations and Trends in Machine Learning*, 3(1):1–122.

[17] Bünger, U., Michalski, J., Crotogino, F., and Kruck, O. (2016). Large-scale underground storage of hydrogen for the grid integration of renewable energy and other applications. *Compendium of Hydrogen Energy*, 4:133–163.

[18] CEN-CENELEC-ETSI Smart Grid Coordination Group (2014). Smart grid set of standards. `https://www.dke.de/resource/blob/765952/e020d215ac4edae2f77a22fa146a4583/extended-set-of-standards-support-smart-grids-deployment-data.pdf`.

[19] Centraal Bureau voor de Statistiek (CBS) and Rijkswaterstaat (RWS). Onderzoek Verplaatsingen in Nederland 2014 (Research on Movements in the Netherlands 2014) - Data Archiving and Networked Services (in Dutch). URL: https://www.cbs.nl.

[20] Chorus, C. G., Arentze, T. A., and Timmermans, H. J. P. (2008). A random regret-minimization model of travel choice. *Transportation Research Part B*, 42:1–18.

[21] CIBSE (2006). *Degree-Days - Theory and Application - TM41: 2006*. Chartered Institution of Building Services Engineer.

[22] Cortes, A. and Martinez, S. (2015). A hierarchical demand-response algorithm for optimal vehicle-to-grid coordination. In *European Control Conference (ECC)*, pages 2425–2430, Linz, Austria.

[23] CPLEX. CPLEX optimizer. URL: http://www-01.ibm.com/software/commerce/optimization/cplex-optimizer/.

[24] De Rosa, M., Bianco, V., Scarpa, F., and Tagliafico, L. (2015). Historical trends and current state of heating and cooling degree days in Italy. *Energy Conversion and Management*, 90:323–335.

[25] del Real, A. J., Arce, A., and Bordons, C. (2007). Hybrid model predictive control of a two-generator power plant integrating photovoltaic panels and a fuel cell. In *46th IEEE Conference on Decision and Control*, pages 5447–5452. IEEE.

[26] Deutscher Wetterdienst (2017). Klimadaten Deutschland-Stundenwerte-FTP server-Hamburg-Fuhlsbüttel-Station ID 1975-2012-2016. `ftp://ftp-cdc.dwd.de/pub/CDC/observations_germany/climate/hourly/`.

[27] Eckstein, J. (1994). Some saddle-function splitting methods for convex programming. *Optimization Methods and Software*, 4(1):75–83.

[28] Enerdata (2015). Odyssee database - transport, households and services. `http://odyssee.enerdata.net/database/`.

[29] Energie Data Services Nederland (EDSN) (2015). Verbruiksprofielen - profielen elektriciteit 2014 (Load profiles - electricity profiles 2014) (in Dutch). URL: http://nedu.nl/portfolio/verbruiksprofielen/.

[30] Eurostat (2015). Number of private households by household composition, number of children and age of youngest child (1000). `http://ec.europa.eu/eurostat/en/web/products-datasets/-/LFST_HHNHTYCH`.

[31] Farahani, S. S., van der Veen, R., Oldenbroek, V., Alavi, F., Lee, E. H. P., van de Wouw, N., van Wijk, A., De Schutter, B., and Lukszo, Z. (2019). Hydrogen-based integrated energy and transport system. *IEEE Systems, Man, and Cybernetics Magazine*, 5(1):37–50.

[32] Fernandes, A., Woudstra, T., van Wijk, A., Verhoef, L., and Aravind, P. V. (2016). Fuel cell electric vehicle as a power plant and SOFC as a natural gas reformer: An exergy analysis of different system designs. *Applied Energy*, 173:13–28.

[33] Garriga, J. L. and Soroush, M. (2010). Model predictive control tuning methods: A review. *Industrial and Engineering Chemistry Research*, 49:3505–3515.

[34] GLPK. GNU Linear Programming Kits. URL: https://www.gnu.org/software/glpk/.

[35] Gou, B., Na, W. K., and Diong, B. (2009). *Fuel Cells: Modeling, Control, and Applications*. CRC press.

[36] Gross, G. and Galiana, F. D. (1987). Short-term load forecasting. *Proceedings of the IEEE*, 75(12):1558–1573.

[37] Guan, Y. and Wang, J. (2014). Uncertainty sets for robust unit commitment. *IEEE Transactions on Power Systems*, 3(29):1439–1440.

[38] Guerrero, J. M., Vasquez, J. C., Mata, J., de Vicuña, L. G., and Castilla, M. (2011). Hierarchical control of droop-controlled AC and DC microgrids - a general approach toward standardization. *IEEE Transactions on Industrial Electronics*, 58(1):158–172.

[39] Gurobi. Gurobi optimization. URL: http://www.gurobi.com/.

[40] Hans, C. A., Nenchev, V., Raisch, J., and Reincke-Collon, C. (2014). Minimax model predictive operation control of microgrids. In *The 19th World Congress of the International Federation of Automatic Control*, pages 10287–10292, Cape Town, South Africa.

[41] Heemels, W. P. M. H., De Schutter, B., and Bemporad, A. (2001). Equivalence of hybrid dynamical models. *Automatica*, 37(7):1085–1091.

[42] Holttinen, H., Tuohy, A., Milligan, M., Lannoye, E., Silva, V., Müller, S., and Söder, L. (2013). The flexibility workout: Managing variable resources and assessing the need for power system modification. *IEEE Power and Energy Magazine*, 11(6):53–62.

[43] Hu, X., Murgovski, N., Johannesson, L. M., and Egardt, B. (2015). Optimal dimensioning and power management of a fuel cell/battery hybrid bus via convex programming. *IEEE/ASME Transactions on Mechatronics*, 20(1):457–468.

[44] Ivy, J. and National Renewable Energy Laboratory (2004). *Summary of electrolytic hydrogen production: Milestone completion report*. National Renewable Energy Laboratory.

[45] Jacobson, M., Delucchi, M., Cameron, M., and Mathiesen, B. (2018). Matching demand with supply at low cost in 139 countries among 20 world regions with 100% intermittent wind, water, and sunlight (WWS) for all purposes. *Renewable Energy*, 123:236–248.

[46] Jakubcionis, M. and Carlsson, J. (2017). Estimation of European Union residential sector space cooling potential. *Energy Policy*, 101:225–235.

[47] Jakubcionis, M. and Carlsson, J. (2018). Estimation of European Union service sector space cooling potential. *Energy Policy*, 113:223–231.

[48] Jaramillo, L. B. and Weidlich, A. (2016). Optimal microgrid scheduling with peak load reduction involving an electrolyzer and flexible loads. *Applied Energy*, 169:857–865.

[49] Kammer, C. and Karimi, A. (2017). Decentralized and distributed transient control for microgrids. *IEEE Transactions on Control Systems Technology*, pages 1–12.

[50] Kempton, W. and Tomić, J. (2005). Vehicle-to-grid power implementation: From stabilizing the grid to supporting large-scale renewable energy. *Journal of Power Sources*, 144(1):280–294.

[51] Khodr, H. M., El Halabi, N., and García-Gracia, M. (2012). Intelligent renewable microgrid scheduling controlled by a virtual power producer: A laboratory experience. *Renewable Energy*, 48:269–275.

[52] Kissock, J. K. (1998). Combined heat and power for buildings using fuel-cell cars. In *Proceedings of the ASME International Solar Energy Conference*, pages 121–132.

[53] Korpås, M. and Holen, A. T. (2006). Operation planning of hydrogen storage connected to wind power operating in a power market. *IEEE Transactions on Energy Conversion*, 21(3):742–749.

[54] Kraftfahrt-Bundesamt (2016). Der Fahrzeugbestand im Überblick am 1. Januar 2016 gegenüber 1. Januar 2015. URL: https://www.kba.de/DE/Statistik/Fahrzeuge/Bestand/Ueberblick/2016/2016_b_ueberblick_pdf.pdf?__blob=publicationFile&v=1.

[55] Kraftfahrt-Bundesamt (2016). Verkehr in Kilometern der deutschen Kraftfahrzeuge im Jahr 2015. URL: https://www.kba.de/DE/Statistik/Kraftverkehr/VerkehrKilometer/2015/2015_vk_kurzbericht_pdf.pdf?__blob=publicationFile&v=1.

[56] Lipman, T. E., Edwards, J. L., and Kammen, D. M. (2004). Fuel cell system economics: Comparing the costs of generating power with stationary and motor vehicle PEM fuel cell systems. *Energy Policy*, 32(1):101–125.

[57] Lipman, T. E., Elke, M., and Lidicker, J. (2018). Hydrogen fuel cell electric vehicle performance and user-response assessment: Results of an extended driver study. *International Journal of Hydrogen Energy*, 43(27):12442–12454.

[58] Longson, W., Chryssochoos, I., Raković, S. V., and Mayne, D. Q. (2004). Robust model predictive control using tubes. *Automatica*, (40):125–133.

[59] Lukszo, Z. and Park Lee, E. (2016). Demand side and dispatchable power plants with electric mobility. In *Smart Grids from a Global Perspective: Bridging Old and New Energy Systems*, pages 163–177. Springer International Publishing.

[60] Maroufmashat, A., Fowler, M., Khavas, S. S., Elkamel, A., Roshandel, R., and Hajimiragha, A. (2016). Mixed integer linear programing based approach for optimal planning and operation of a smart urban energy network to support the hydrogen economy. *International Journal of Hydrogen Energy*, 41:7700–7716.

[61] Mc Namara, P., Negenborn, R. R., De Schutter, B., and Lightbody, G. (2013). Optimal coordination of a multiple HVDC link system using centralized and distributed control. *IEEE Transactions on Control Systems Technology*, 21(2):302–314.

[62] Milieu Centraal (2016). Kleine windmolens ("Small wind turbines") (in Dutch). URL: https://www.milieucentraal.nl/klimaat-en-aarde/energiebronnen/windenergie/kleine-windmolens/.

[63] National Renewable Energy Laboratory (2015). PVWatts Calculator. URL: http://pvwatts.nrel.gov/pvwatts.php.

[64] NEDU (2017). Profielen aardgas & elektriciteit. URL: http://www.nedu.nl/documenten/verbruiksprofielen/.

[65] Oldenbroek, V., Verhoef, L. A., and van Wijk, A. J. M. (2017). Fuel cell electric vehicle as a power plant: Fully renewable integrated transport and energy system design and analysis for smart city areas. *International Journal of Hydrogen Energy*, 42(12):8166–8196.

[66] Padhy, N. P. (2004). Unit commitment–a bibliographical survey. *IEEE Transactions on Power Systems*, 19(2):1196–1205.

[67] Parhizi, S., Lotfi, H., Khodaei, A., and Bahramirad, S. (2015). State of the art in research on microgrids: A review. *IEEE Access*, 3:890–925.

[68] Parisio, A. and Glielmo, L. (2013). Stochastic model predictive control for economic/environmental operation management of microgrids. In *European Control Conference (ECC)*, pages 2014–2019, Zürich, Switzerland.

[69] Parisio, A., Rikos, E., and Glielmo, L. (2014). A model predictive control approach to microgrid operation optimization. *IEEE Transactions on Control Systems Technology*, 22(5):1813–1827.

[70] Park Lee, E. H. and Lukszo, Z. (2016). Scheduling fuel cell electric vehicles as power plants in a community microgrid. In *Proceedings of IEEE PES Innovative Smart Grid Technologies, Europe*, Ljubljana, Slovenia.

[71] Park Lee, E. H., Lukszo, Z., and Herder, P. (2017). Static volume-based and control-based contracts for coordinating vehicle-to-grid supply in a microgrid. In *Proceedings of Innovative Smart Grid Technologies (ISGT) European Conference*, pages 1–6.

[72] Park Lee, E. H., Lukszo, Z., and Herder, P. (2018). Conceptualization of vehicle-to-grid contract types and their formalization in agent-based models. *Complexity*, 2018.

[73] Parsons, G. R., Hidrue, M. K., Kempton, W., and Gardner, M. P. (2014). Willingness to pay for vehicle-to-grid (V2G) electric vehicles and their contract terms. *Energy Economics*, 42(0):313–324.

[74] Peel, M. C., Finlayson, B. L., and McMahon, T. A. (2007). Updated world map of the Köppen-Geiger climate classification. *Hydrology and Earth System Sciences*, 11:1633–1644.

[75] Peng, C., Lei, S., Hou, Y., and Wu, F. (2015). Uncertainty management in power system operation. *CSEE Journal of Power and Energy Systems*, 1(1):28–35.

[76] Persson, U. and Werner, S. (2015). Quantifying the heating and cooling demand in Europe: Work package 2, background report 4. URL: https://hre.aau.dk/wp-content/uploads/2018/09/STRATEGO-WP2-Background-Report-4-Heat-Cold-Demands.pdf.

[77] Petrollese, M., Valverde, L., Cocco, D., Cau, G., and Guerra, J. (2016). Real-time integration of optimal generation scheduling with MPC for the energy management of a renewable hydrogen-based microgrid. *Applied Energy*, 166:96–106.

[78] Prodan, I. and Zio, E. (2014). A model predictive control framework for reliable microgrid energy management. *Electrical Power and Energy Systems*, 61:399–409.

[79] Rodatz, P., Paganelli, G., Sciarretta, A., and Guzzella, L. (2005). Optimal power management of an experimental fuel cell/supercapacitor-powered hybrid vehicle. *Control Engineering Practice*, 13(1):41–53.

[80] Royal Netherlands Meteorological Institute (KNMI) (2015). Uurgegevens van het weer in Nederland (Hourly weather data in the Netherlands) (in Dutch). URL: http://knmi.nl/nederland-nu/klimatologie/uurgegevens.

[81] Samuelsen, S. (2017). The automotive future belongs to fuel cells: Range, adaptability, and refueling time will ultimately put hydrogen fuel cells ahead of batteries. *IEEE Spectrum*, 54(2):38–43.

[82] Schiffer, J., Ortega, R., Astolfi, A., Raisch, J., and Sezi, T. (2014). Conditions for stability of droop-controlled inverter-based microgrids. *Automatica*, 50:2457–2469.

[83] Schiffer, J., Zonetti, D., Ortega, R., Stanković, A. M., Sezi, T., and Raisch, J. (2016). A survey on modeling of microgrids - from fundamental physics to phasors and voltage sources. *Automatica*, 74:135–150.

[84] Shinoda, K., Park Lee, E., Nakano, M., and Lukszo, Z. (2016). Optimization model for a microgrid with fuel cell vehicles. In *13th IEEE International Conference on Networking, Sensing and Control (ICNSC)*, pages 1–6.

[85] Tazelaar, E., Shen, Y., Veenhuizen, P. A., Hofman, T., and van den Bosch, P. P. J. (2012). Sizing stack and battery of a fuel cell hybrid distribution truck. *Oil & Gas Science and Technology*, 67(4):563–573.

[86] U.S. Department of Energy (2012). Wind and water program: Community wind benefits. URL: http://www.nrel.gov/docs/fy13osti/56386.pdf.

[87] van Hessem, D. H. and Bosgra, O. H. (2003). A full solution to the constrained stochastic closed-loop MPC problem via state and innovations feedback and its receding horizon implementation. In *42nd IEEE Conference on Decision and Control*, pages 929–934. IEEE.

[88] van Wijk, A. J. M. and Verhoef, L. (2014). *Our Car as Power Plant*. Delft University Press. ISBN: 9781614993766.

[89] Veldman, E., Gaillard, M., Gibescu, M., Slootweg, J., and Kling, W. (2010). Modelling future residential load profiles. In *Proceedings of the Innovation for Sustainable Production*, pages 64–68, Bruges, Belgium. I-SUP.

[90] Verzijlbergh, R. A., Lukszo, Z., and Ilic, M. D. (2012). Comparing different EV charging strategies in liberalized power systems. In *International Conference on the European Energy Market*, pages 1–8.

[91] Vidueira, J. M., Contreras, A., and Veziroglu, T. N. (2003). PV autonomous installation to produce hydrogen via electrolysis, and its use in FC buses. *International Journal of Hydrogen Energy*, 28(9):927–937.

[92] Walters, M., Kuhlmann, A., and Ogrzewalla, J. (2015). Fuel cell range extender for battery electric vehicles. In *International Conference on Electrical Systems for Aircraft, Railway, Ship Propulsion and Road Vehicles (ESARS)*, Aachen, Germany.

[93] Wang, J. J. and Song, W. (2017). An algorithm twisted from generalized ADMM for multi-block separable convex minimization models. *Journal of Computational and Applied Mathematics*, 309:342–358.

[94] Werner, S. (2016). European space cooling demands. *Energy*, 110:148–156.

[95] Wolsink, M. (2012). The research agenda on social acceptance of distributed generation in smart grids: Renewable as common pool resources. *Renewable and Sustainable Energy Reviews*, 16(1):822–835.

[96] Yazdanian, M. and Mehrizi-Sani, A. (2014). Distributed control techniques in microgrids. *IEEE Transactions on Smart Grids*, 5(6):2901–2909.

[97] Zhang, L., Gari, N., and Hmurcik, L. V. (2014). Energy management in a microgrid with distributed energy resources. *Energy Conversion and Management*, 78:297–305.